FACULTAD DE
CIENCIAS
UNIVERSIDAD AUTÓNOMA DE MADRID

Universidad Autónoma de Madrid

Department of Condensed Matter Physics

Calorimetric and thermodynamic study of molecular glasses and crystals of butanol

Thesis presented by

Merzak Hassaine

for the degree of Doctor in Physics

Thesis Director:

Miguel Ángel Ramos Ruiz

June, 2013

Agradecimientos

Esta Tesis ha sido desarrollada en el Departamento de Física de la Materia Condensada de la Universidad Autónoma de Madrid (UAM), en el laboratorio de Bajas Temperaturas. Me gustaría agradecer al laboratorio todos los medios puestos a mi disposición para realizar este trabajo y a la AECI por la financiación de mis estudios.

Esta tesis ha sido el fruto de mucho trabajo e ilusión durante cinco años junto a personas a las que he tenido la suerte de conocer y a las que tengo muchas cosas que agradecer.

En primer lugar, me gustaría dar las gracias de manera muy especial a mi director de tesis, Miguel Ángel Ramos, sin el nada de esto hubiera sido posible, le agradezco la confianza que ha depositado en mí, la formación científica que he recibido de él, su apoyo constante, y por su cuidadosa revisión. Asimismo quería dar las gracias a Sebastián Vieira, y a todos los profesores del laboratorio de bajas temperaturas, Raúl Villar, Nicolás Agrait, Hermann Suderow, José Gabriel Rodrigo, Gabino Rubio y Fakhad Aliev, por su apoyo.

Quiero dar las gracias a todas las personas en el laboratorio que han ayudado a que los experimentos salgan adelante, a Andrés Buendía por sus consejos y su ayuda, a Rosa que hace que no nos falte nada en el laboratorio, a Manolo, José, Santiago, Juanma, Macarena y Elsa por su disponibilidad, y sus ánimos constantes.

Gracias a todas las personas que he tenido la suerte de colaborar con ellos, Dr. Rafael Jiménez-Riobóo (CSIC, Madrid), Dr. Ivan Shmyt'ko (Russian Academy of Sciences, Moscow) y Dr. Alexander Krivchikov (Verkin Institute, Kiev).

A mis compañeros en el laboratorio y en el departamento, Bisher, Tomas, Yan, Ahmed, David, Carlos, Andrés C, Charalambos, Siya, Teresa, Edmund, Manuel, Roberto, Juanpe, Isabel, Vanesa, Ana, José Augusto, Prassana, Antón, Guillermo, Eduardo, Mohammed, Michelle y Curro, gracias por su apoyo y que han hecho que estos años sean más agradables. A Bisher, le agradezco su ayuda de los primeros días, y a Tomas le agradezco su ayuda y su apoyo hasta el último momento. Gracias.

Quiero dar las gracias a todos mis amigos los que están en Argelia y los que he conocido en Madrid durante estos años. Que han confiado en mí y me han apoyado y animado a superarme.

Por último, quisiera dar las gracias a mi familia, a mis hermanos y hermanas, a mis padres, que les debo todo. A mi madre por su apoyo incondicional, aunque no le guste que esté lejos, en Madrid, y de manera muy especial quiero dar las gracias a mi padre, por lo que ha hecho, para que podemos seguir adelante. Gracias por todo.

Table of contents

Abstract 7
Resumen 9

Chapter 1: Introduction 11

1.1 Liquids, crystals and glasses 12
1.2 Motivation and objectives 14
References 16

Chapter 2: The glass transition and the glass state 17

2.1 Fundamentals of the glass transition and theoretical background 17
2.1.1 Phenomenology of the glass transition 17
2.1.2 Fragile and strong glass-forming liquids 21
2.1.3 The Kauzmann paradox and the ideal glass 23
2.1.4 Theories and models 25
2.1.4.1 Free volume theory 25
2.1.4.2 Adam-Gibbs theory 26
2.1.4.3 Energy Landscape 28
2.1.4.4 Mode coupling theory (MCT) 29
2.1.4.5 Random first order theory (RFOT) 31
2.2 Low-temperature properties of glasses 32
2.2.1 Tunneling Model (TM) 36
2.2.2 Soft Potential Model (SPM) 40
References 45

Chapter 3: Experimental.....47

3.1 Experimental system.....48
3.2 Calorimetric cells.....49
3.3 Materials and preparation of the samples.....50
3.4 Experimental methods of calorimetry.....52
3.4.1 Adiabatic method.....52
3.4.2 Relaxation methods.....53
3.4.3 Quasi-adiabatic ontinuous method.....56
3.4.4 Experimental operation.....58
3.5 Heat capacity measurements of the addenda (empty cell).....60
3.5.1 At liquid nitrogen temperatures.....60
3.5.2 At liquid helium temperatures.....61
References.....64

Chapter 4: Calorimetric, thermodynamic and structural study of butanol isomers.....65

4.1 Experimental results on n-butnaol.....66
4.2 Experimental results on sec-butanol.....75
4.3 Experimental results on tert-butanol.....79
4.4 Experimental results on isobutanol.....85
4.5 Other experiments.....90
4.5.1 X-ray diffraction.....90
4.5.1.1 Experimental setup and measuring procedures.....90
4.5.1.2 Results.....91
4.5.2 Brillouin scattering.....93
4.5.2.1 Experimental setup and measuring procedures.....93
4.5.2.2 Results.....94
4.6 Discussion.....97
4.6.1 The so-called “glacial state” of n-butanol.....97

4.6.2 Thermodynamic properties……100
References……106

Chapter 5: Thermal properties at low temperature of butanol isomers……109

5.1 Experimental results on n-butanol……110
5.2 Experimental results on sec-butanol……114
5.3 Experimental results on tert-butanol……116
5.4 Experimental results on isobutanol……117
5.5 Other experiments……120
5.5.1 Thermal conductivity……121
5.5.1.1 Experimental setup……121
5.5.1.2 Results……122
5.5.2 Brillouin scattering at low temperatures……123
5.5.2.1 Experimental setup……123
5.5.1.2 Results……123
5.6 Discussion……125
5.6.1 The so-called "glacial state" of n-butanol……125
5.6.2 Low-temperature properties of butanol crystals……127
5.6.3 Low-temperature properties of butanol glasses……128
5.6.4 Residual entropy and Kauzmann temperature of butanol glasses……135
5.6.4.1 n-butanol entropy……136
5.6.4.2 sec-butanol entropy……140
5.6.4.3 isobutanol entropy……143
5.3.4.4 General discussion……145
References……148

Chapter 6: General conclusions……151

Index of figures and tables……157
List of publications……161

Abstract

Glasses at low temperatures show universal physical properties that are attributed to the low-energy excitations which characterize all kinds of amorphous solids, and significantly different from the behavior of fully-ordered crystals well explained by the Debye theory. Many theories and models have been proposed to explain these glassy features and related phenomena. However, the low-temperature universal properties of glasses, as well as the glass transition itself, are still one of the major unsolved and debated problems of condensed matter physics.

Thermal as well as several other universal low-temperature properties of glasses or amorphous solids have been well explained and successfully accounted for by the Tunneling Model (TM) below 1K. Nevertheless, above 1K the also rich and universal behavior of glasses, such as the broad maximum of the specific heat in the representation C_p / T^3 or the "plateau" in the thermal conductivity, remain unsolved. One of the approaches most often used to explain and account for this behavior is the soft-potential model (SPM), which will be used here to analyze our results.

In order to better understand and make progress in the investigation of the so-called low-temperature universal properties of non-crystalline solids and the phenomena of the glass transition and the glassy state, we have conducted an exhaustive calorimetric study on the butanol isomers system (n-butanol, sec-butanol, isobutanol and *tert*-butanol), and have measured their specific heat in a wide low temperature range, under the same experimental conditions. These measurements and the corresponding theoretical analyses have provided a consistent set of calorimetric and thermodynamic data of glasses and crystals of the different butanol isomers. We will also present other experiments conducted to complement the results obtained by our specific heat measurements, which have addressed other thermal, structural, and elastoacoustic properties.

Specifically, we have performed a comparative analysis of low-temperature thermal properties of the glassy phases among different butanol isomers, to assess the influence of chemical isomerism and the location of hydrogen bonding

on lattice dynamics of these glasses. We have also made a direct comparison with the lower monoalcohols previously measured by our group, especially the propanol isomers. In addition, we also expect to shed light on the disputed solid "glacial" phase reportedly found in n-butanol (1-butanol) around 120 K.

Finally, the entropy curves of the different phases of these isomers of butanol have been obtained, and hence the so-called Kauzmann temperature of glasses T_K and their "residual entropy" at zero Kelvin have been determined. These and other available thermodynamic data of butanol isomers will be discussed, by comparing our results with proposed correlations found in the literature.

Resumen

Las propiedades físicas (en particular, las propiedades térmicas) de los sólidos no cristalinos a bajas temperaturas presentan un comportamiento universal, atribuido a las excitaciones de baja energía que caracterizan a todos los tipos de sólidos amorfos, y que difiere significativamente del observado en los cristales completamente ordenados que siguen la teoría de Debye. Se han propuesto muchas teorías y modelos para explicar estas propiedades características de los vidrios y otros fenómenos relacionados. No obstante, las propiedades universales de los vidrios a bajas temperaturas, así como la propia transición vítrea, siguen constituyendo uno de los principales problemas sin resolver y más debatidos en el área de la física de la materia condensada.

Las propiedades térmicas, así como otras varias propiedades a bajas temperaturas de los vidrios o sólidos amorfos, han sido bien explicadas y representadas con éxito por el modelo de túnel (TM) por debajo de 1 K. Sin embargo, el comportamiento universal de los vidrios por encima de 1 K, tal como el máximo del calor específico en la representación C_p / T^3 o el "plateau" en la conductividad térmica, siguen siendo un problema sin resolver. Uno de los métodos más utilizados para explicar este comportamiento, es el modelo de potenciales blandos (SPM, por sus siglas en inglés), que utilizaremos para el análisis de los resultados.

Con el objetivo de progresar en la investigación de las llamadas propiedades universales de bajas temperaturas de los sólidos no cristalinos, y del propio fenómeno de la transición vítrea y del estado vítreo, hemos llevado a cabo un estudio calorimétrico exhaustivo del sistema de los isómeros del butanol (n-butanol, sec-butanol, isobutanol y *tert*-butanol) y hemos medido su calor específico en un amplio rango de bajas temperaturas, en unas mismas condiciones experimentales. Estas medidas y los correspondientes análisis teóricos nos van a proporcionar una serie consistente de datos calorimétricos y termodinámicos para las fases de vidrio y cristal de los diferentes isómeros del butanol. También presentaremos otros experimentos realizados para

complementar los resultados de nuestras medidas de calor específico, y que han abordado el estudio de otras propiedades térmicas, estructurales y elastoacústicas.

En concreto, hemos realizado un análisis comparativo de las propiedades térmicas a bajas temperaturas de las fases vítreas entre diferentes isómeros de butanol, para evaluar la influencia del isomerismo químico y de la posición que ocupa el enlace de hidrógeno en la molécula sobre la dinámica de red de estos vidrios. También hemos hecho una comparación directa con los monoalcoholes inferiores ya estudiados previamente en el laboratorio, especialmente los isómeros del propanol. Además, esperamos arrojar luz sobre la polémica fase sólida “glacial” reportada en el n-butanol (1-butanol) alrededor de 120 K.

Por último, hemos calculado las curvas de entropía de las diferentes fases de los isómeros del butanol, determinando así las llamadas temperaturas de Kauzmann T_K de los vidrios y sus "entropías residuales" a cero Kelvin. Se discutirán estos y otros datos termodinámicos de los isómeros del butanol, comparando los resultados con algunas correlaciones propuestas en la literatura.

1 Introduction

The art and technology of glass long preceded their scientific understanding. Investigations of ancient glasses take us to the very dawn of civilization; it appears that glass was first made in Mesopotamia in western Asia. Objects dated to 4000 B.C. have been found. From this we find them in the successive civilizations to our days.

19th century gave birth to industries with mechanized glasswork, the modern methods of making glass in large quantities. In fact, following the industrial revolution, glass making did become the business of factories. In the 20th century glass became an integral part of human life, but also the evolution of manufacturing techniques and the scientific understanding of glasses were started. Growth of glass science is evidently connected with the growth of chemistry and physics.

So, glass has been made into practical and decorative objects since ancient time and it is still very important in applications. It plays an important role in various scientific fields, in industry, telecommunications, etc. [Zallen 1983]. It is used at home, such the most familiar windows glass or the electric bulb. It is also found in new technology applications such as amorphous semiconductors, optic fiber optic waveguides, and in new energy sources (photovoltaic energy) used in the solar cells. We certainly find glass in our research laboratory: besides usual glassware, our own calorimetric experiments at low temperatures were realized in a cryostat entirely made of glass. The examples are numerous, we encounter more frequently noncrystalline than crystalline solids in our everyday life.

Therefore, we live in a world in which glasses play a very important role in all aspects of our daily life and this is enough reason for us to study the science of these glasses [Rao 2002, Zallen 1983].

Formerly the glasses have been only produced by cooling the melts. However, with the evolution of the science and industry, many amorphous solids are now prepared by various methods other than the traditional liquid-cooling method. On the other hand, the glass transition phenomenon has been recognized since a long time as one of the major topics in condensed matter physics. In spite

of its considerable scientific impact there still exists a fairly widespread lack of understanding the nature of the glass transition.

1.1 Liquids, crystals and glasses

Traditionally, solid-state physics has meant crystal physics. Solidity and crystallinity are treated as synonymous in the standard texts on condensed matter. Yet, one of the most active fields of solid-state research in last decades has been the study of solids that are not crystals [Zallen 1983, Elliott 1990].

Therefore, it might be worth that before starting to talk about glasses and the glassy state, we give some definitions of the principal states of matter.

Liquids: Liquids like gases take the shape of their container because they are fluids, but the liquid does not necessarily fill it. In contrast the solid is the substance that does not flow, its viscosity is $\eta \geq 10^{13} - 10^{14}$ poise.

Crystals: Crystals are solids for which the atomic (groups of atoms or molecules) positions exhibit long-range order (periodicity).

Amorphous solids: Amorphous solids or non-crystalline solids are the solids which do not possess long-range translational order. The equilibrium of atomic (groups of atoms or molecules) position is disordered, and the long-range order is absent, as schematized in Fig 1.1. The glass is an amorphous solid that present a glass transition.

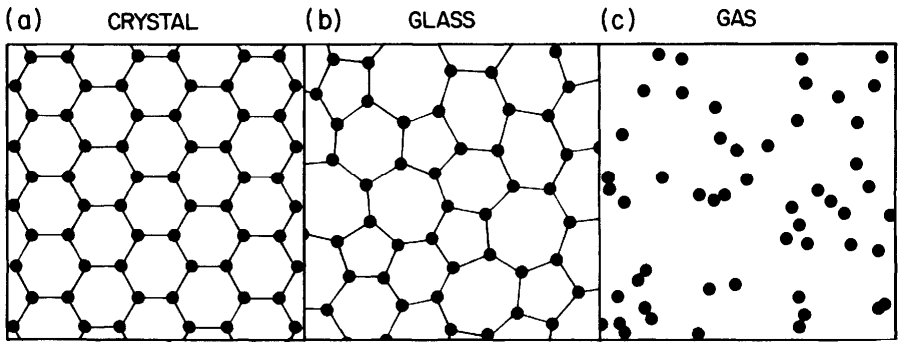

Fig 1.1 Schematic sketches of the atomic arrangements in (a) a crystalline solid, (b) amorphous solid, and (c) a gas [Zallen 1983]

Without further deepen the definitions, this classification is, of course, useful as a first rough division between different states of matter.

In nature, processes of crystallization and glass-formation are induced by increasing pressure or by decreasing temperature. The simplest way to produce a glass is by supercooling a liquid. So, by decreasing the temperature of the liquid state, the liquid solidifies; two different solidifications are possible, as shown in Fig 1.2. If the rate of cooling is sufficiently low, we usually obtain the liquid-crystal transition at/or below the melting temperature T_m (or T_f, for freezing temperature), with discontinuity in the entropy S or the volume V. But at higher cooling rates, T_m is bypassed, the liquid phase is maintained becoming more and more viscous and the solidification liquid-glass (vitrification) eventually occurs with a small slope change in volume at the glass transition T_g. [Zallen 1983].

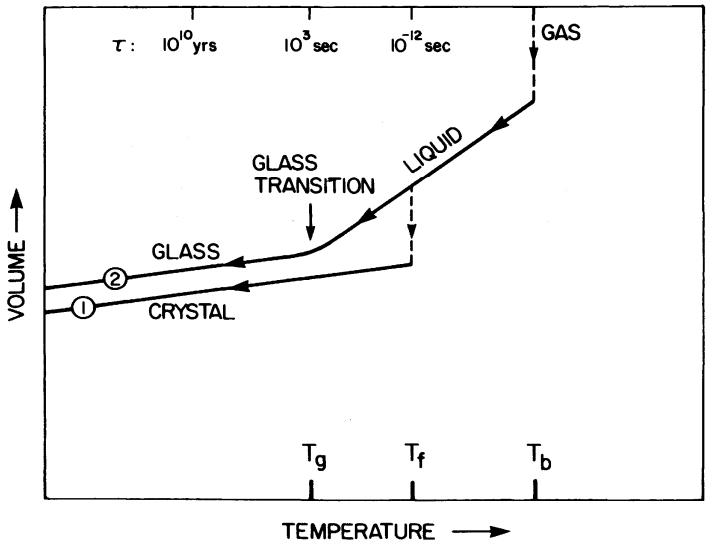

Fig 1.2 The two general cooling paths by which an assembly of atoms in the liquid state can condense into the solid state. Route 1 is the path to the crystalline state; route 2 is the rapid-quench path to the amorphous solid state (glass). [Zallen 1983]

Even if the glass transition has been studied and observed by different techniques, and many approaches have been made to understand the glass transition phenomena, given its complexity none of these theory appears

successful to explain it in all its aspects. Although some characteristics have been clarified, its origin remains, however, one of the major unsolved and debated problems of condensed matter physics. As stated by the well-known Nobel Laureate P. W. Anderson: "*The deepest and most interesting unsolved problem in solid state theory is probably the nature of glass and the glass transition*." [Anderson 1995]

On the other hand, at low temperatures the glasses present very different properties from those of the crystals. Thus, despite the fact that glasses or amorphous solids were recognized as different to the crystals, before 1970 most solid-state physicists, if asked to describe the behaviour of the heat capacity and the thermal conductivity of pure fused silica below 1 K, would have predicted it to be very similar to that of crystalline quartz [Phillips 1981]. It was assumed that structural differences do not contribute, because the wavelength and the mean free path of phonons in this region would increase, thus the effects of disorder being negligible. It was not until the experiments of specific heat and thermal conductivity in different amorphous solids performed by Zeller and Pohl [Zeller 1971] that clear evidence was given that glasses or amorphous solids exhibited thermal properties very different from those of the crystalline counterparts.

In addition to the clear evidence that the amorphous solids exhibit very different thermal properties from those of the crystals, the second important finding is that these were indeed very similar among themselves (the universal glassy behaviour). The glass always shows a higher specific heat and much lower thermal conductivity then the corresponding crystal.

1.2 Motivation and objectives

We cannot begin this section without recalling the sentence of Anderson [Anderson 1995] cited just before.

The principal motivation of this thesis is trying to better understand and to make progress in the investigation of the so-called low temperature universal properties of non-crystalline solids and the phenomenon of the glass transition and the glassy state. The materials chosen for this purpose are simple alcohols. In particular, glass-forming molecular liquids are good and appealing systems to

investigate the nature of both the glass-transition phenomenon and the universal low-temperature properties of glasses, since they present a very convenient temperature transformation range below room temperature.

It seems instructive to compare the same property, such as the glass transition temperature T_g or the low temperatures properties, for different glass-formers and/or the same family of glass formers under the same conditions. In particular, it is very interesting to study the properties of different glasses of the same substance in different chemicals structures (isomers) under the same experimental conditions and theoretical analyses. This will allow us to carry out a comparative study for different molecular glasses of the same substance, in order to assess the effects of changing the spatial arrangement of atoms and hydrogen bonding in the lattice on the thermodynamic magnitudes of the glass transition and on the low-temperature properties.

Therefore, in this work we will be most interested in a comparative analysis of low-temperature thermal properties of the glassy phases among different butanol isomers. Moreover, this will allow us a direct comparison with the lower monoalcohols previously measured by our group, especially the propanol isomers.

We also expect to shed light on the disputed solid "glacial" phase reportedly found in 1-butanol at 120 K (between the glass and crystal phases).

Finally, we will provide calorimetric and thermodynamic data of all butanol isomers, and discuss the proposed correlations in the literature with liquid fragility. In addition, we will conduct an analysis of specific-heat data curves in order to calculate the residual entropy in the zero-temperature limit and the so-called Kauzmann temperature for the studied glasses.

After this short introduction, in the next chapters we will begin by giving a theoretical background of the glassy state and the glass transition, and we will describe the materials and methods used to prepare the different samples, as well as the setup and experimental techniques employed. Then, the experimental data directly obtained from the measurements will be presented, both at liquid-nitrogen temperatures, where the different phases are prepared and characterized, and the phase transitions measured, and at (liquid-helium) low temperatures. Then data analysis and interpretation will follow. Finally, the main conclusions of the work will be summarized.

References

[Anderson 1995]: P. W. Anderson, Science 267, pp.1615-1616 (1995).

[Elliott 1990]: S. R. Elliott, *Physics of Amorphous Materials*, 2nd ed. (Longman, 1990).

[Phillips 1981]: W. A. Phillips (ed.), *Amorphous Solids: Low Temperature Properties* (Topics in Current Physics, Vol. 24, Springer, 1981).

[Rao 2002]: K. J. Rao, *Structural chemistry of glasses*, (Elsevier science Ltd, 2002).

[Zallen 1983]: R. Zallen, *The Physics of Amorphous Solids*, (Wiley, 1983).

[Zeller 1971]: R. C. Zeller and R. O. Pohl, Phys. Rev. B 4, 2029 (1971).

2 The glass transition and the glass state

2.1 Fundamentals of the glass transition and theoretical background

2.1.1 Phenomenology of the glass transition

As said before, when a liquid is cooled two different events may occur (see Fig 1.2). Either crystallization takes place at the melting point T_m, or the liquid will become supercooled for temperatures below T_m, becoming more viscous with decreasing temperature, and may ultimately form a glass [Zallen 1983].

Generally speaking, when cooling the liquid slowly enough, we observe the liquid–crystal transition at (or below) T_m. In order to avoid the crystallization, the liquid has to be cooled rapidly from T_m through the region of crystallization (difficult or "dangerous" zone for people working on glasses) represented in Fig 2.1. Nevertheless, many more substances than often believed can be kept supercooled below T_m without crystallizing for more or less long times.

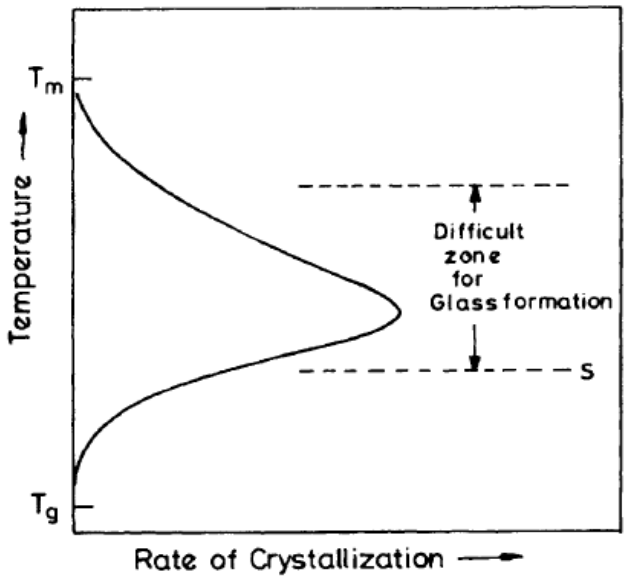

Fig 2.1 Behavior of crystallization rate as a function of temperature [Rao 2002].

Crystallization is governed by two factors, the nucleation and the growth rate that are dependent on the viscosity of the melt [Rao 2002]. The cooling rates can be compared to

$$v = \frac{L(T_m - T)}{3\pi a^2 \eta T_m} \tag{2.1}$$

where v is the velocity of crystallization, L is the latent heat of fusion, η is the viscosity of the material, and a is the typical distance through which the particles have to move during the crystallization.

The glass transition or vitrification occurs by further decreasing temperature T or increasing pressure P. Then, the structural relaxation time of the supercooled liquid (SCL) becomes longer and longer when approaching the glass transition. Hence the viscosity η of the liquid, that represents the resistance to the flow, increases considerably, which reflects a severe increase in the relaxation times at T_g, as shown in Fig 1.2 (previous chapter): the relaxation time τ in the liquid region is typically about $\approx 10^{-12}$ s, whereas is about $\approx 10^3$ s at the glass transition.

It is useful and traditional to account for the viscoelastic behavior of glass-forming liquids following the idea of Maxwell, according to which liquids behave (mechanically) like solids at times shorter than a certain time scale. This time scale can be taken as the fundamental definition of shear relaxation time τ. In its simplest form, $G(t)$ can be expressed as $G(t) = G_\infty \exp(-t/\tau)$, where G_∞ is the infinite frequency (i.e. zero time) shear modulus. Within the Maxwell model a single (or average) exponential relaxation time is assumed, directly implying [Cavagna 2009] that the relaxation time τ and the shear viscosity η are linearly linked through the Maxwell's relation

$$\tau = \frac{\eta}{G_\infty} \tag{2.2}$$

The kinetic grounds of the laboratory glass transition are evident from (2.2), where a usually defined viscosity $\eta(T_g) \equiv 10^{12}$ Pa·s is directly connected to a typical relaxation time $\tau(T_g) \approx 10^2 – 10^3$ s at the glass transition.

From the thermodynamic point of view, it is obvious that the glass transition is not a standard first-order transition as the crystal-liquid one. It looks like, in principle, as a second-order one, but even that has been (and still is) a matter of vivid discussion for decades. Let us briefly summarize below the basic points.

At the glass transition the first derivative quantities (2.3) of the Gibbs free energy (V and S) remain continuous:

$$\left(\frac{\partial G}{\partial P}\right)_T = V \quad \text{and} \quad \left(\frac{\partial G}{\partial T}\right)_P = -S\,, \tag{2.3}$$

while the thermodynamic coefficients (specific heat C_p, thermal expansion α, and compressibility β), i.e. the corresponding second derivative quantities (2.4), (2.5) and (2.6) of the Gibbs free energy G, exhibit (apparent) discontinuities:

$$\left(\frac{\partial^2 G}{\partial T^2}\right)_P = -\left(\frac{\partial S}{\partial T}\right)_P = -\frac{C_P}{T} \tag{2.4}$$

$$\left(\frac{\partial^2 G}{\partial P^2}\right)_T = \left(\frac{\partial V}{\partial P}\right)_T = -V\beta \tag{2.5}$$

$$\left(\frac{\partial^2 G}{\partial P \partial T}\right) = -\left(\frac{\partial S}{\partial P}\right)_T = \left(\frac{\partial V}{\partial T}\right)_P = V\alpha \tag{2.6}$$

The glass transition could therefore be treated apparently as a second-order phase transition in the Ehrenfest sense. There is not a consensus however about this statement. Figure 2.2 shows a typical liquid which can either crystallize or form a glass. By employing a low cooling rate the glass transition T_g occurs at T_{ga}, whereas by a higher cooling rate it occurs at T_{gb}. The glass transition temperature T_g depends on the technique used to measure it, on its thermal history, and particularly on the rate of cooling the supercooled liquid, where T_g increases with increasing cooling rate. The thermodynamic and dynamic properties of a glass therefore depend upon how it was formed.

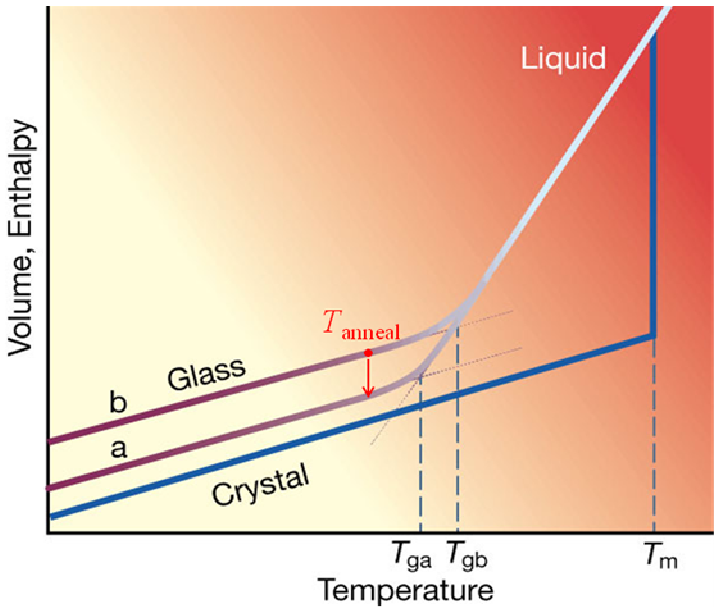

Fig 2.2 Temperature dependence of a liquid's volume V or enthalpy H at constant pressure. T_m is the melting temperature. A slow cooling rate produces a glass transition at T_{ga}; a faster cooling rate leads to a glass transition at T_{gb}. The thermal expansion coefficient $\alpha_p=(\partial \ln V/\partial T)_p$ and the isobaric heat capacity $C_p=(\partial H/\partial T)_p$ change abruptly but continuously at T_g [Debenedetti 2001]. T_{anneal} is a possible temperature of annealing (ageing) of the glass.

In addition, it is well known that an amorphous solid in the glassy state is out of thermodynamical equilibrium. Hence ageing (or annealing) of the glassy state close to, but below, the glass transition T_g, allows it to "relax". During this process the structure and energy of the system will tend toward the equilibrium state (at least, to a more stable glassy state).

Therefore, it is essential to give some conventional definition of the temperature associated to the glass transition. During the cooling, the transition to the glassy state is continuous and the glass transition is not well defined. So, the glass transition is usually determined by calorimetry, where the glass transition temperature T_g is typically determined as the midpoint temperature of the specific-heat jump from the glassy to the liquid state (see, for example, the inset of Fig. 2.3) at a given heating rate (10 K/min) [Gutzow 1995]. Obviously, other physical magnitudes obtained from other experimental techniques can also

be used to assess T_g, though once again the so-obtained values for T_g would somewhat depend on the followed experimental method.

Alternatively, it is often convenient to use the fictive temperature T_f [Elliott 1990], which is the temperature obtained at the intersection point of the extrapolated liquid and glass enthalpy curves.

2.1.2 Fragile and strong glass-forming liquids

According to a phenomenological definition, glass transition takes place at temperature T_g, where the viscosity of a supercooled liquid reaches 10^{13} poise. The increase in viscosity in these systems is directly proportional to the increase in relaxational time τ.

For some glass-forming liquids (*strong* liquids), τ grows at low temperatures following the Arrhenius law

$$\tau = \tau_0 \exp\left(\frac{A}{T}\right), \tag{2.7}$$

where A is constant.

However, for most glass-forming liquids (*fragile* liquids) the temperature dependence of relaxation times is more complex, and the increase in τ is well fitted by a super-Arrhenius law

$$\tau = \tau_0 \exp\left(\frac{A}{T - T_{VF}}\right), \tag{2.8}$$

called the Vogel-Fulcher-Tammann (VFT) law, where T_{VF} is the Vogel-Fulcher temperature, which can be obtained from data extrapolation below T_g.

Figure 2.3 represents the viscosity logarithm variation as a function of a reduced inverse temperature scale T_g/T using T_g as a normalizing parameter. This so-called Angell plot [Angell 1976] has been used to classify supercooled liquids into ”strong” and ”fragile”, thereby introducing an interesting framework to describe structural relaxation in liquids.

Fragile liquids are those exhibiting a rapid breakdown of viscosity and relaxation time with increasing temperature above T_g, in contrast with strong liquids which do not change so much around the glass transition and remain

rather viscous in the supercooled liquid state. Fragile glass-forming liquids are typically substances with non-directional bonding and hence are more prone to "thermal degradation", whereas strong glass-forming liquids use to be covalent oxides whose inter-molecular structure is very robust against thermal energy.

As it is also shown in the inset of Fig. 2.3, the jump in C_p at T_g is generally large for fragile liquids and small for strong liquids, despite some exceptions as hydrogen-bonded alcohols.

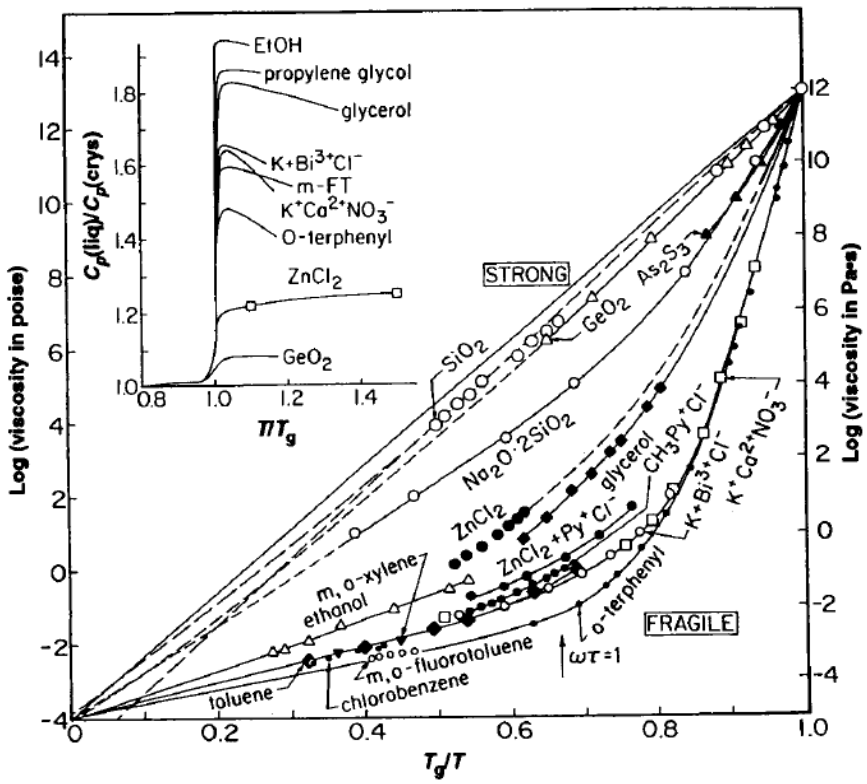

Fig 2.3 Temperature dependence (using T_g as normalizing parameter) of viscosity logarithm for several glass-forming liquids. Reproduced from [Angell 1995].

In any case, this strong-fragile pattern is widely used to characterize the fragility of liquids or, in other words, to separate out those glass-formers having, respectively, stronger and weaker T_g/T-dependence on log η. One way to quantify the overall T_g/T-dependence of log (η) or log (τ) of glass formers is the so-called

fragility or steepness index m, that is defined as the slope of the fragility plot $\log_{10}\langle\tau\rangle$ versus T_g/T evaluated at T_g [Angell 2006].

$$m = \left(\frac{d \log_{10}\langle\tau\rangle}{dT_g / T} \right)_{T=T_g} \tag{2.9}$$

The fragility index m is usually considered as an essential characteristic of the kinetic and relaxational behavior of undercooled liquids. Several proposals or models have been introduced in the literature to correlate the kinetic properties of undercooled liquids with their thermodynamic behavior around the glass transition.

Still, one of the main problems to be solved in the physics of glass-forming liquids is to fully understand this abrupt *dynamic arrest* (i.e., a steep increase in the relaxation time τ) observed, especially in fragile glass-formers, approaching T_g from above, and the corresponding divergence of τ at a finite temperature T_{VF} as predicted by the VFT law.

2.1.3 The Kauzmann paradox and the ideal glass

Near the melting point the liquid entropy is larger than the crystalline entropy. However, when supercooling the liquid below the melting point, in absence of crystal nucleation, the liquid entropy is found to decrease with decreasing temperature much more rapidly than the crystalline entropy does. There is therefore a temperature T_K at which a crossover between the two (extrapolated) entropies occurs, and the liquid entropy would become lower than the crystalline entropy. This is the so-called Kauzmann paradox.

Figure 2.4 shows the temperature dependence of the entropy difference (ΔS) between several supercooled liquids and their corresponding crystals, as was described by Kauzmann in 1948 [Kauzmann 1948]. By extrapolating the measured curves of the supercooled liquids, the excess entropy ΔS is going to vanish in most cases at a finite temperature, which is usually called the Kauzmann temperature T_K or the "ideal glass transition" temperature. Obviously, the glass transition temperature T_g cannot fall below T_K without violating the basic laws of Thermodynamics, since the configurational entropy of the liquid would be lower (i.e. negative) than the null configurational entropy of the fully-

ordered crystal, assuming very similar vibrational contributions for crystals and glasses. Nevertheless, from Fig. 2.4 one would expect that by conducting slower and slower cooling rates and hence decreasing the experimental T_g, it could be possible to achieve such a disordered state with negative entropy! This is the so-called Kauzmann paradox or "entropy crisis" that is still a vivid matter of discussion. In brief, the central question that any proper theory of the glass transition should be answered is: Why this thermodynamic "entropy crisis" is systematically avoided by a kinetic process (the dramatic increasing viscosity at T_g and the corresponding departure from the supercooled-liquid equilibrium curve)?

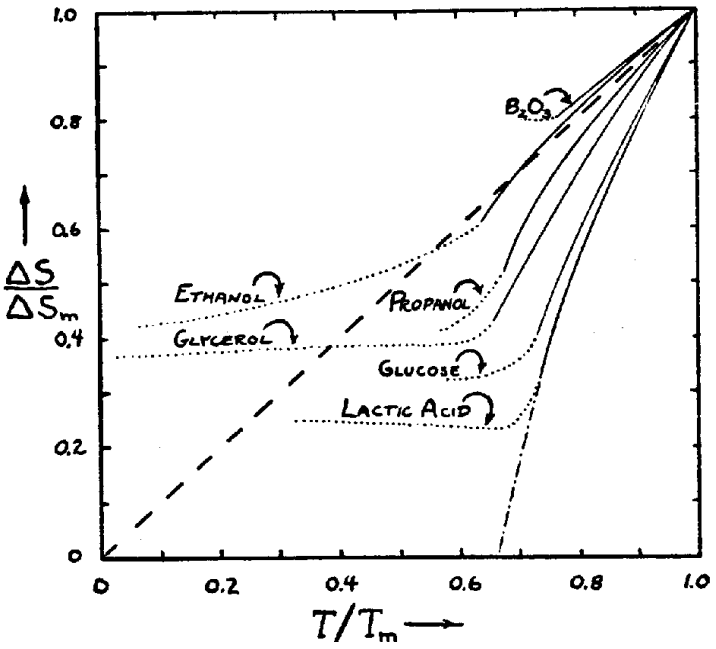

Fig 2.4 Temperature dependence of the entropy difference between several supercooled liquids and their stable crystal, normalized by their value at the melting point [Kauzmann 1948]. Solid lines are the obtained values in the supercooled liquid state above T_g, dotted lines are in the glassy state below T_g.

Since the Kauzmann temperature is the temperature at which the configurational entropy of the liquid becomes zero, some theoreticians have proposed the existence of an underlying (ideal) second-order phase transition precisely occurring at T_K when the entropy would vanish. Unfortunately, this

ideal glass transition is never observed experimentally because the laboratory glass transition occurs before and hence $T_K < T_g$.

2.1.4 Theories and models

During the last century there has been (and still is) a considerable amount of research and efforts aiming to understand the glass transition phenomenon and the structural relaxation dynamics of supercooled liquids. Many different theories and models have been proposed to explain this phase transition, even though whether or not it is a genuine phase transition is a matter of debate and controversy! In this section we will briefly summarize some of the most relevant theories on the glass transition. For the interested reader and to extend these and other theories more in detail, an excellent and recent review can be found in [Cavagna 2009].

2.1.4.1 Free volume theory

The free volume theory [Cohen and Turnbull 1959] is among the firsts approaches developed and has its historical importance. The basic idea is that the liquid-glass transition is a macroscopic manifestation of changes occurring in the microscopic distribution of molecular *free volume*. The theory of free volume was originally developed for a fluid of hard spheres which simulates the liquid. The total volume of a liquid is supposed to be divided into the part "occupied" by the molecules V_{oc}, and the other part of volume in which the molecules are free to move permitting the diffusive motion, which is termed the "free volume".

In this model the free volume is independent of temperature and no local *free energy* is required to redistribute the free volume.

Free volume theory has also been applied to the problem of viscosity of liquids: The empirical Doolittle equation establishes a relation between the viscosity and the free volume

$$\eta = A \exp\left(\frac{B V_{oc}}{V_f} \right) \tag{2.10}$$

where A and B are constants.

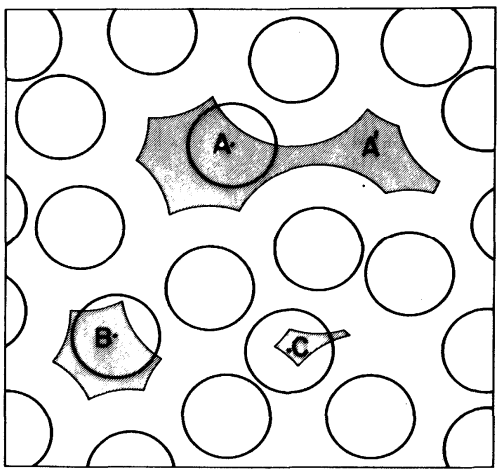

Fig 2.5 Visualization of the free-volume notion for a two-dimensional hard-sphere system. The shaded areas show the region accessible, in this configuration, to the centers of three molecules. Molecule A is capable of taking a diffusive step to a new position, while B and C are confined within small cages [Zallen 1983].

Later on, Cohen and Grest [Cohen and Grest 1979] extended the free volume theory. They used "percolation theory" to account for the exchange of free volume between nearest-neighbouring "liquid-like" cells and hence were able to study the thermodynamic behavior and the glass transition itself. Despite all their efforts and approximations, their theory always predicted a percolative first-order transition, too far from reality as to be considered seriously, in spite of being otherwise a theory relatively simple and conceptually appealing [Zallen 1983].

2.1.4.2 Adam-Gibbs theory

Adams and Gibbs proposed in 1965 a theory that establishes a link between the relaxation time in the supercooled liquid and the configurational entropy [Adam and Gibbs 1965]. The connection between entropy and glass transition is based on the concept of cooperative rearranging regions (CRR). According to the model the relaxation has its origin in cooperative rearrangements of groups of atoms or molecules, which size increases with decreasing temperature.

Molecular motions are thermally activated and the activation free energy is taken as the energy barrier of each molecule multiplied by the number of molecules that are necessary to form a CRR with a large enough size to have a transition from one configuration to another. If we consider a system of N particles and assume that it can be decomposed into CRR of size z, and if the configurational entropy of the whole system is S_c, the one of the subsystems is given by $s_c = z\ S_c/N$. Therefore, the kinetic relaxation time (and hence the viscosity) is directly related to the thermodynamic entropy [Elliott 1990]

$$\tau = \tau_0 \exp\left(\frac{B}{TS_c(T)}\right) \tag{2.11}$$

where η_0 and B are constants.

Furthermore, the vanishing of the configurational entropy leads to the divergence of the relaxation time. The temperature dependence of the configurational entropy can be obtained by integration of the difference of the specific heat of the liquid from its corresponding crystal

$$S_c = \int_{T_K}^{T} \frac{\Delta C_p}{T} dT \tag{2.12}$$

If we assume the approximation $\Delta C_p(T)=K/T$, then we obtain through eq. (2.12) the VFT expression:

$$\tau = \tau_0 \exp\left(\frac{BT_K}{K(T-T_K)}\right) \tag{2.13}$$

where the Kauzmann temperature T_K is now identical to the Vogel-Fulcher-Tammann temperature T_{VF} –see eq. (2.8)–, and $A=B/K$. It is found however that for certain materials the value of the Kauzmann temperature T_K is above the one of Vogel-Fulcher temperature [Binder and Kob 2005]. In addition, the nature of CRR is not defined in a precise way, and hence their size, the number of particles they contain (generally a few molecules at T_g), etc. Nevertheless, the main merit of the theory is thus to propose a connection between the relaxation dynamics of glass formers and their thermodynamic quantities.

2.1.4.3 Energy landscape

In 1969 Goldstein proposed a topographic viewpoint of condensed phases that is known as the energy landscape paradigm [Debenedetti 2001]. The landscape energy is the potential energy in the configurational space; it can be understood as a set of peaks, valleys, saddle points, and basins in three dimensions.

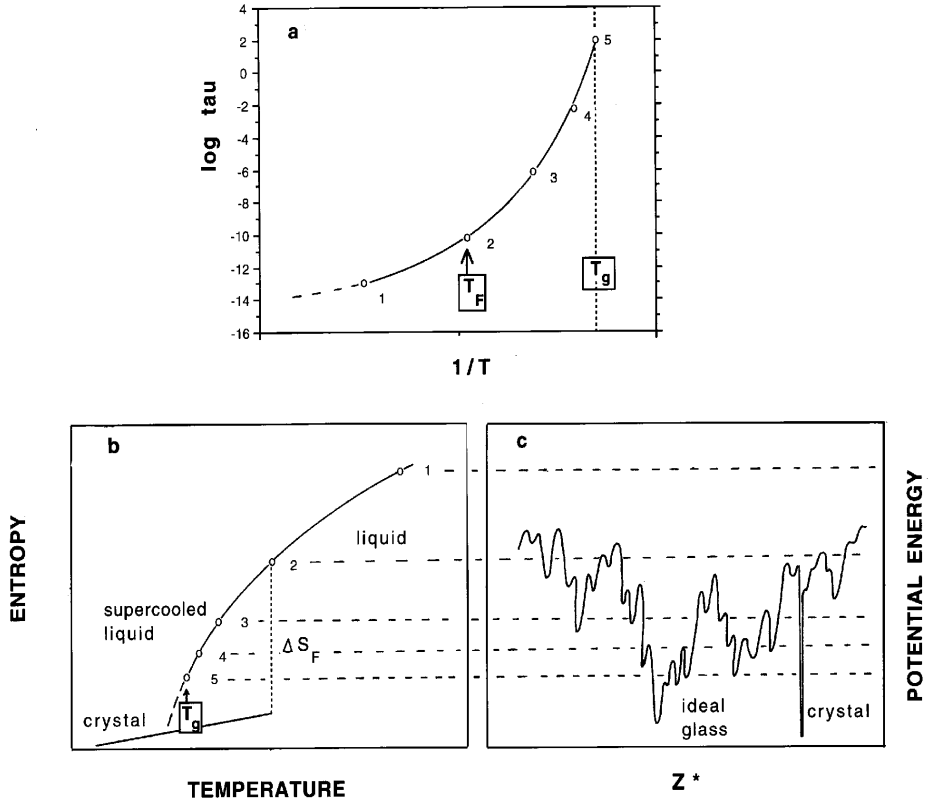

Fig 2.6 Illustration of the relation between relaxation time, entropy, and excitation level on the potential energy hypersurface for a fragile glassforming system [Angell 1997]. See details in the text.

The idea is that, a supercooled liquid explores the phase space mainly through activated jumps between different amorphous minima, separated by potential energy barriers [Cavagna 2009]. For a constant number of particles at a fixed volume V, the energy landscape is independent of temperature, although the

fraction of space that is statistically accessible decreases with decreasing temperature.

Figure 2.6 shows the relationship between the relaxation time, the entropy and the energy levels in the potential energy hypersurface. The point 1 is located in the liquid diffusive regime, at point 2 (the melting point of the material) the system starts to feel the landscape, and will be more affected as it approaches the point 5. With still some excess entropy, the system goes out of equilibrium being trapped in a minimum as a "glass". The ideal glass corresponds to the configuration that has energy within the lowest well except the crystal. This well would be the one that should be occupied at temperature T_K, if the supercooled liquid could be cooled slowly enough.

2.1.4.4 Mode coupling theory (MCT)

The mode coupling theory (MCT) was developed in order to describe the dynamics of liquids and dense gases. Here we will just discuss certain aspects of MCT that are of interest for the supercooled liquid and the glass transition [Leutheusser 1984, Bengtzelius 1984].

The core part of MCT is a nonlinear set of integro-differential equations for time-dependent correlation functions. The so-called mode coupling function $\Phi(q,t)$ is obtained by normalizing the intermediate scattering function $F(q,t)=\langle\delta\rho_q(t)\delta\rho^*_q(0)\rangle$ by the static structure factor $S_q=\langle\delta\rho_q\delta\rho^*_q\rangle$, where $\delta\rho_q(t)$ is fluctuation of the density for wave vector q at time t. After some transformations this may be closed to the single equation:

$$\frac{d^2}{dt^2}\phi_q(t)+\Omega_q^2\frac{d}{dt}\phi_q(t)+\int_0^t m_q(t-t')dt'\frac{d}{dt'}\phi_q(t')=0 \qquad (2.14)$$

Ω_q is the microscopic frequency that can be obtained from the static structure factor, and $m_q(t)$ is the memory function independent of time, but dependent on q.

Equation (2.14) can be derived and solved under certain approximations. These equations depend on temperature and density. It is found that for high temperature (or low densities), $\Phi(q,t)$ decays to zero in the long-time limit.

Accordingly there is a critical temperature, $T_c > T_g$, where the ergodicity is dynamically broken. The MCT describes the glass transition as a bifurcation from ergodic to non-ergodic behavior below a critical temperature T_c [Barrat 1990].

If the temperature of the liquid is lowered to T_g, the correlation function develops a plateau (see Fig. 2.7), and two time scales can be identified. Roughly speaking, we can say that there is a fast process describing the relaxation of the function to the plateau, and a slow process due to the decay of function from the plateau. Conventionally, these two processes are respectively called β (fast) and α (slow) relaxation.

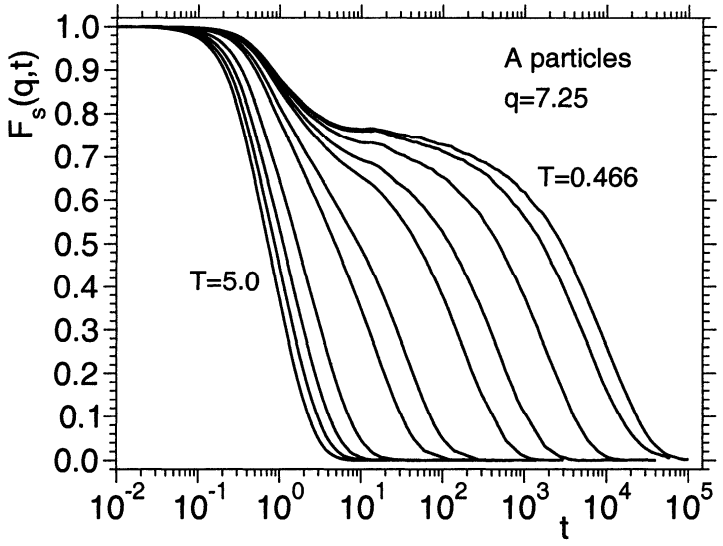

Figure 2.7 The dynamic correlation function in a Lennard-Jones system. In this case the function is the incoherent intermediate scattering function F_s *(q, t),* evaluated at the value of q where the static structure factor has the main peak. At high temperatures the decay is exponential, but when the temperature get close to T_g a plateau is formed and relaxation proceeds in two steps. Figure from [Kob 1995].

MCT predicts a critical temperature T_c at which relaxation times for density fluctuations diverge, without any singular behavior in the pair correlations, and the estimated critical temperature is usually located much (20%) above T_g. Therefore the glass-forming liquids are still able to relax, within observation

times at T_c, T_c being above T_g. Thus, the whole range of temperatures ($T_g \leq T \leq T_c$) is not covered by mode coupling predictions. The theory gives a good description of the dynamics of supercooled liquids above T_g, but not of the glass state [Kob 2005].

2.1.4.5 Random First Order Transition (RFOT) theory

Another promising approach is the so-called random first order transition (RFOT) or mosaic theory, developed by Wolynes and co-workers in a series of papers in the late 1980s. This theory is directly inspired by the phenomenology of p-spin models. They elaborated a theory, RFOT, in which the increase of a characteristic lenght-scale ξ_{RFOT} in the supercooled liquid is due to a decrease of configurational entropy [Kirkpatrick 1987, 1989].

To understand the dynamics of a supercooled liquid, we need a mechanism able to describe hopping between potential energy minima. This mechanism is given in RFOT by the same kind of local cooperative rearrangements described by Goldstein in 1969 (landscape energy) and by the Adam-Gibbs theory [Adam and Gibbs 1965]. What is new in the RFOT theory is the nature of the entropic force which drives these cooperative rearrangements and the existence of surface tension between different cooperative regions [Kirkpatrick 1989].

The main assumption of RFOT is that, at each temperature, the typical length-scale ζ_{RFOT} is given by the balance between free energy gain $\Delta F_{gain} = -TS_c(T)R^d$ and the surface cost $\Delta F_{cost} = YR^\theta$; $\theta \leq d-1$. Because the cooperative rearrangement happens independently of the position of other particles in the surroundings, there is generally an energy cost to be paid [Cavagna 2009], due to the mismatch at the interface between the rearranging region and the rest of the system. That is, a region of linear size R, in order to be rearranged, must overcome the free energy barrier

$$\Delta F = -TS_c(T)R^d + YR^\theta \tag{2.15}$$

The critical length-scale of the system follows from balancing of entropic gain $-TS_c(T)R^d$ and the surface cost YR^θ.

Within the RFOT, the length-scale $\xi \propto \left(1/S_c \right)^{\frac{1}{d-\theta}}$, whereas in Adams-Gibbs theory $\xi \propto \left(1/S_c \right)^{\frac{1}{d}}$.

This is the first time that surface tension is introduced in the context of supercooled liquids, and it also plays the very important role of determining the critical size of cooperative rearrangements.

Near T_K, configurational entropy vanishes linearly, $S_c \sim T - T_K$ [Kirkpatrick 1989]. This implies

$$\xi_{RFOT} = \left(\frac{1}{T - T_k} \right)^{\frac{1}{d-\theta}}, \tag{2.16}$$

whereas in Adams-Gibbs theory one has

$$\xi_{AG} = \left(\frac{1}{T - T_k} \right)^{\frac{1}{d}} \tag{2.17}$$

2.2 Low-temperatures properties of glasses

As introduced in chapter 1, glasses or amorphous solids exhibit universal properties at low temperatures which are very different from those of the crystalline solids [Zeller 1971, Phillips 1981]. Its origin remains, however, one of the major unsolved and debated problems of condensed matter physics, that is usually known as the universal behavior of glasses at low temperatures.

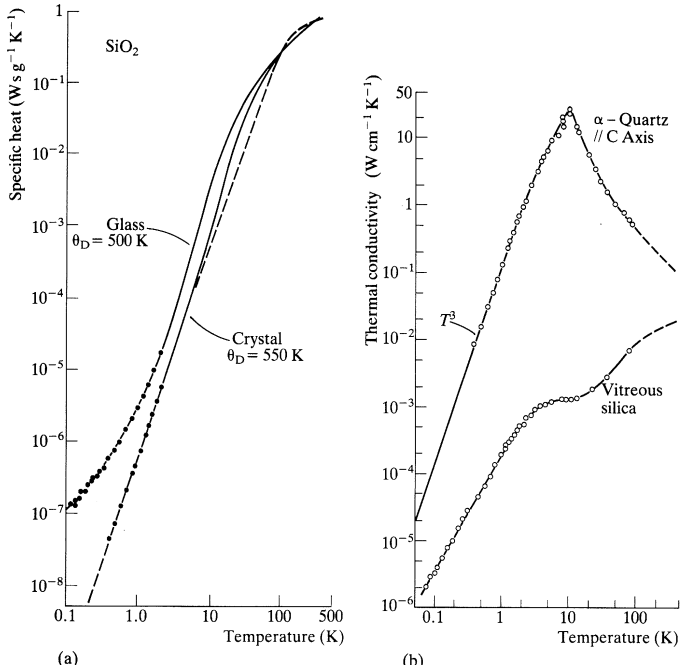

Fig 2.8 Specific heat (a) and thermal conductivity (b) of crystalline and amorphous phases of SiO_2 [Zeller 1971].

Figure 2.8 (a) shows the specific heat for crystalline and amorphous SiO_2 (vitreous silica) as a function of temperature. The specific heat of the quartz crystal coincides with T^3 law as predicted by the Debye model, while the specific heat in the amorphous SiO_2 is well above the one of its crystalline counterpart. This suggests that vitreous silica contains additional low energy excitations, which contribute significantly to heat capacity of amorphous solids.

Figure 2.8 (b) shows the thermal conductivity of quartz crystal and vitreous silica. The thermal conductivity of the amorphous material is much smaller than the one of its crystalline counterpart. The reduction of the thermal conductivity compared to crystalline materials indicates that glasses contain additional scattering mechanisms for phonons which are not present in crystalline materials [Zeller 1971].

In particular, below 1 K the specific heat follows a quasilinear dependence on T, and the thermal conductivity shows a T^2 dependence [Zeller 1971, Phillips 1981].

In summary, the specific heat of glasses strongly deviates from the expected $C_{\text{Debye}} \propto T^3$ dependence (due to the contribution of acoustic phonons). Furthermore, in the usual C_p/T^3 representation (Fig. 2.9) it exhibits a broad maximum, in contrast to the constant C_p/T^3 level observed in the crystal state. On the other hand, the thermal conductivity κ presents an ubiquitous plateau in the same range of temperatures.

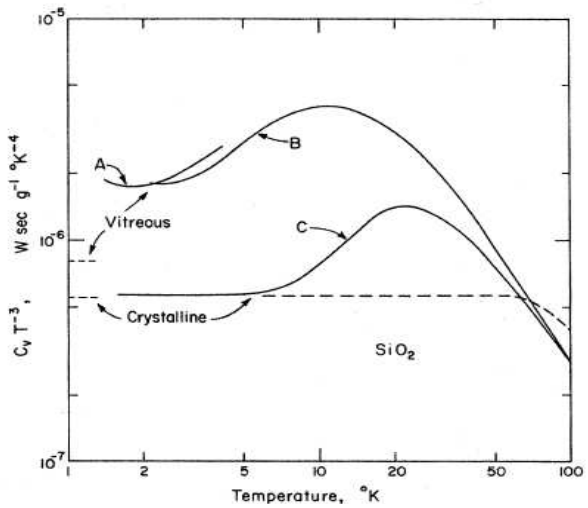

Fig 2.9 Specific heat of vitreous SiO_2 and crystal quartz, plotted as C_p/T^3 vs T [Zeller 1971].

This universal behavior of amorphous solids is not restricted to thermal properties. The elastic and dielectric behavior of amorphous solids at low temperature also differs completely from that of crystalline solids; the acoustic and dielectric absorption is strongly enhanced compared with crystals [Phillips 1981]. All these phenomena were attributed to the unknown excitations related to the amorphous solids.

This feature becomes even more striking when we consider the acoustic attenuation of lower frequency phonons, in the ultrasonic, sonic and even the subsonic frequency regime (from 10^9 Hz to 10^2 Hz). The technique used is wave attenuation, in which the quantity α, the inverse of the attenuation length l of the acoustic energy in the propagating wave, is measured. l is also called the phonon

mean free path, a physical quantity that can also be determined from thermal conductivity data.

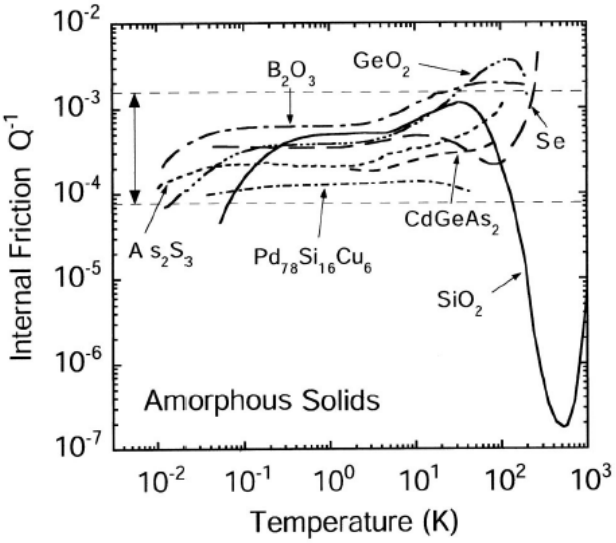

Fig 2.10 Acoustic attenuation, expressed as internal friction Q^{-1}, of seven different amorphous solids measured at different frequencies (from ~10^2 to 10^5 Hz), [Topp and Cahill 1996]. The double arrow marks the range observed on all amorphous solids studied to date [Pohl 2001].

Figure 2.10 contains a collection of internal friction data obtained from a variety of amorphous solids in a wide range of measuring frequencies. Above 10 K the internal friction is seen to depend on the material. Below 10 K, however, Q^{-1} is found to be independent of temperature, and within an order of magnitude also independent of the chemical composition of the amorphous solid, as had also been found in thermal conductivity [Pohl 2001].

Below 10 K all amorphous solids investigated (with the possible exception of Si and Ge) show very similar anomalous thermal and acoustical properties. This provides strong evidence that Debye-like phonons exist in glasses, and are scattered by additional excitations which can be represented most simply by two-level systems, or more generally by highly anharmonic oscillators [Phillips 1981].

Different models have been proposed to explain these universal properties exhibited by glasses or amorphous solids at low temperatures. As already said,

below 1 K the specific heat C_p depends approximately linearly on temperature T, and the thermal conductivity κ varies as T^2. This thermal behavior, as well as the abovementioned acoustic properties below 1 K, has been explained by the Tunneling Model [Anderson 1972, Phillips 1972], to be described in the next section. In contrast, there is not such a consensus for the rest of universal glassy properties above 1 K, and several very different approaches have been proposed. Among them, the phenomenological soft-potential model (SPM) [Parshin 1994, Ramos and Buchenau 1998] which can be regarded as an extension of the tunneling model (TM) [Phillips 1981], is one of the best accepted and most often considered, and hence we will describe it with a little more detail in section 2.2.2.

2.2.1 Tunneling Model

The phenomenological tunneling model (TM) [Anderson 1972, Phillips 1972] postulated the existence of atoms or small groups of atoms in amorphous solids which can tunnel between two configurations of very similar energy (two-level systems, TLS), in contrast to crystals, in which the atoms have a single energy minimum. At low temperatures these atoms cannot overcome the potential barrier between two minima via thermal excitation. But they can get to the other minimum through quantum mechanical tunneling.

In figure 2.11, the double-well potential consisting of two harmonic potentials separated by a potential barrier is depicted. V_B denotes the height of the barrier between the two minima. These minima of the single harmonic potentials will in general have a potential difference Δ called asymmetry energy, and d is the distance between the two wells along the generalized coordinate.

At low enough temperatures, only the two lowest energy levels will contribute significantly to thermodynamic quantities. The energy difference E between those two levels is given by

$$E = \sqrt{\Delta_0^2 + \Delta^2}\ , \tag{2.18}$$

where Δ_0 is the energy splitting arising from quantum mechanical tunneling through the potential barrier. Assuming two symmetric potentials separated by a high enough potential barrier V_B,

$$\Delta_0 = \hbar\Omega \exp^{-\lambda}, \tag{2.19}$$

where Ω is roughly the angular frequency of oscillation within one single well, and

$$\lambda = \frac{d}{\hbar}\sqrt{2mV_B} \quad , \tag{2.20}$$

where λ is the tunneling parameter and m is an effective mass of the particle moving in the double-well potential.

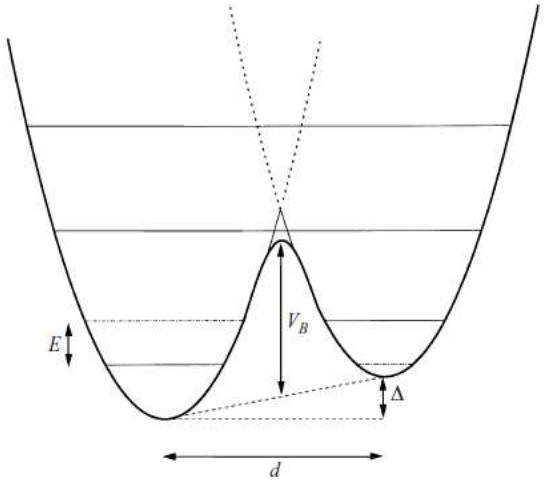

Fig 2.11 Schematic illustration of the double-well potential used in the TM, with its basic parameters. The two lowest energy levels, the asymmetry energy Δ, the distance d between the wells and the height of the potential barrier V_B.

In the standard tunneling model the tunneling parameter λ and the asymmetry energy Δ are assumed to be independent of each other having a uniform distribution function

$$P(\Delta, \lambda) = P_0 \tag{2.21}$$

The effect of the strain field ε_j induced by the elastic (sound) wave in the tunneling system is (neglecting possible small variations in Δ_0) to change the asymmetry Δ of the double-well potential by an amount characterized by a coupling constant

$$\gamma_j = \frac{1}{2}\frac{\partial \Delta}{\partial \varepsilon_j} \quad , \tag{2.22}$$

where $j=l,t$ stand for the longitudinal and transverse phonon branches, respectively.

Below 1 K the dominant process is the so-called one-phonon-process. In this process a transition is induced between the ground and the excited state including the emission or absorption of one thermal phonon. The energy of the phonons in this temperature range is comparable to the energy splitting of the tunneling systems. The calculation of the relaxation rate for the one-phonon-process gives [Phillips 1981]

$$\tau^{-1} = \left(\frac{\gamma_l^2}{v_l^5} + \frac{2\gamma_t^2}{v_t^5} \right) \frac{E^3}{2\pi\rho\hbar^4} u^2 \coth\left[E \big/ 2k_B T \right] \tag{2.23}$$

where v and ρ are respectively, the sound velocity and mass density of the material, respectively, and $u=E/\Delta_0$. From (2.23) one can see that the minimum relaxation time $\tau_{\min}$ occurs in the case of symmetric potentials ($\Delta=0$, $\Delta_0=E$).

To calculate the contribution of the tunneling states to the specific heat, it is often convenient to use as variables the energy difference E and the relaxation time τ. By making the Jacobian transformation, it is obtained that

$$g(E,\tau) = \frac{P_0}{2\tau(1-\tau_{\min}(E)/\tau)^{1/2}} \tag{2.24}$$

The free energy of a simple system of two levels is

$$F(E) = -k_B T \ln\left[\cosh(E/2k_B T)\right] \tag{2.25}$$

Taking into account that the specific heat at constant volume is given by $C_v = -T(\partial^2 F/\partial^2 T)_v$, and by integrating over all two-level systems

$$C_p = C_v = k_B \int_0^\infty n(E) \frac{(E/2k_B T)^2}{\cosh^2(E/2k_B T)} \tag{2.26}$$

By integrating (2.24) from $\tau_{\min}$ up to an experimental $t_{\exp}$ (time of the heat capacity measurement), one obtains [Phillips 1981] the density of states per unit volume in an energy interval as

$$n(E) = \frac{1}{2} P_0 \ln(4t_{\exp}/\tau_{\min}) \tag{2.27}$$

And by replacing it in (2.26), it is finally obtained

$$C_p \approx \frac{\pi}{12} P_0 k_B^2 T \ln(4t_{\exp}/\tau_{\min}) \,. \tag{2.28}$$

From (2.28) we can observe the quasilinear dependence for the specific heat on temperature with a small logarithmic increase with measuring time.

Although the terms tunneling states and two-level systems (TLS) are often used interchangeably, they do not mean always necessarily the same. The tunneling model (TM) is more general and assumes that in amorphous solids there is a continuous distribution of Δ_0 as well as of Δ. In some cases, the specific distribution of the chosen variables and the corresponding relaxation times are not very important, and the tunneling states can be replaced by an ensemble of two-level systems (TLS) only characterized by their energy E, and whose density can be considered as constant, $n(E) \approx n_{\mathrm{TLS}}$. In this simpler case:

$$C_p \approx C_v = \frac{\pi^2}{6} n_{TLS} k_B^2 T \tag{2.29}$$

Therefore, with the supposition that the density of tunneling states is independent of the energy, the temperature dependence is strictly linear, which is in good agreement with experiments.

The Tunneling Model is also able to explain the observed T^2 behavior of the thermal conductivity κ of amorphous solids at very low temperatures [Phillips 1981]. In general, the thermal conductivity can be expressed by

$$\kappa = \frac{1}{3} \int_0^{\omega_{Debye}} d\omega \sum_j C_{Debye,j}(\omega,T) v_j l_j(\omega) \tag{2.30}$$

where $C_{Debye,j}(\omega,T)\mathrm{d}\omega$ is the specific heat per unit volume contributed by longitudinal ($j=l$) and transverse ($j=t$) sound waves, and $l_j(\omega)$ is the mean free path for the corresponding acoustic phonons at the frequency ω.

At very low temperatures, the dominant process is the resonant scattering by tunneling states, and the inverse mean free path can be shown to be

$$l_{j,res}^{-1}(\omega) = \frac{\pi \gamma_j^2 \omega}{\rho v_j^3} P_0 \tanh\left(\frac{\hbar\omega}{2k_B T}\right) \tag{2.31}$$

Replacing (2.31) into (2.30) and integrating, one obtains

$$\kappa = \frac{\rho k_B^3}{6\pi\hbar^2}\left(\sum_j \frac{v_j}{P_0 \gamma_j^2}\right) T^2 \tag{2.32}$$

The thermal conductivity κ indeed shows a T^2 dependence, which is in very good agreement with experimental results at the lowest temperatures.

2.2.2 Soft Potential Model (SPM)

As mentioned before, the TM explains very good the behavior of the amorphous solids and agrees very well with the experimental data below 1 K, but does not explain the behavior of glasses or amorphous solids above 1 K, such as the broad maximum of the specific heat in the representation C_p/T^3 or the plateau in the thermal conductivity. One of the approaches most often used to explain and account for this behavior is the soft potential model (SPM). SPM was first proposed by Karpov, Klinger and Ignat'ev [Karpov et al 1982], and extended by Il'in, Karpov and Parshin [Il'in et al 1987], and further by Buchenau and co-workers [Buchenau 1992].

In the SPM, the potential of the soft modes is assumed to have a general form $V(x) = W\,(D_1\,x + D_2\,x^2 + x^4)$ [Ramos and Buchenau 1998], where x is any generalized spatial coordinate, and the energy W is the stabilizing fourth-order term assumed to be the same for all atomic potentials, and constitutes the basic parameter of the model. Each mode has its own first-order (asymmetry D_1) and second-order (restoring force D_2) terms, which can be either positive or negative, hence giving rise to a distribution of double-well potentials (TLS) and more or less harmonic single-well potentials (soft vibrations), as can be seen in Fig. 2.11. The Tunneling Model could therefore be regarded as a subpart of the SPM. The parameter W marks the crossover from the TLS-dominated region (minimum of specific heat in C_p/T^3) at the lowest temperatures to the soft-modes region above it. Similarly to the Tunneling Model, a random distribution of potentials is assumed in the SPM: $P(D_1, D_2) = P_s$.

In brief, very good agreement has been found between the SPM predictions and the experimental data (see [Parshin 1994] and [Ramos and Buchenau 1998] as reviews).

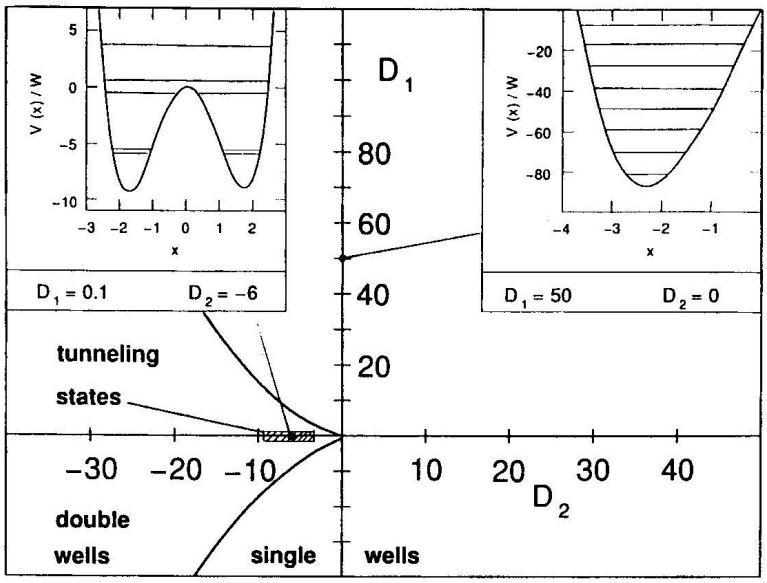

Fig 2.12: Single and double-well regions in the D_1-D_2 plane of the soft-potential model. Insets: Potentials and energy levels of a typical tunneling state (left) and of a typical vibrational state (right) [Ramos and Buchenau 1998].

Figure 2.12 shows the different single– and double–well regions of the potential in the D_1-D_2 plane. The insets in the figure show the potential shapes and the energy levels of a typical tunneling state (left) and of a typical vibrational state (right). Assuming modes with different D_1 and D_2 values at different places in the glass, one obtains a broad distribution of soft modes ranging from tunneling to vibrational states [Ramos and Buchenau 1998].

To calculate the total specific heat of a glass at low temperatures, within the SPM, one must add to the usual Debye contribution by the acoustic phonons

$$C_{Debye} = \frac{2\pi^2}{5}\left(\frac{k_B^4}{\hbar^3 \rho v_D^3}\right) T^3 \tag{2.33}$$

where v_D is the Debye-averaged sound velocity $1/v_D^3 = 1/3\ (1/v_L^3 + 2/v_T^3)$, the contribution by all the relevant low-energy excitations present in those single– and double–well *soft potentials* that coexist with usual lattice vibrations (phonons), and following the assumed distribution $P(D_1, D_2) = P_s$.

As said above, the analytical description of the tunneling states within the SPM can be mostly taken from the tunneling model. Hence, to calculate the distribution function $P(\Delta, \lambda)$ in the SPM, we need expressions for Δ and λ as a function of D_1 and D_2. According to the SPM, it is found [Ramos and Buchenau 1998] approximately that

$$\Delta_0 = W|D_2|^{3/2} \exp\left(1 - \frac{\sqrt{2}}{3}|D_2|^{3/2}\right) \tag{2.34}$$

$$\Delta = WD_1\sqrt{2(|D_2| - 1)} \tag{2.35}$$

From these equations and making use of (2.18) and the dimensionless parameter $u=E/\Delta_0$, the density of tunnelling states is found approximately to be

$$P(E,u) \approx \left(\frac{2}{9}\right)^{1/3} \frac{P_s}{W} \frac{1}{u\sqrt{1-u^2}} \ln^{-2/3}(40W/Eu) \tag{2.36}$$

The specific heat of these two level systems is thus approximately

$$C_{p,TLS}(T) \approx \frac{\pi^2}{6}\left(\frac{1}{9}\right)^{1/2} \frac{P_s}{W} k_B^2 T \ln^{1/3}\left(\frac{t_{\exp}}{\tau_{\min}(k_B T)}\right) \tag{2.37}$$

On the other hand, the density of quasi-harmonic *soft* vibrational states was found to be [Ramos and Buchenau 1998]

$$g_s(h\nu) = \frac{1}{8}\frac{P_s}{W}\left(\frac{h\nu}{W}\right)^4 \tag{2.38}$$

Since the heat capacity of a single harmonic oscillator is given by

$$C_h(x) = k_B \frac{x^2 e^{-x}}{(1-e^{-x})^2} \tag{2.39}$$

where $x = \dfrac{\hbar\omega}{k_B T}$, then the contribution of quasi-harmonic soft vibrations to the specific heat can be evaluated by

$$C_{p,s} = \int_0^\infty d\nu g(\nu) C_h(x) \tag{2.40}$$

and hence

$$C_{p,SPM} = \frac{2\pi^6}{21} P_s k_B \left(\frac{k_B T}{W}\right)^5 \tag{2.41}$$

In summary, within the SPM the total contribution to the specific heat at low temperature is given by

$$C_p = C_{TLS}\,T + C_D\,T^3 + C_{sm}\,T^5 \tag{2.42}$$

where the different terms correspond to the contributions of the two level systems (2.37), Debye lattice vibrations (2.33) and soft quasiharmonic modes (2.41), respectively.

Now, we will summarize the main SPM predictions for the low-temperature thermal conductivity of glasses. According to the soft potential model [Buchenau 1992], the inverse phonon mean-free-path can be subdivided into three components describing sound-wave resonant scattering by tunneling states and quasilocalized low-frequency vibrations, as well as by classical relaxation processes [Buchenau 1992, Ramos and Buchenau 1998]

$$l_j^{-1} = l_{res,tunn}^{-1} + l_{rel,class}^{-1} + l_{res,vib}^{-1} \tag{2.43}$$

First, the mean free path for the resonant scattering by the tunneling states is given by

$$l_{rel,tunn}^{-1} = \frac{\pi\omega C_j^{tunn}}{v}\tanh\left[\frac{\hbar\omega}{2k_BT}\right] \tag{2.44}$$

where j stands for l and t in the longitudinal or transverse case, respectively, and $C_j^{tunn} = P_0\gamma_j^2 \big/ \rho v_j^2$

Secondly, the mean free path of the sound waves under the influence of classical relaxation processes is

$$l_{rel,class}^{-1} = \frac{\pi\omega C_j}{v_j}\left(\frac{k_BT}{W}\right)^{3/4}\ln^{-1/4}(1/\omega\tau_0) \tag{2.45}$$

where $C_j = P_0\gamma_j^2 \big/ W\rho v_j^2$

Finally, the third part due to the quasilocalized low-frequency vibrations follows the relation

$$l_{res,vib}^{-1} = \frac{\pi\omega C_j}{v_j}\frac{1}{8}\left(\frac{\hbar\omega}{W}\right)^3 \tag{2.46}$$

By using the Debye approximation for the density of states of the sound waves transporting heat, and making use of the expression (2.30) of the thermal conductivity and of (2.39), it is obtained

$$\kappa = \frac{1}{6\pi^2}\int_0^\infty d\omega\omega^2 C_h(x)\left(\frac{l_l}{v_l^2}+\frac{2l_t}{v_t^2}\right) \tag{2.47}$$

And now by inserting the three corresponding equations of the different contributions to the mean free path in (2.43) and then in (2.47), and replacing the variable ω by x and the temperature T by the dimensionless variable $z = \frac{k_B T}{W}$, the thermal conductivity is found to follow the general equation:

$$\kappa = \frac{2k_B}{3\pi}\left(\frac{W}{h}\right)^2\left(\frac{1}{C_l v_l}+\frac{2}{C_t v_t}\right)F(z) \tag{2.48}$$

with

$$F(z) = \int_0^\infty dx \frac{x^3 e^{-x}}{(1-e^{-x})^2}\frac{z^2}{1.1\tanh(x/2)+0.7z^{3/4}+x^3 z^3/8} \ . \tag{2.49}$$

The function $F(z)$ depends only on the normalized temperature $z = k_B T/W$, when $z \le k_B T/4W$. Moreover, $F(z)$ can be approximated [Ramos and Buchenau 1998] as

$$F(z) = \frac{9z^2}{1.1+0.7z+3z^2} \tag{2.50}$$

And by defining an average $\overline{C}$ over C_l and C_t

$$\overline{C} = \frac{1/v_l + 2/v_t}{1/C_l v_l + 2/C_t v_t} \tag{2.51}$$

the thermal conductivity κ becomes

$$\kappa = \frac{6k_B}{\pi\overline{C}}\left(\frac{W}{h}\right)^2\left(\frac{1}{v_l}+\frac{2}{v_t}\right)\frac{z^2}{1.1+0.7z+3z^2} \ . \tag{2.52}$$

The soft potential model therefore provides a quantitative description [Ramos and Buchenau 1998] of the low-temperature specific heat and thermal conductivity of glasses, as well as of other low-temperature and/or low-frequency properties of glasses, so that we will later apply this model to discuss and interpret our experimental results in chapter 5.

References

[Adam and Gibbs 1965]: G. Adam and J. H. Gibbs. J. Chem. Phys., 43, 139, (1965).

[Anderson 1972]: P.W. Anderson, B. I. Halperin, and C. M. Varna, Phil. Mag. 25, 1 (1972).

[Angell 1976]: C. A. Angell and H. Kanno, Science 193, 1121 (1976).

[Angell 1997]: C. A. Angell, J. Res. Natl. Inst. Stand. Technol. 102, 171 (1997).

[Angell 1995]: C. A. Angell, Science 267, 1924 (1995).

[Barrat 1990]: J.-L. Barratt and A. Latz, Condens. Matter 2, 4289 (1990).

[Bengtzelius 1984]: U Bengtzelius, W Gotze and A Sjolander J. Phys. C: Solid State Phys. 17 5915 (1984).

[Binder and Kob 2005]: Kurt Binder and Walter Kob. *Glassy Materials and Disordered Solids,* World Scientific Publishing (2005).

[Buchenau 1992]: U. Buchenau, Yu. M. Galperin, V. L. Gurevich, D. A. Parshin, M. A. Ramos, and H. R. Schober, Phys. Rev. B46, 2798 (1992).

[Cavagna 2009]: A. Cavagna. *"Supercooled liquids for pedestrians".* Physics Reports 476, 51 (2009).

[Cohen and Grest 1979]: M. H. Cohen and G. S. Grest. Phys. Rev. B. 20 1077 (1979).

[Cohen and Turnbull 1959]: M. H. Cohen and D. Turnbull, J. Chem. Phys. 31, 1164 (1959).

[Debenedetti 2001]: P. G. Debenedetti and F. H. Stillinger. Nature 410, 259 (2001)

[Elliott 1990]: S. R. Elliott, *Physics of Amorphous Materials*, 2nd ed. (Longman, 1990).

[Gutzow 1995]: I. Gutzow and J. Schmelzer, *The Vitreous State*, (Springer, Berlin, 1995).

[Il'in et al 1987]: M. A. Il'in, V. G. Karpov and D. A. Parshin, Zh. Eksp. Teor. Fiz. 92, 291 (1987).

[Karpov et al 1982]: V. G. Karpov, M. I. Klinger, and F. Ignat'ev, Solid State Commun. 44, 333 (1982).

[Kauzmann 1948]: W.Kauzmann, Chem. Rev. 43, 219 (1948).

[Kirkpatrick 1987]: T. R. Kirkpatrick, and P. G. Wolynes, Phys. Rev. A 35, 3072 (1987); T. R. Kirkpatrick, and D. Thirumalai, Phys. Rev. Lett. 58, 2091 (1987); T. R. Kirkpatrick, and P. G. Wolynes, Phys. Rev. B 36, 8552 (1987).

[Kirkpatrick 1989]: T. R. Kirkpatrick, D. Thirumalai, and P. G. Wolynes, Phys. Rev. A 40, 1045 (1989).

[Kob 1995]: W. Kob and H. C. Andersen. Phys. Rev. E, 52, 4134, (1995).

[Leutheusser 1984]: E Leutheusser Phys. Rev. A 29, 2765 (1984).

[Parshin 1994]: D. A. Parshin. Solid State 36, 991, (1994).

[Phillips 1972]: W. A. Phillips, J. Low Temp. Phys. **7**, 351 (1972).

[Phillips 1981]: W. A. Phillips (ed.), *Amorphous Solids: Low Temperature Properties* (Topics in Current Physics, Vol. 24, Springer, 1981).

[Pohl 2001]: R.O. Pohl, X. Liu, and E. Thompson. Reviews of Modern Physics, 74, 991, (2002).

[Ramos and Buchenau 1998]: M. A. Ramos and U. Buchenau, *Tunneling Systems in Amorphous and Crystalline Solids*, ed. by P. Esquinazi (Springer, Berlin, 1998).

[Topp and Cahill 1996]: K. A. Topp, D. G. Cahill. Z. Phys. B. 101, 235 (1996).

[Zallen 1983]: R. Zallen, *The Physics of Amorphous Solids*, (Wiley, 1983).

[Zeller and Pohl 1971]: R. C. Zeller and R. O. Pohl, Phys. Rev. B 4, 2029 (1971).

3 Experimental

Most heat capacity measurements at low temperatures have been made with the quasi-adiabatic calorimeters, developed by Gaede [Gaede 1902], and especially by Nernst and Eucken 1910 [Nernst 1910, Eucken 1909], shortly after the first successful production of liquid ^{4}He in 1908. Considerable advances in the production and measurement of low temperatures were realized, since the development of the very sensitive phosphor-bronze thermometer by Keesom and Van den Ende [Keesom 1932]. The application of liquid ^{4}He and ^{3}He for the production of low temperatures, and the discovery of adiabatic demagnetization [Giauque 1933] as a means to reach very low temperatures, were a big step in the field of cryogenic applications.

In spite of this progress, the experimental methods have been continuously improved and are still improving. The technical difficulties arising in low temperature calorimetry is the drastic decrease in thermal energy. On the cooling from room temperature to liquid helium temperatures the specific heat of any material decreases by three to four orders of magnitude, and becomes extremely small at absolute zero. The small heat capacity of solids at liquid helium, and at lower temperatures, creates difficulties, because of the influence of the surroundings, for example vibration, that can lead to significant errors in the determination of the heat capacity [Barron 1999].

Therefore, measurements of the heat capacity of solids at low temperatures have always been a challenging task, but they are of major interest since the specific heat is one of the most valuable thermodynamical quantities to be considered when studying liquids or solids [Gmelin 1987], and for the relevant information to check theories and models, as well as about the thermodynamic properties and its phase transitions.

3.1 Experimental system

The experimental set-up consists in a glass cryostat used with liquid helium or liquid nitrogen depending on the temperature range wanted, with a double chamber insert to allow an independent thermal control, within a high vacuum environment reaching between 10^{-7} and 10^{-8} mbar at low temperatures (after have beginning the vacuum operation at ambient temperatures). To decrease the temperature from 4.2 to 1.6 K, it is done simply by pumping over the helium bath (see Fig 3.1 (a)).

A programmable current source and a micro-voltmeter (Keithley) are used to supply and determine the exact power applied to the sample. Another pair of these apparatus is used for the thermometer. A programmable controller (DRC-91 CA Lake Shore) is used to monitor and control the temperature of the thermal sink (inner chamber) via the electrical heater and a silicon diode as thermal sensor. An automatized calorimetric program allows us to control and communicate with these different instrumentations.

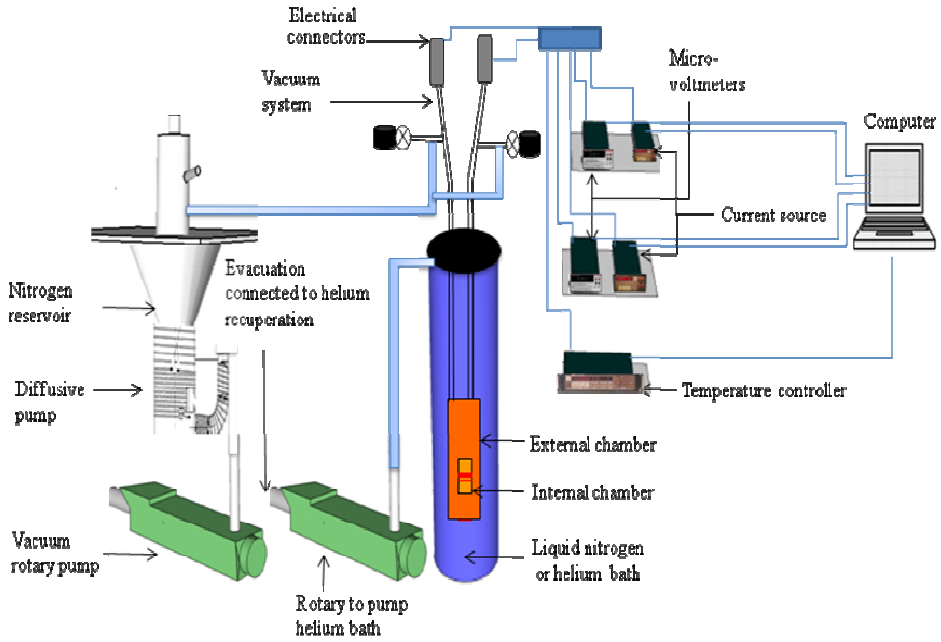

Fig 3.1 (a) Schematic illustration of the experimental system.

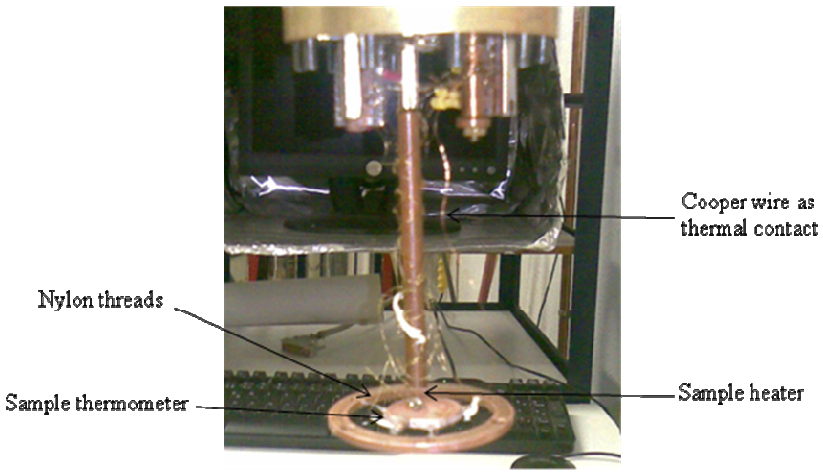

Fig 3.1 (b) photo of the calorimetric cell suspended from the circular support (ring) by nylon threads.

3.2 Calorimetric cells

The major problem when performing experiments with these materials is that they are in liquid phase at room temperature. This impedes using standard calorimetric cells for measuring the specific heat. With the aim of measuring the specific heat of the samples with sufficient precision, adequate cells are required.

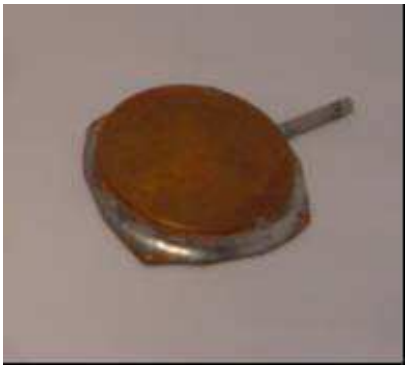

Fig 3.2 the calorimetric cell.

Thus, it is necessary to optimize the amount of alcohol sample against the mass of copper in the cell. The empty cell is of copper and has a typical mass m=1.5 g, and very thin walls (see fig 3.2), and can hold ~ 0.6 g of alcohol sample (or any liquid). A carbon ceramic sensor (CCS) is used as thermometer, which is attached onto the lower surface of the cell. One resistor of 1kΩ used as heater and a pure-copper wire used as thermal contact (chosen as to have relaxation time ~ 10^2 s in the relevant temperature range) to control the thermal equilibrium are glued on the upper surface of the calorimetric cell. Then the sample is suspended by nylon threads as shown in Fig. 3.1 (b). All the wires of connections for thermometers and heaters were anchored in a copper block having a good contact with the walls of the cold reservoir, to ensure that contribution of the heat by wires is minimal.

On the other hand, to prepare quenched glasses or avoid crystallizations by fast cooling (quenching), with this experimental system and by using these cells, maximum cooling rates attainable in the transformation range of typical molecular glass-forming liquids (~100 K), are around -20 K/min, whereas there is no limitation to conduct cooling or heating processes as slow as desired.

3.3 Materials and preparation of the samples

High purity samples of the different butanol position isomers were used: 463 mg of 1-butanol (n-butanol) $CH_3CH_2CH_2CH_2OH$ (99.8% pure), 564 mg of its isomer 2-butanol (sec-butanol) $H_3CH_2CH(OH)CH_3$ (99.5% pure), 531 mg of its isomer isobutanol $CH_3CH_2CH_2CH_2OH$ (99.5% pure) and 479 mg of its last isomer tert-butanol or 2-methyl-2-propanol $CH_4H_{10}O$ (99.5% pure). They were purchased from Sigma Aldrich. Immediately upon them receipt under standardized conditions, they were stored in a dry glove box, and then used without further purification. Then, liquid samples were introduced by clean syringes into the cleaned cells and sealed mechanically. This operation is realized into the dry glove box to avoid contact with air moisture.

In Fig. 3.3, we show the structure of the butanol molecule and the position of the hydroxyl group responsible for the hydrogen bonding in the solid state, that are significantly different in each case.

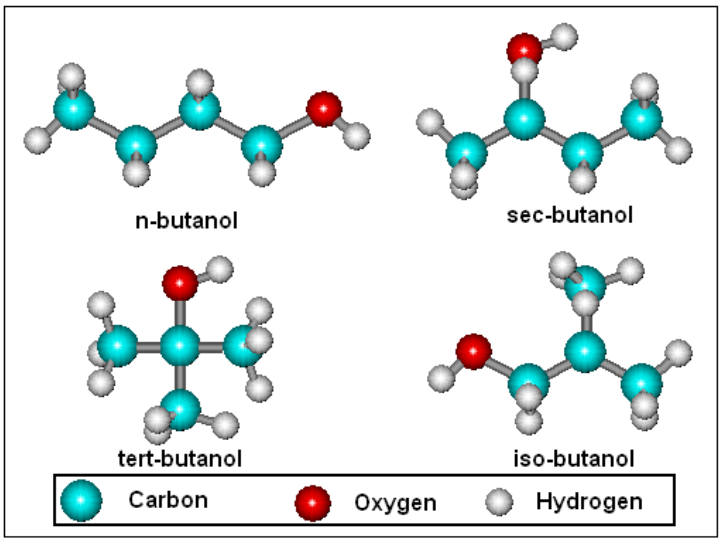

Fig 3.3 Schematic molecular structure of the four different position isomers of butanol. Note the different position of the hydroxyl group within the butanol molecular chain in each case.

Before filling the cells with liquid, these were subjected to several processes of cleaning: We immerse them in acid nitric bath to clean the impurities of the welds, and then eliminate the acid by warming the cells. After this, we immerse them in acetone bath and then heated again. Finally, they are subjected to the last bath with the sample that will be measured. Once this cleaning cycle is realized, we introduce the cells during some time into an oven at 70 °C to evaporate any residues. And then, they are kept in the glove box.

Once the cells were filled with liquid and the seal was made, we must check that there is no leak. For that, we do a dynamic vacuum using the diffusive pump by pumping over the cell. A smallest leak can be easily detected in the diffusive pump, knowing that the alcohols have height volatility or by comparison of the weight of the cell before and after this dynamic vacuum operation. We also point out that, after each measurement run the cell is weighed and compared to its weight before being measured. By doing so, we have the guarantee that the specific heat measured is truly the one of the mass considered. It is also important to completely fill the cells, to ensure that there are not important thermal inhomogeneities, and hence having a good thermal equilibrium.

3.4 Experimental methods of calorimetry

Heat capacity of materials as a function of temperature is a source of important information concerning their molecular structure.

In the calorimetric specific heat experiments realized in this work, we have used two different measurement techniques, depending on the required temperature range. To measure the specific heat at low temperatures we use two alternative relaxation methods, and to characterize and measure the specific heat of different phases at intermediate temperatures, we use a quasiadiabatic continuous method.

The principle of the heat capacity measurement is to record the temperature rise of the sample upon supplying a known amount of energy. Let us remembering the classical definition of the specific heat $C_p, C_p(T) = \lim_{\Delta T \to 0} (Q/\Delta T)_P / M$ where Q is a heat energy input "pulse" that causes a small temperature rise ΔT in a specimen of mass M. In the next subsections, we will describe the most relevant calorimetric methods typically employed to measure the heat capacity in the laboratory.

3.4.1 Adiabatic method

The most simple and best known method to measure heat capacity is the adiabatic (or Nernst) method [Gmelin 1987, Nernst 1910]. Although we will not make use of the adiabatic method in this thesis, we will briefly describe it, due to its significance as basic reference.

In an ideal adiabatic system the power applied to the calorimetric cell P_{heat} is proportional to the temperature increase via:

$$P_{heat} = C_p(T)\frac{dT}{dt} \tag{3.1}$$

Experimentally the heat pulse is applied by a heater (Joule effect) during time *t,* and the temperature is measured by the thermometer, the power $P_{heat} = V_h I_h$ where V_h and I_h are the drop in the heating resistive element, and the electric current flowing through it.

$$C_p(T)\frac{dT}{dt} = V_h I_h \tag{3.2}$$

Hence the heat capacity is directly obtained by applying heat pulses $Q=V_h I_h \Delta t$ and measuring the produced increase of temperature $\Delta T= (T_f - T_i)$, from which C_p is obtained at the temperature T_m, which is the midpoint of the temperature increment,

$$C_p(T_m) = \frac{Q}{\Delta T} = \frac{V_h I_h \Delta t}{T_f - T_i} \tag{3.3}$$

In practice, the excellent thermal isolation and the minimization of stray heat leaks, and also the long measuring times to achieve specific heat data, makes the adiabatic method inapplicable in many cases. This has led to the development of several other calorimetric techniques, such as relaxation calorimetry, AC-temperature calorimetry or diffusive heat pulse calorimetry [Barron 1999].

3.4.2 Relaxation methods

In addition to those difficulties or convenience of use, the adiabatic method is appropriate for measurements in which the internal relaxation time t_i of the sample is sufficiently small ($t_i << \tau$). When employing the adiabatic method, it is also recommended to use cells of a relatively high mass, but this has its energy and time cost to cool the system to very low temperatures.

So, in contrast to the adiabatic method, in the thermal relaxations methods [Bachmann 1972], the sample holder is connected to the temperature-controlled thermal reservoir through a wire (cooper in our case) as a thermal link.

The simplified form of the heat conduction equation relates a constant heating power P ($P = V_h I_h$), with the variation of energy in the cell and the energy losses through the thermal contact:

$$P = C_p(T)\frac{dT}{dt} + \int_{T_0}^{T_1} K_H(T)dT \tag{3.4}$$

where we assume that the main energy loss occurs through the contact wire. If the heat capacity of the cell, C_p, is nearly constant for small temperature changes,

and the thermal conductance of the wire, K_H, is either linear or nearly constant between T_0 and T_1, eq (3.4) becomes

$$P = C_p(T)\frac{dT}{dt} + K_H \Delta \mathrm{T} \tag{3.5}$$

The solution for this linear differential equation is:

$$\Delta t = \frac{P}{K_H}\left[1 - \exp\left(-\frac{t}{\tau}\right)\right]; \qquad \tau = \frac{C_p}{K_H} \tag{3.6}$$

When the relaxation time τ is much larger than the typical time of the experiment, $\tau >> \tau_{exp}$, the solution becomes the usual adiabatic case (see eq. (3.3))

$$\Delta T \approx \frac{P}{K_H}\left[1 - \left(1 - \frac{t}{\tau}\right)\right] = \frac{P}{C_p}t \Rightarrow C_p = \frac{P\Delta t}{\Delta T} \tag{3.7}$$

where Δt is the fixed time for heating the cell at power P. In this adiabatic solution, the temperature remains constant when no power is applied (quasi-adiabatic case). The increase in temperature remains constant: $\Delta T_\infty = P/K_H$. When the heating power is switched off, the temperature T of the cell decay exponentially with the time t:

$$T(t) = T_0(t) + \Delta T_\infty \exp\left(-\frac{t}{\tau}\right) \tag{3.8}$$

The linear fitting of the exponential decay in a semi-log plot (fig 3.4 relaxation part) gives the time constant τ, the thermal conductance parameter is directly $K_H = P/\Delta T_\infty$, and hence the value of heat capacity is obtained

$$C_p = K_H \tau \tag{3.9}$$

When the relaxations times to equilibrium are getting larger (typically with increasing temperature), an alternative non-standard relaxation method can be used. In this "faster" relaxation method [Perez-Enciso 2007] we replace the long time of heating by a shorter time of heating without waiting until the steady-state thermal equilibrium has been reached. So, ΔT_∞; is not measured directly, but determined from a linear fit of the heating curve (3.6), and after having determined the relaxation time τ form the cooling-curve fit, by simply making a variable change $\delta = [1 - \exp(-t/\tau)]$, we obtain $\Delta T = (P/K_H)\,\delta$. Thus, a simple least-squares linear fit provides the parameter K_H, and the heat capacity is obtained again from equation (3.9).

In figure 3.4, and 3.5, we present an example of real experimental points obtained for isobutanol using the two different methods, the standard relaxation method (let us call it relaxation I), and the alternative non-standard relaxation method (let us call it relaxation II), at the same temperature 10 K where the time begins to be too long.

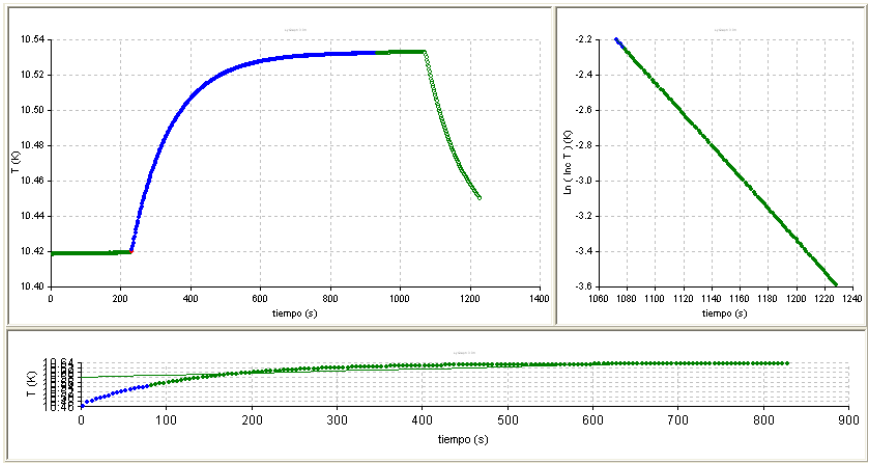

Fig 3.4 Example of a real experimental point (direct capture from screen) obtained for isobutanol using the standard relaxation method (relaxation I).

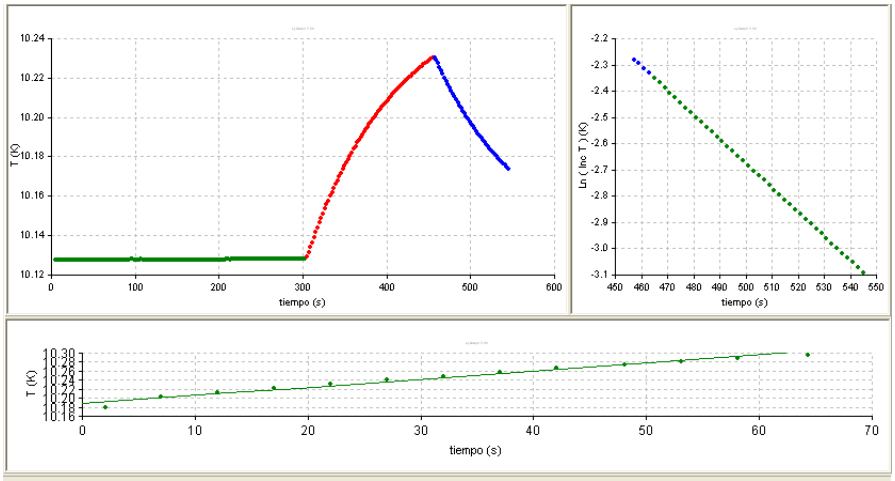

Fig 3.5 Example of a real experimental point (direct capture from screen) obtained for isobutanol using the non-standard relaxation method (relaxation II).

3.4.3 Quasi-adiabatic continuous method

For measurements above 77 K we have used a quasi-adiabatic continuous method. This method provides a continuous data recording of the heat capacity as shown in figure 3.6, and the advantage of simplicity of use. As disadvantage this classical continuous method, have not a good precision because it application need an ideal adiabatic case).

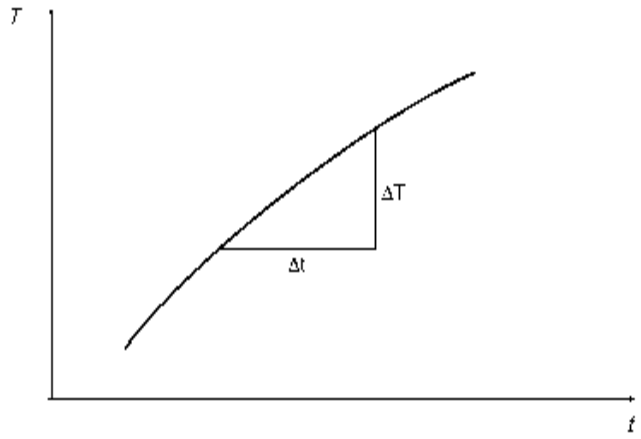

Fig 3.6 Schematic illustration of the continuous method

However, in laboratory was developed one variant more precise for the realistic case "quasi-adiabatic" [Perez-Enciso 2007]. The method was developed especially to measure the heat capacity, and characterize calorimetrically the different prepared phases.

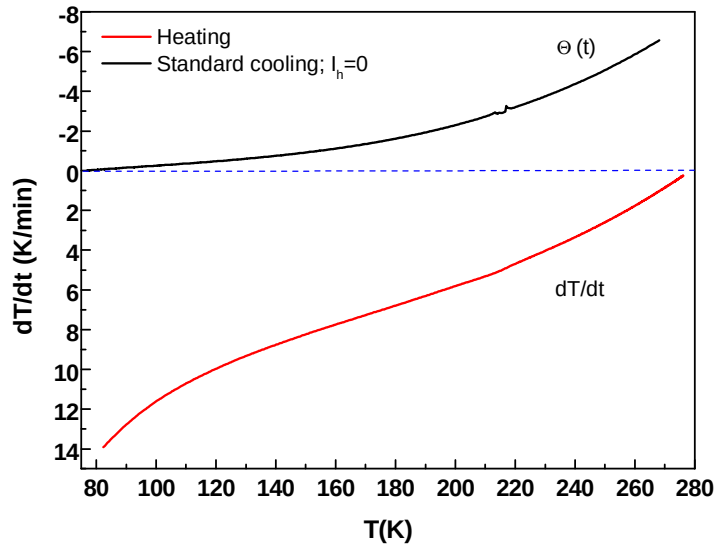

Fig 3.7 Experimental run of the empty cell. The black curve represent the standard cooling (I_h=0 with the thermal reservoir fixed at 77K), the red curve represent a heating run at fixed power.

The calorimetric cell is in contact with the thermal reservoir at 77 K through an effective thermal link (mainly arising from blackbody thermal radiation plus conduction through the electrical wiring).

Therefore, the equation of heat transport [Perez-Enciso 2007] contains both a cooling P_{cool} and heating P_{heat} power terms

$$C_p\left(\frac{dT}{dt}\right) = P_{heat} + P_{cool} = V_h I_h + C_p\Theta(T) \tag{3.10}$$

$\Theta(T) \equiv (dT/dt)_{drift}$ is the intrinsic negative thermal drift of the system which is measured as a function of temperature by standard cooling at I_h=0, with the thermal reservoir fixed at 77 K (see fig 3.7).

The heat capacity of the cell can be determined from:

$$C_p = \frac{V_h I_h}{\left(\frac{dT}{dt} - \Theta(T)\right)} \tag{3.11}$$

Furthermore, a direct display of the measured *dT/dt* curves as a function of temperature *T*, for a constant applied power, allows us to monitor first-order transitions such as melting and crystallization processes, and also allows

providing a large amount of data taken continuously, and has advantage of simplicity.

This method requires an instantaneous distribution of heat within the addenda and in the sample, and hence, relatively small samples are recommended, and the carful choice of materials used. And also, the heating powers (heating rates) should be chosen small enough to guarantee a uniform distribution of temperature.

3.4.4 Experimental operation

In practice, an automatized calorimetric program allows us to choose among the different methods [Perez-Enciso 2007]. The application is composed of different functional modules: heat capacity with different methods, and other modules for the data analysis, and automation of temperature controllers.

The power applied by the heaters and the temperature reading by the thermometers are nothing else that voltage and current measurements. So, as said before, in these specific heat measurements the instrumentation consists of two pairs of precision current sources and high-sensitivity micro-voltmeters (Keithley), assigned respectively for the heater and thermometer. In these experiments, temperature is the central parameter, a precision thermometry is needed, and hence well-calibrated thermometers are used. Due to the wide temperature range of interest, several kind of thermometers and calibration curves can be selected within the program. Different types of calibration files can be imported, either as polynomial fits (Chebyshev, power series, logarithmic, inverse power series, etc) or calibration data to be interpolated. At any time, the current in the resistance thermometers is automatically set, so that the voltage drop is a selectable value (typically a few millivolts). Current polarity is also changed to avoid thermoelectric offset. To reduce the maximum possible, the effects of electrical noise and interferences, all the instrumentation used including the computer are grounded to the same point.

In addition, we can choose among several temperature controllers (a programmable controller DRC-91 CA Lake Shore) for temperature stabilization or ramping of the cryostat inner.

Once the instrumentation and thermometry has been selected, we choose the measurement method, we introduce the measurements parameters, and then we start the run. After one heat capacity data point at a given temperature has been obtained, the program automatically changes the chamber temperature to a required amount (selectable). When the conditions (the introduced parameters) for a new run are given, a new heat-capacity measurement is started. As long as the conditions are fulfilled the experiment continues to operate automatically, unless, by an order from us. As the heat capacity of the cell is known from the last run, the program automatically determines the heating power to obtain the selected percent increase in temperature, in a given heating time which is also pre-selected.

In the standard relaxation method, heating is stopped when the slope is similar enough to the initial one, and ΔT_∞ is obtained by extrapolation of the slopes to the end of heating time. The program will fit the relaxation curve for the data between upper and lower limits. Those limits are selected as percent values of ΔT_∞, typically between 5% and 80%. Good exponential fits are obtained only if the extrapolated drift of the first part of the run is correctly subtracted from the recorded data. This is also true for the fits in both the heating and cooling parts of the fast relaxation method.

Moreover, the program opens graphic windows on the screen to show instantaneously the semilogarithmic plots of the running experiment, and the corresponding linear fits (see fig 3.4 and 3.5) to monitor the good thermal behavior of the experiment. This linear behavior of the semilogarithmic plot guarantees the existence of a well defined relaxation time τ for the thermal link and improves the accuracy of the measurement.

On the other hand, the continuous method is run by simply recording the temperature reading of the thermometer(s) as a function of time $T(t)$, also recording the instantaneous voltage drop in the heater and any other required parameters . Having these data, specific-heat curves are obtained by doing the instantaneous derivative of the temperature T with respect to time t, and using Eq. (3.11).

3.5 Heat-capacity measurement of the addenda (Empty cell)

The heat capacity of the calorimetric cell, after being emptied and remounted with the same conditions as before, is measured separately and then subtracted from the total (filled cell) measured values. In the case when using similar cells but slightly different in weight, this small difference is taken into account by considering the specific heat of copper.

3.5.1 At liquid nitrogen temperatures

The heat capacity of the empty cell was measured by the quasi-adiabatic continuous method in a wide temperature range (from room temperature to liquid nitrogen temperature), corresponding to the range of the measurements to be used in our experiments, and using similar conditions among different runs and rates of heating.

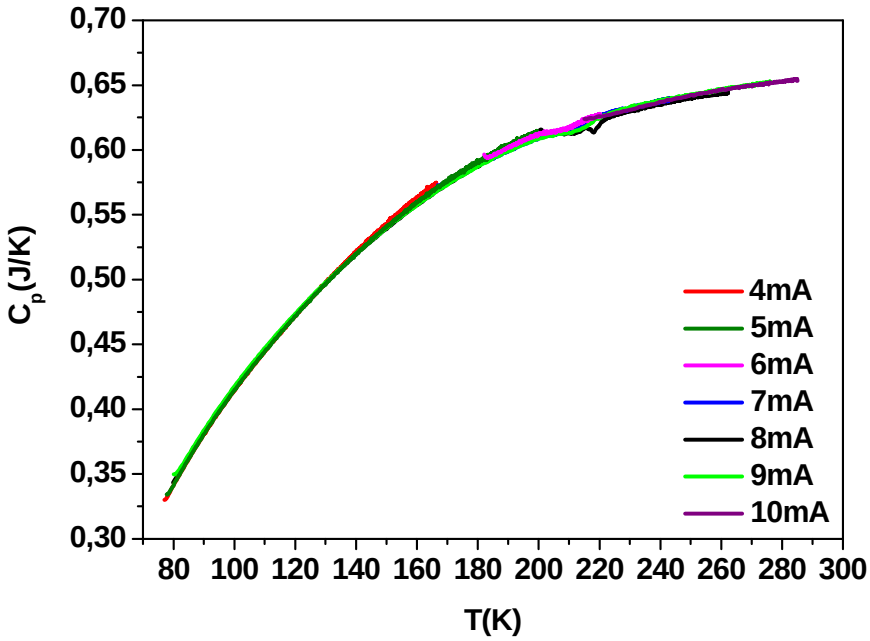

Fig 3.8 Heat capacity of the empty cell by different experimental runs, after having used different powers of heating (heating rates).

Figure 3.8 shows the very good agreement between the different runs at different rates of heating, hence supporting the validity of this calorimetric method. Once the curves C_p (T) have been obtained, a simple polynomial fit for these experimental data is made, as shown in figure 3.9, a simple polynomial fit of third degree, agrees very well with the experimental data. So, by making use of these polynomial coefficients and by considering the specific heat of copper, the contribution of the empty cell will be subtracted from the measured total heat capacity in each case.

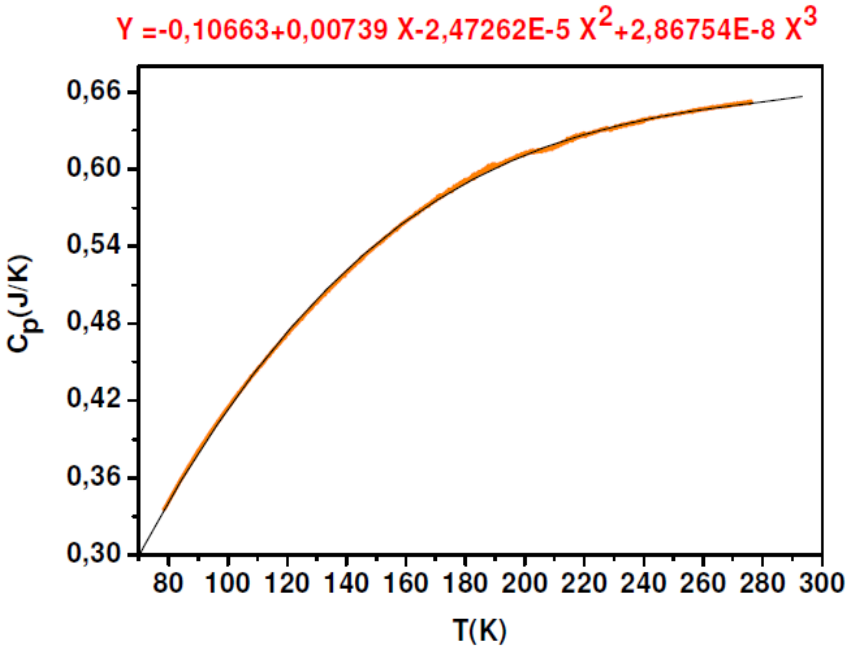

Fig 3.9 Polynomial fit to the experimental data covering the whole interval.

3.5.2 At liquid helium temperatures

At low temperatures, also the heat capacity of the empty cell was measured by using both the standard relaxation method, and the alternative (non-standard) relaxation method. We have obtained a very good agreement between the two methods and among different experimental runs, as can be seen in Fig 3.10.

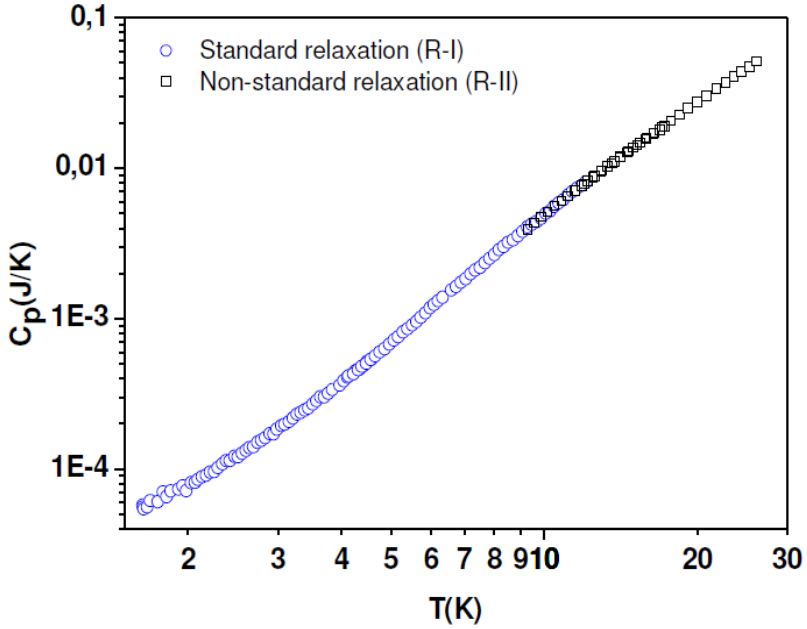

Fig 3.10 Heat capacity of the empty cell measured by using both the standard relaxation method and the fast relaxation method in log-log representation.

After having measured and obtained the experimental data, we performed polynomial fits to build up a continuous function that can be used at any temperature of the range measured. So, to be precise as most as possible, when doing the polynomials fit, we divided the whole range of low-temperature measurements, into two ranges: one at the lowest temperatures (1.6-6.3) K and the second one for the rest of the interval (6.3-30) K.

We have fitted these experimental data with a simple least-square linear fit in a C_p/T vs T^2 plot. After trying several polynoms of different degrees, we have selected the ones that agree better with the experimental data and have a good connection between them, as shown in fig 3.11 in log-log representation of C_p/T vs T^2. Once the polynoms have been selected, we set the validity of its application.

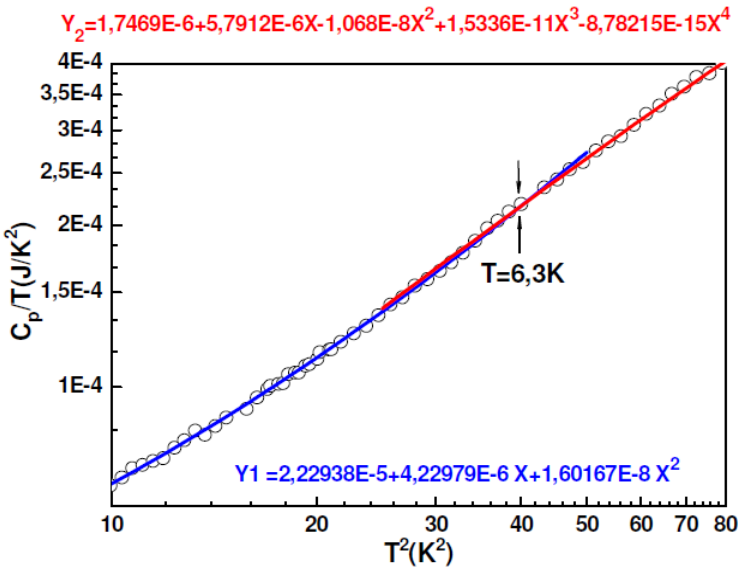

Fig 3.11 Polynomials fits and the selected limit (6.3 K) of its validity range (lower limit for one range and upper for the other).

As, it is also very important to check the contribution of the empty cell in total specific heat, by comparing the heat capacity of the addenda with respect to the specific heat of the sample (Fig 3.12), to make sure that specific heat of sample is widely greater (~ 40%) compared to the empty cell.

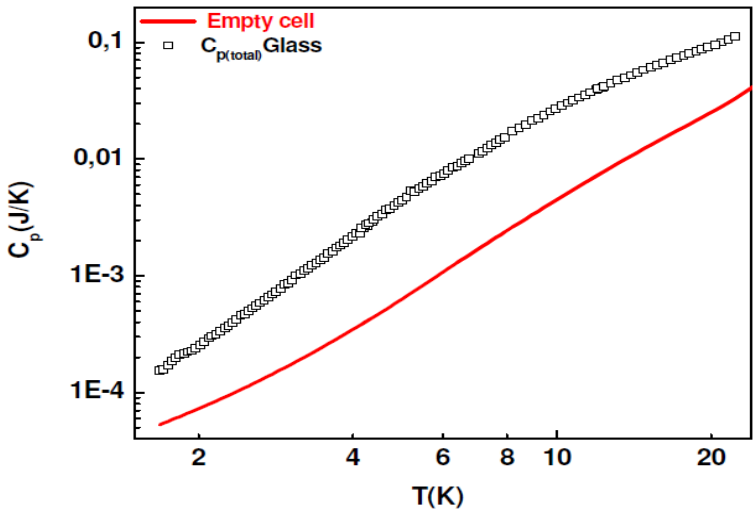

Fig 3.12 Total heat capacity of the sample (in this case 2-butanol glass) together with the heat capacity of the empty cell.

References

[Bachmann 1972]: R. Bachmann, F.J. DiSalvo Jr., T.H. Geballe, R.L. Greene, R.E. Howard, C.N. King, H.C. Kirsch, K.N. Lee, R.E. Schwall, H.U. Thomas and R.B. Zubeck, Rev. Sci. Instrum. 43, 205 (1972).

[Barron 1999]: T.H.K. Barron and G.K. White, *Heat Capacity and Thermal Expansion at Low Temperatures*, Kluwer, New York (1999).

[Eucken 1909]: A. Eucken, Z. Phys, 10, 586 (1909).

[Gaede 1902]: W. Gaede, Z. Phys, 4, 105 (1902).

[Giauque 1947]: W. F. Giauque and C. W. Clark. *J. Am. Chem. Soc.* 54. 3135 (1933).

[Gmelin 1979]: E. Gmelin, Thermochim. Acta 29, 1 (1979).

[Keesom 1932]: W. H. Keesom and J. N. Van den Ende, Commun. Kamerlingh onnes Lab. Univ. Leiden, 219B 2196 (1932).

[Nernst 1910]: W. Nernst, Sitzungsber. K. Preuss. Akad. Wiss, 12, 261 (1910).

[Perez-Enciso 2007]: E. Perez-Enciso and M. A. Ramos, Termochim. Acta 461, 50 (2007).

4 Calorimetric, thermodynamic and structural studies of butanol isomers

We have conducted calorimetric experiments on butanol isomers, characterized the phase diagram of each one, and measured the specific heat of the different phases obtained in the temperature range of their preparation. In the case of n-butanol, these calorimetric and thermodynamic studies were complemented by employing X-ray diffraction and Brillouin-scattering experiments to study its phase diagram and the very nature of its "glacial state". That will be discussed in section 4.6.1. We have also studied and measured the specific heat of the different solid states of each butanol isomer at low temperatures, as well as its thermal conductivity. That will be presented in the next chapter 5.

Both specific-heat measurements and calorimetric studies on the phase diagram in the 77K–300K temperature range of the different substances studied in this thesis were conducted by employing a versatile low-temperature calorimetric system, especially designed for glass-forming liquids (described in chapter 3). In particular, we used a quasi-adiabatic continuous method that allows accurate heat-capacity determination after coherent cooling and heating runs, using liquid nitrogen as thermal bath.

As it has been indicated in chapter 2, when cooling a liquid we can obtain either a glass or a crystalline state (depending of the cooling rate and the material). In practice, when producing the different phases of any material, the most important issue is to ensure that the phase formed is pure. If we cool the system fast enough to avoid crystallization (see sec 2.1.1) we obtain the glassy state. If instead we cool more slowly or stop the cooling in the metastable region between the melting temperature and the glass transition temperature, the system can crystallize after some time (depending on the system, the crystallization may be spontaneous or take place in several hours or days). To check this, in the case of the crystalline phase, when heating the crystal we verify that the specific heat does not show any variation around the glass transition temperature, with no break until the melting temperature. In the case of the glassy phases, we first record $T(t)$ within the continuous method when cooling the liquid, to observe that

there are no jumps in dT/dt (that would indicate that there is crystallization or a partial crystallization). Secondly, in the heating process we observe the glass transition, then crystallization if the material has a tendency to crystallize, and we characterize the phase transition and evaluate its enthalpy of crystallization H_{cryst}. In addition, we repeat this process for lower cooling rates in order to estimate the lower limit of cooling rate.

4.1 Experimental results on n-butanol

First of all, we will present our experimental results on n-butanol (also called 1-butanol): Studies on the glass and crystal states of n-butanol have been previously reported [Counsell 1965, Nan 2007]. Furthermore, a controversial "glacial state" has been also reported to exist [Bol'shakov 2005, Tanaka 2005]. This additional "glacial phase" has been debated in literature [Wypych 2007]. To shed light on the controversial issue of this "glacial state", we have paid more attention to this phase, which we have investigated through calorimetric experiments, and also by complementary Brillouin-scattering and X-ray diffraction experiments which were conducted by our collaborators.

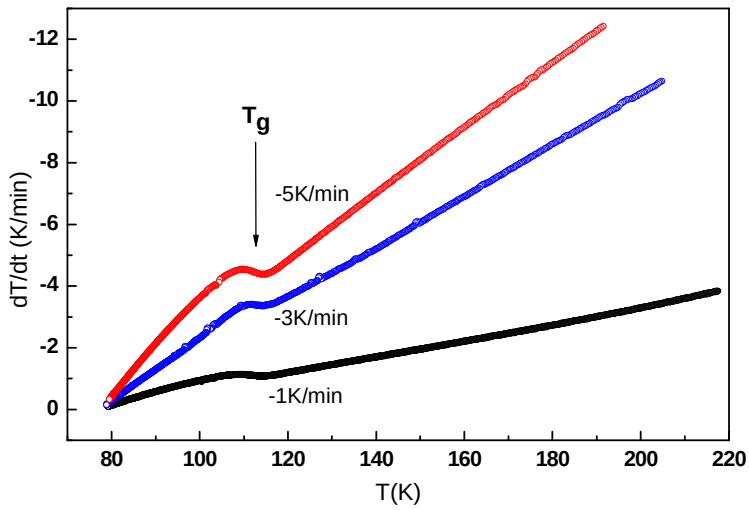

Fig 4.1 A directly measured variation of temperature as a function of time, showing different rates of cooling to prepare the glass of n-butanol.

As expected, by supercooling the liquid of n-butanol at even moderate rates (< 0.2 K/min), we can easily obtain its glass state. We observe a break in dT/dt (the glass transition) around 115 K as shown in Fig 4.1.

Once the glass state of n-butanol is obtained, by applying a continuous heating run (see Fig 4.2) at a constant and relatively high applied power of 145 mW (corresponding to a heating rate around 7 K/min for the SCL), we observe the glass transition around 111 K, followed by an exothermic process (a first-order transition) above 145 K. This crystallization process ends almost at the melting temperature around 183 K, at this heating rate.

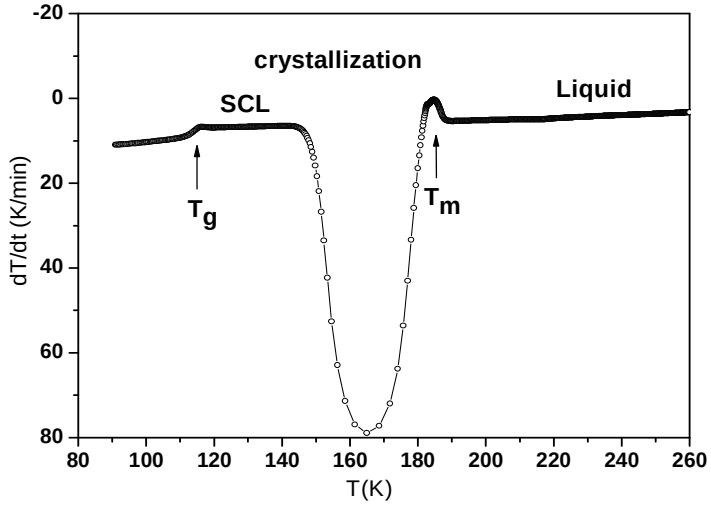

Fig 4.2 Thermogram as a function of temperature from the glass to the liquid of n-butanol, by applying a continuous heating run at constant power of 145 mW, which corresponds to a heating rate around 7 K/min of the SCL prior to crystallization, exhibiting a single crystallization process.

However, in order to study the three different solid phases of n-butanol, we have conducted the experiments depicted in figures 4.3 and 4.4. We begin by supercooling the liquid below T_g (see fig 4.3). Then, by heating the glass at moderate heating rates (around +2 K/min), the glass transition is observed at T_g = 111 K. When further heating the SCL above T_g, and after the heating is turned off around 130 K as shown in Fig 4.3, the SCL undergoes an exothermic process (an

apparent first-order transition) into the so-called "glacial state". Afterwards, this glacial phase does not exhibit any feature when is cooled.

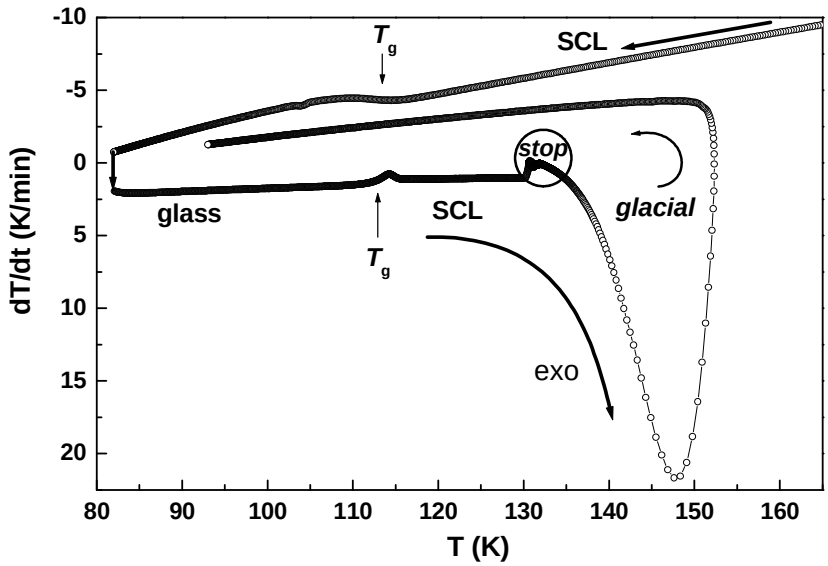

Fig 4.3 Typical thermogram, in absolute d*T*/dt units, showing the preparation of the metastable "glacial" state: First, a glass is obtained by simply supercooling the liquid. Then, the glass state is heated at a constant applied power through its glass transition T_g = 111 K, until the heating process is stopped around 130 K. Then, an irreversible exothermic process supercooled liquid (SCL)→glacial state occurs.

Once the glacial state has been obtained, this remains metastable, and when further heated above 155 K, it exhibits another exothermic, first-order transition into the stable crystal. This is illustrated in Fig. 4.4, when repeated cooling and heating cycles below the melting point (T_m = 184 K) show the stability of the crystal obtained by heating from the glacial phase. These and other performed thermal cycles of the obtained crystal, by cooling and heating it below T_m = 184 K, demonstrate that this is a stable crystalline state indeed, since no further transitions have been then observed.

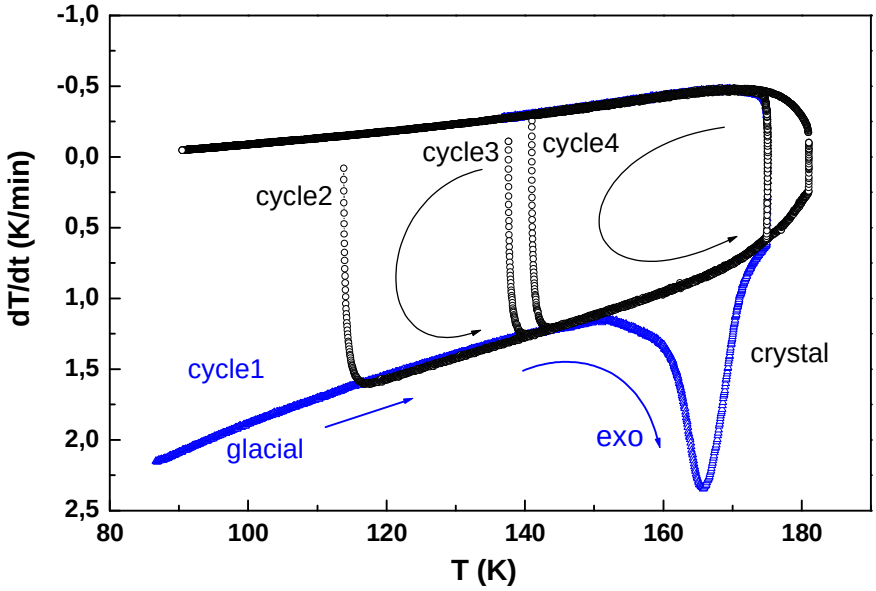

Fig. 4.4 Thermogram showing a first thermal cycle by heating the glacial state of *n*-butanol that exothermically transforms into the crystal state above 155 K. Subsequent and repeated cooling and heating cycles below the melting point (T_m = 184 K) show the stability of the obtained crystal state.

On the other hand, we have been able to obtain this kind of glacial state, either by heating the glass above T_g or also by directly cooling the liquid down to a stabilization temperature, within the temperature range 125–145 K, approximately. An example is shown in Fig 4.5.

In Fig. 4.6, we show the heating thermograms of several glacial phases previously obtained at slightly different temperature ranges, by following different thermal protocols. In all cases, the transition of those glacial phases into the stable crystal begins around 155–160 K, with an exothermic peak at 163–164 K.

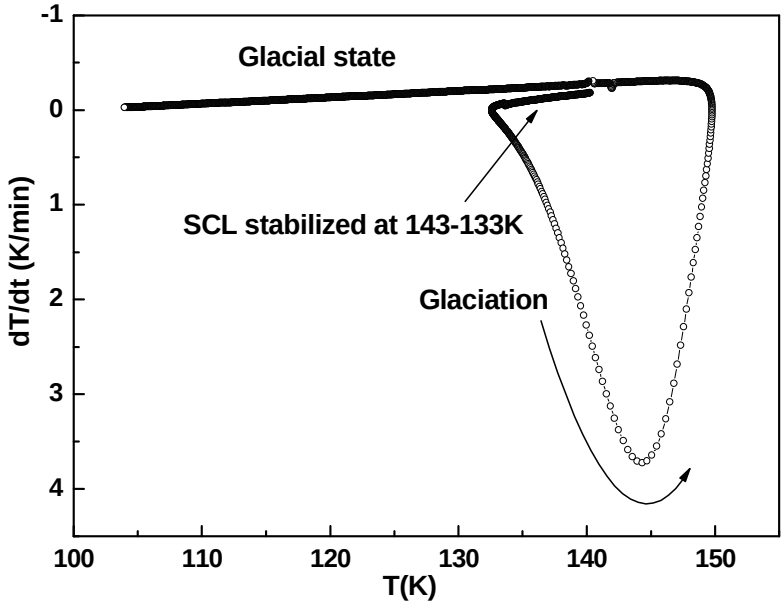

Fig 4.5 A glacial state obtained directly by cooling the liquid n-butanol from 250 K then stabilized around 135 K.

It is worth mentioning that when we tried to obtain the glacial state by employing helium exchange gas to avoid self-heating and stop temperature increase, we always observed curves such as those shown with dashed lines (curves e and f) in Fig. 4.6. A small feature at around 111 K followed by a exothermic peak at 135−140 K, before the usual crystallization, clearly indicates that by doing so we are interrupting the "glaciation" process, leaving a portion of supercooled liquid which becomes a glass. In fact, when it is heated, the corresponding (partial) glass transition at $T_g \approx 111$ K and the end of the "glaciation" below 140 K follow, before the whole of the glacial phase eventually crystallizes then above 155 K, as usual. Comparing their heat capacity curves with that of the glass sample (see inset in Fig. 4.6), one can estimate that a very low percentage of the sample had remained glass in these particular experiments.

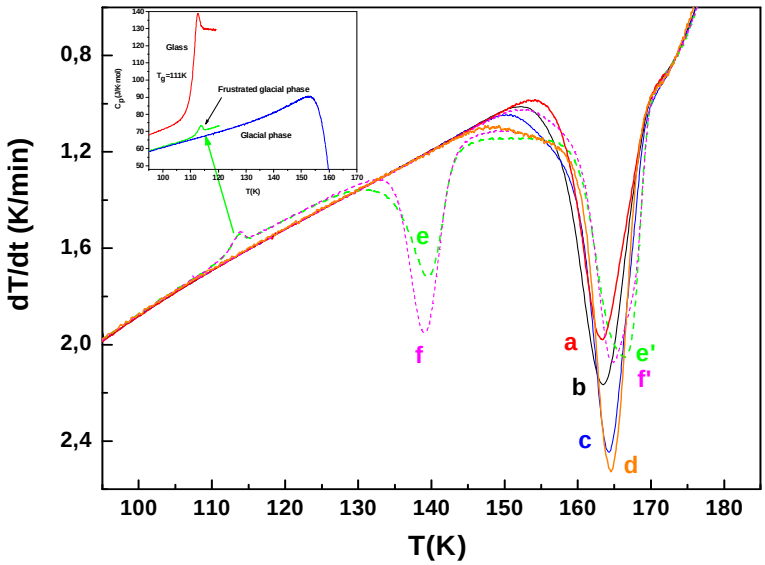

Fig 4.6 Heating thermograms of several *glacial phases* previously obtained following different crystallization histories. Taking the "glaciation" temperature range as the full width at half maximum of the exothermic peak, the depicted thermograms correspond to glaciation at: 138–153 K (a); 137–150 K (b); 138–148 K (c); 139–145 K (d). Dashed curves (e,e') and (f,f') correspond to *glaciation* processes interrupted by supplying helium exchange gas. The inset shows that the latter exhibit in their specific-heat curves a glass-transition feature around 5–10% of the total sample.

We observe that the higher the temperature range of the first *glaciation* step, the smaller the enthalpy of crystallization thereafter. This can be simply traced back to a previously larger entropy loss during its corresponding *glaciation* step, in turn due to a larger fraction of well-crystallized sample. For example, curve a of Fig. 4.6 was produced after annealing the heated glass at 125 K for 4 hours, and then the glaciation proceeded slowly until an effective final temperature of 153 K. (We will define here the initial and final temperatures by the full width at half maximum of the exothermic peak). The entropy variation of this process is determined to be −31.5±1 J/mol·K, and the corresponding later crystallization around 163 K gives −6.2±0.5 J/mol·K. On the other hand, curves b and c obtained by cooling the liquid in a controlled way, and exhibiting final temperatures of "glaciation" 3–5 K lower, gave entropy losses of −28±1 J/mol·K

and −26.5±1 J/mol·K, respectively, and −7.1±0.4 J/mol·K and −7.7±0.4 J/mol·K for their subsequent crystallizations around 164 K. Curve d gives values almost identical to curve c. It is worth noticing that the entropy losses around 139 K of curves e and f (allegedly, the continuation of the interrupted glaciation) are −2.0±0.2 J/mol·K and −2.3±0.2 J/mol·K, respectively. Therefore, they are well within the 5−10% range of the typical entropy losses at the "glaciation" event, in good agreement with the above-mentioned fact that their specific-heat curves exhibited a glass-transition feature around 5−10% of the full-glass sample.

After characterizing the phase diagram of n-butanol, the obtained results for the molar specific heat of the three different states of n-butanol (measured at heating rates around +2 K/min) are presented in Fig. 4.7.

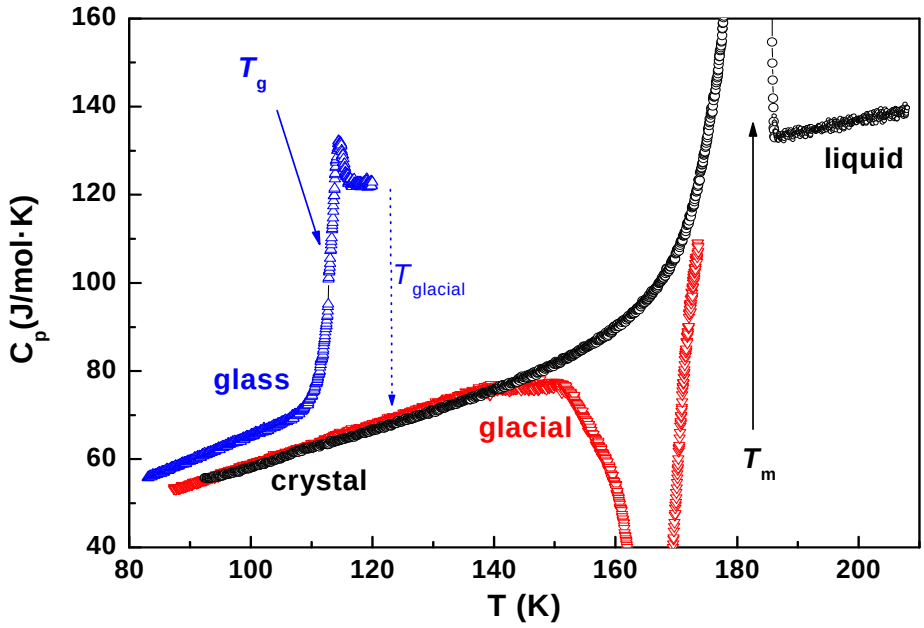

Fig 4.7 Temperature dependence of the specific heat of *n*-butanol for the glass (Δ), *glacial* (∇) and crystal (O) states around the glass-transition temperature region. The glass-transition temperature T_g, the glaciation transition observed by heating $T_{glacial}$, and the melting temperature T_m are graphically indicated.

The glass transition is observed at $T_g \approx 111$ K, in good agreement with literature [Tan 2007]. Then, the "glacial state" is obtained by heating at $T_{glacial} > 125$ K, and measured from lower temperatures after cooling it. The exothermic crystallization process, discussed above, is observed here as an apparent minimum in the heat capacity at $T > 155$ K. The so-obtained stable crystal does not exhibit any phase transition, when measured in the whole measured temperature range below its melting point at $T_m = 184$ K. We want to remark that specific heats of crystal and *glacial* states are very similar between them, but clearly different from the glass values.

As we have seen in chapter 2, the glass transition temperature T_g depends on several factors, particularly on the rate of cooling of the supercooled liquid. Our experimental system by using helium gas as exchange gas in its external chamber allows us to vary the cooling rates (up to –20 K/min around T ≈ 100 K). We have measured differently prepared glasses (we already presented some of them in figure 4.1), although here we present two differently prepared either by slow cooling (SC) or by fast cooling (FC) of the corresponding liquid, at around –0.2 K/min and –20 K/min, respectively. All measurements were performed by applying the same heating power of ≈ 2.5 mW, which corresponds to heating rates of ≈ 1.2 K/min around the glass transition.

The temperature T_g of the glass transition has been determined as the midpoint temperature of the jump between the specific-heat extrapolated curves of the glass and supercooled liquid states [Gutzow 1995], as graphically indicated in Fig. 4.8. In the same way, we have also determined the discontinuity $\Delta C_p(T_g) = C_p^{liquid}(T_g) - C_p^{glass}(T_g)$ between the linearly extrapolated specific heat of the glassy state and that of the SCL evaluated at T_g. Following this method, we have obtained $T_g = 111 \pm 1$K and $\Delta C_p(T_g) = 48 \pm 2$ J/mol·K.

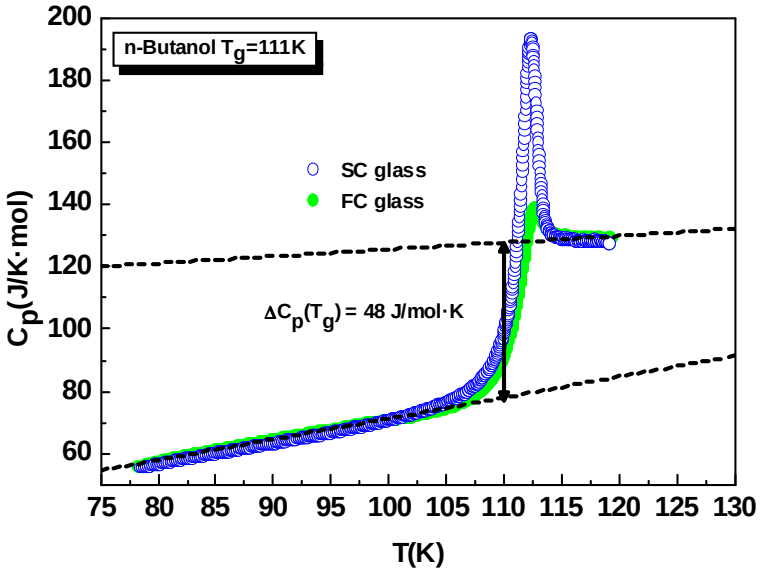

Fig 4.8 Specific heat of differently prepared glasses of n-butanol. Open symbols correspond to glass from slowly cooling of the liquid (–0.2 K/min) whereas the solid green symbols correspond to a much faster cooling (–20 K/min). Glass-transition temperatures T_g and specific-heat discontinuities $\Delta C_p(T_g)$ are shown by arrows.

The only difference within experimental error between FC and SC glasses, is a big increase of the "overshoot" observed at the T_g peak for the more slowly cooled ones, as can be seen in Fig. 4.8.

From the specific-heat curves of the different studied glasses, we have also calculated, and plotted in Fig. 4.9, the corresponding curves for their configurational enthalpy by means of:

$$\Delta H_{conf} = \int_{T_0}^{T} (C_p - C_{p,glass})dT \qquad (4.1)$$

where T_0 is a fixed reference temperature in the supercooled liquid state and $C_{p,glass}$ is the extrapolated linear curve of the corresponding glass state, that is essentially the vibrational contribution to be subtracted. From the enthalpy curves, one can obtain the so-called fictive temperature T_f, which is defined as the intersection point of the equilibrium-liquid configurational enthalpy with that extrapolated from the glass [Elliott 1990]. By doing so, we obtain T_f =110 K for the FC glass and T_f =108 K for the SC one.

Therefore, as expected, the fictive temperature T_f decreases with slower cooling of the liquid to obtain the glass state. This is directly related to the "overshoot" in the C_p peak that implies larger enthalpy or entropy losses at the glass transition.

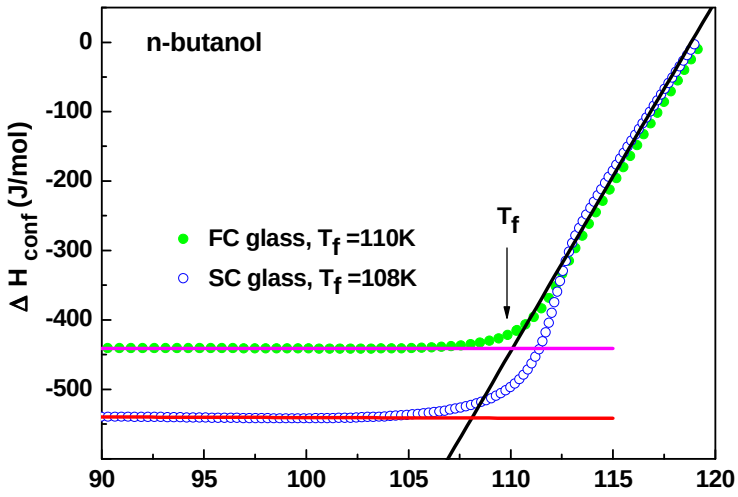

Fig 4.9 Configurational enthalpy of a fast cooled (FC) glass, and a slow cooled (SC) glass for 1-butanol. The method followed to determine their fictive temperatures, T_f, is also graphically shown.

4.2 Experimental results on sec-butanol

On the other hand, sec-butanol is a very good glass former. When supercooling its liquid at very slow rates (< 0.2 K/min around T_g) we still obtain easily the glass state around 120 K as can be seen in Fig 4.10.

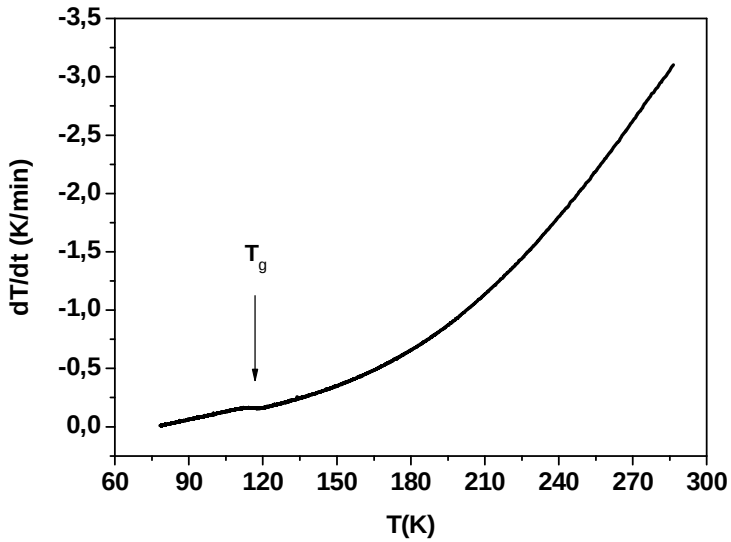

Fig 4.10 A directly measured variation of temperature as a function of time, showing the glass transition of 2-butanol, at a cooling rate of -0.2 K/min around the glass transition.

On the contrary to n-butanol, sec-butanol showed no tendency to crystallize. We annealed its supercooled liquid (SCL) for one day at different temperatures below its melting point and we were not able to obtain the crystalline state. It has been nevertheless reported [Andon 1971] that crystallization of 2-butanol occurred after the sample was cooled and warmed several times during 15 days in the temperature range 150-180 K.

In Fig. 4.11 we present the measured specific heat curve $C_p(T)$ of glass 2-butanol and its supercooled liquid (SCL) to above 200K.

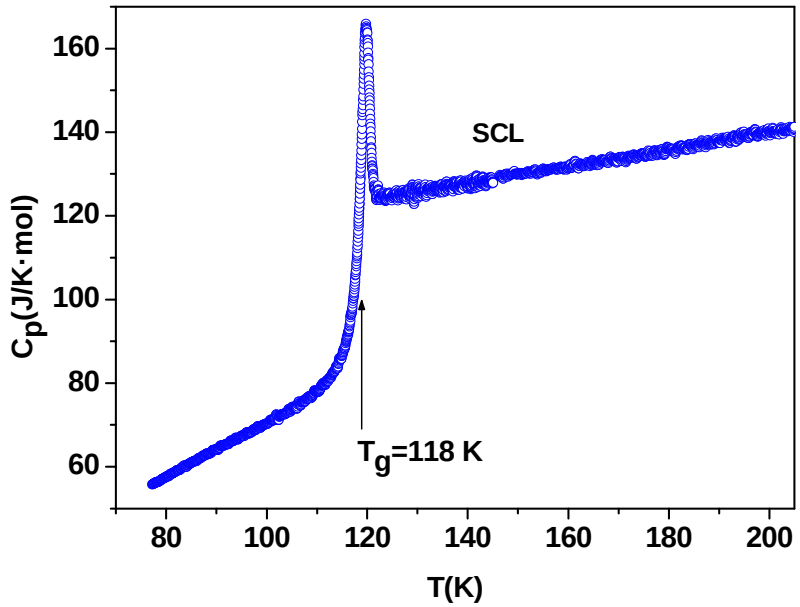

Fig 4.11 Molar specific heat of glass 2-butanol and its supercooled liquid (SCL) to above 200K.

In the same way as in n-butanol, we have measured two differently prepared glasses of 2-butanol, either by slow cooling (SC) or by fast cooling (FC) of the corresponding liquid, at around –0.2 K/min and –20 K/min, respectively. All measurements were performed by applying the same heating power of 2.5 mW, which corresponds to heating rates of ≈ 1 K/min, measured around its glass transitions.

The temperature T_g of the glass transition has been determined as the midpoint temperature of the jump between the specific-heat extrapolated curves of the glass and supercooled liquid states, as graphically indicated in Fig. 4.12. In the same way, we have also determined the discontinuity $\Delta C_p(T_g) = C_p^{liquid}(T_g) - C_p^{glass}(T_g)$ between the linearly extrapolated specific heat of the glassy state and that of the SCL evaluated at T_g. Following this method, we have obtained T_g = 118±1 K and $\Delta C_p(T_g)$ = 40±2 J/mol·K for sec-butanol.

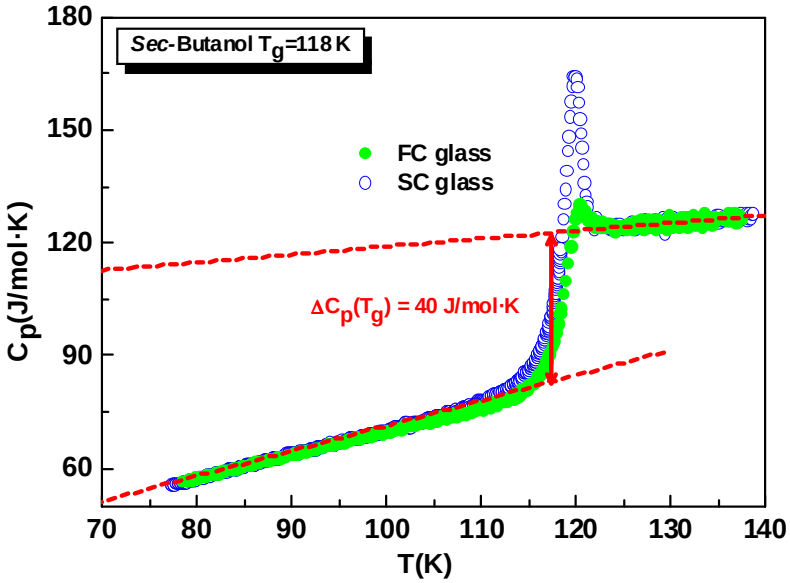

Fig 4.12 Specific heat of differently prepared glasses of 2-butanol. Open symbols correspond to glass from slowly cooling of the liquid (–0.2 K/min) whereas the solid green symbols correspond to a much faster cooling (–20 K/min). Glass-transition temperatures T_g and specific-heat discontinuities $\Delta C_p(T_g)$ are shown by arrows.

From the specific-heat curves (Fig. 4.12) of the different studied glasses, we have also calculated, and plotted in Fig. 4.13, the corresponding curves for their configurational enthalpy by means of equation (4.1). We obtain T_f=117 K for the FC glass and T_f=114 K for the SC one.

Therefore, as expected, the fictive temperature T_f decreases with slower cooling of the liquid to obtain the glass state. This is directly related to the "overshoot" in the C_p peak that implies larger enthalpy or entropy losses at the glass transition, when the glass was previously formed by cooling the liquid.

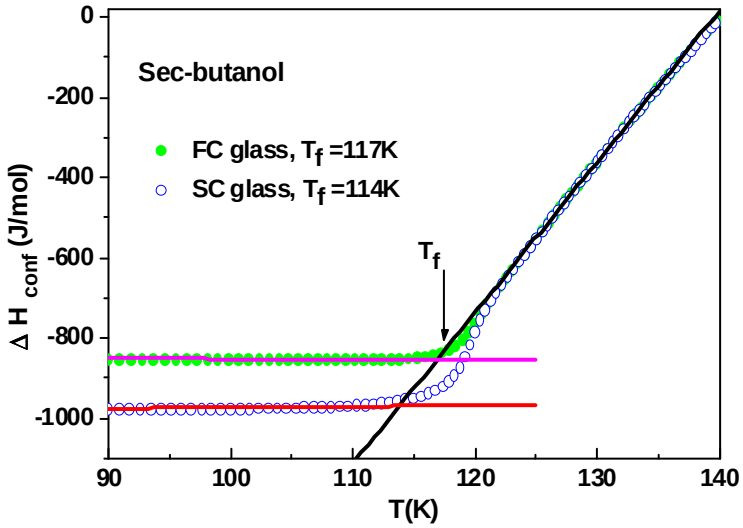

Fig 4.13 Configurational enthalpy of a fast cooled (FC) glass, and a slow cooled (SC) glass for 2-butanol. The method followed to determine their fictive temperatures, T_f, is also graphically shown.

4.3 Experimental results on tert-butanol

Contrary to the two first studied isomers, tert-butanol possesses a high melting temperature. At ambient temperature it is in a very viscous state or already in solid state, and to introduce it in the calorimetric cell we were required to heat it slightly.

In literature, the behavior of tert-butanol in the solid states has been studied by using various experimental techniques. Unfortunately, the results obtained for the solid states are controversial. Much interest was paid to characterize its structural nature [Mc Gregor 2006], and its molecular dynamics [Nishchenko 2011]. In calorimetric measurements, three crystalline phases were found by Oetting [Oetting 1963]. Dilatometric studies [Neu 1968] showed that a further phase of tert-butanol exists, and Mc Gregor *et al.* in their structural studies also conducted a DSC experiment, and also reported the existence of another crystalline phase [Mc Gregor 2006].

We have conducted calorimetric experiments on tert-butanol, by using our experimental system applying the continuous method to characterize the phase transitions. When cooling the liquid of tert-butanol from 310 K with a moderate cooling rate (–3 K/min around 300K), we observe a first phase transition around 285 K followed by a second transition around 260 K (see Fig 4.14). Let us call them crystal-I and crystal-II, respectively.

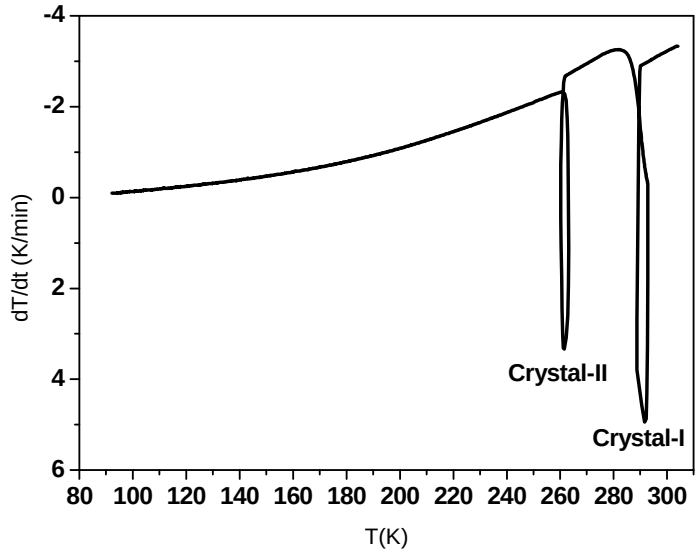

Fig 4.14 Variation of temperature as a function of time, from 310 K to 77 K, showing the two consecutive crystallization processes of tert-butanol.

When heating the crystal (crystal-II) from nitrogen temperature, we do not observe any variation in *dT/dt* until a small peak in the pre-melting region. Then, melting is observed around 293 K.

Before studying with more detail these crystalline phases, we have done several experimental runs gradually increasing the rates of cooling, with the aim of bypassing this strong crystallization and therefore obtain the glass state. Unfortunately, we were not been able to obtain the glass of tert-butanol, even with the maximal rates of cooling (–80 K/min around 290 K) allowed by our calorimetric system: the liquid always crystallizes, as shown in Fig 4.15.

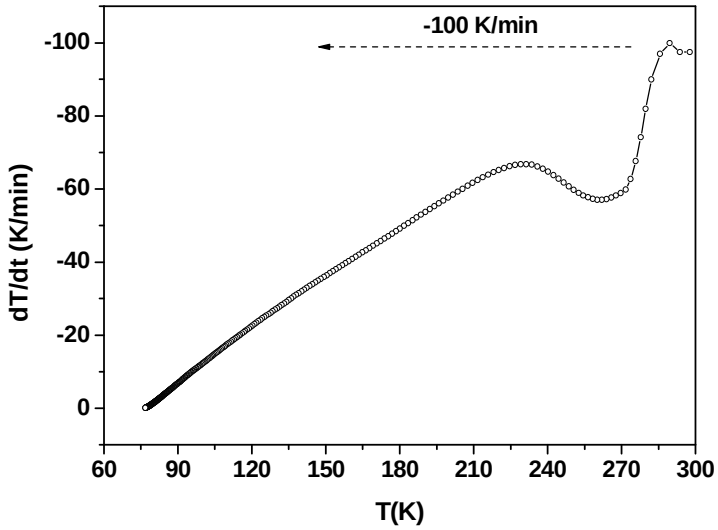

Fig 4.15 A directly measured variation of temperature as a function of time, showing the persistent crystallization in spite of the quench of liquid tert-butanol (-80 K/min around 280 K temperature of crystallization).

When heating the crystalline phases obtained by the fast cooling, all of them present an exothermic peak around 200-220 K, as shown in Fig 4.16.

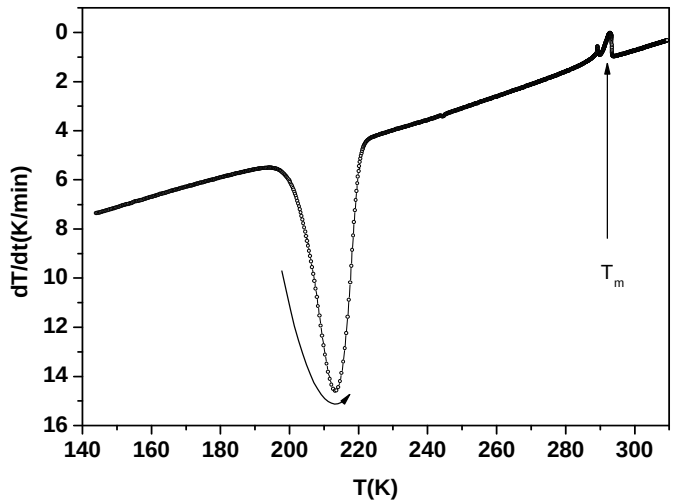

Fig 4.16 Heating of the crystal obtained by the very fast cooling. An exothermic transition is observed at 210 K, followed by a peak in pre-melting region and eventually the melting.

It seems that the crystallization occurred by fast cooling was aborted (interrupted). This exothermic peak has also been attributed to an anomaly due to a possible ordering of the methyl groups [McGregor 2006]. By following the heating, the crystal does not show any variation until the small peak in the pre-melting region, and then melting occurs at T=293 K, exactly like in the case of the slowly prepared crystal.

However, we will focus now on the crystals of tert-butanol by performing some specific experiments. Cooling the liquid from T = 310 K to T = 270 K (just before the second crystallization), we obtain the so-called crystal-I. Then, by heating this crystal applying the same power as before, the crystal-I does not present any variation or peak (transition) until it melts into the liquid at $T \approx$ 293K, as can be seen in Fig 4.17.

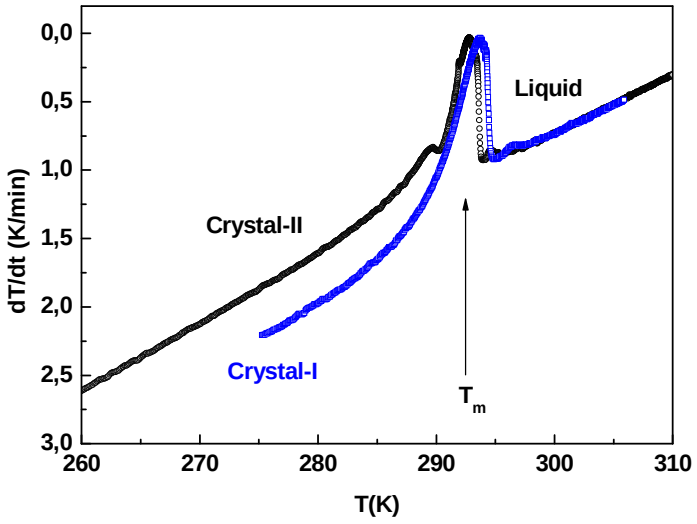

Fig 4.17 *dT/dt* of the heating of the crystal-I from 275K and its liquid state, plotted together with crystal-II heated by the same heating power.

Then, we tried to prepare the crystal-I by very slow cooling (-0.5 K/min) in order to get it "more stable". Once the crystal is obtained, we continued the cooling in standard conditions, the second transition (crystal-II) occurs, but at slightly lower temperatures than usual ($T \approx$ 250 K). When heating this crystal-II the small peak in pre-melting region (see Fig 4.18 a) is more pronounced and clear than when the crystals are prepared slightly faster (at standard conditions).

When we performed another experiment by stabilizing the SCL just below the pre-melting region for 10 hours, followed by cooling slowly the annealed SCL, we also obtain the two known crystals. But in this case, when heating the crystal-II we obtain an exothermic transition mixed with the fusion (see Fig 4.18 b).

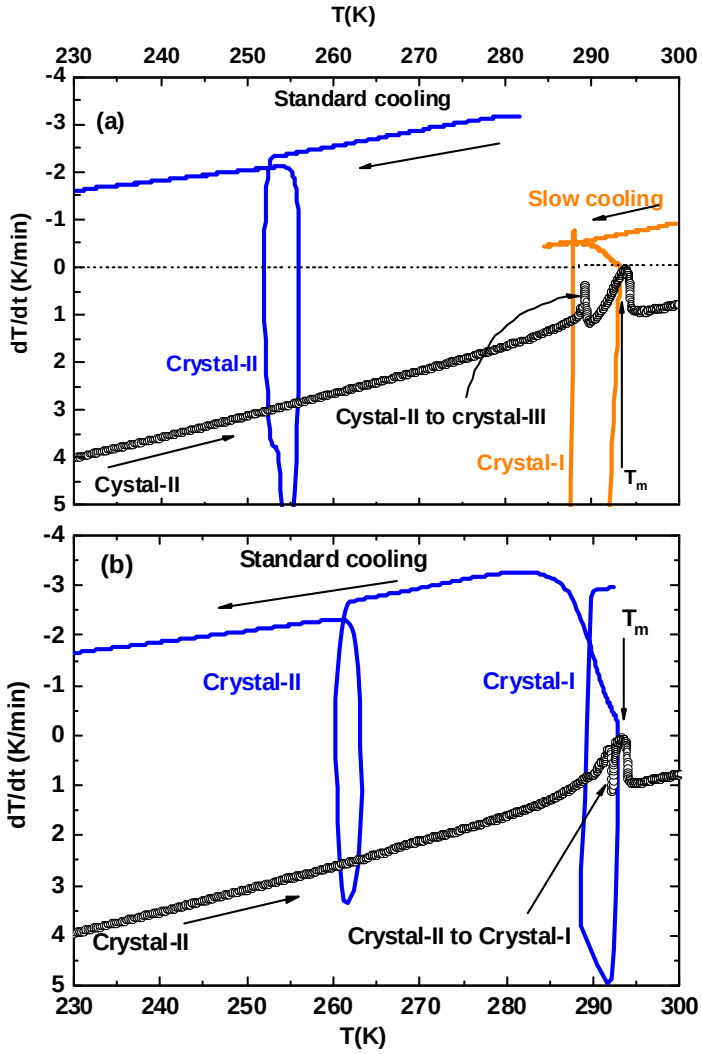

Fig 4.18 Thermograms as a function of temperature of tert-butanol. (a) shows crystal-I obtained by very slow cooling (orange curve), followed by the second crystallization (blue curve) and the corresponding heating run (black curve). (b) crystal-I obtained after stabilizing the SCL in the pre-melting region, followed by crystal-II (blue curve), and its corresponding heating run (black curve).

Finally, in Fig 4.19 we present the obtained molar specific heat of the two different crystals, I and II, the fusion and the specific heat of liquid tert-butanol. As can be seen the specific heat value of crystal-II is higher than the specific heat of crystal-I.

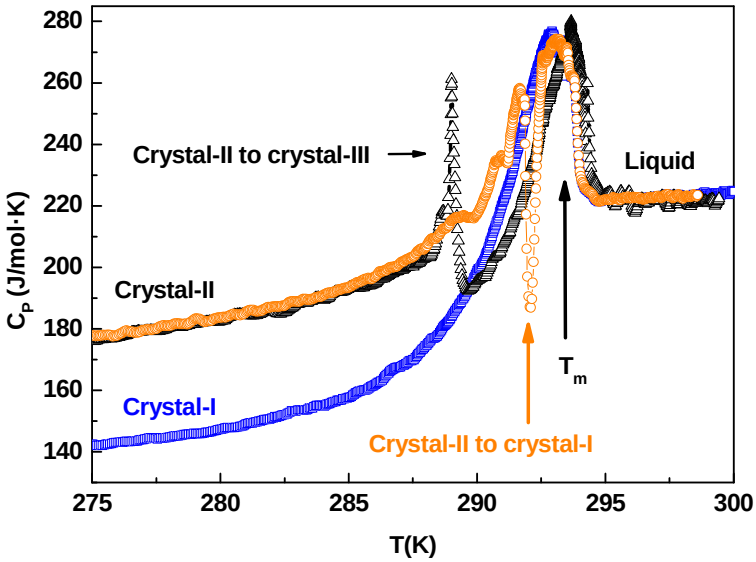

Fig 4.19 Specific heat of different crystals tert-butanol. Orange circles and black triangles represent the specific heat of crystal-II, including the transitions to crystal-III and crystal-I very close to the melting temperature. Blue squares represent the specific heat of crystal I.

From those calorimetric studies we have found that tert-butanol has a strong tendency to transform in the crystalline state. In spite of having quenched the liquid tert-butanol at −80 K/min around the temperature of crystallization 280 K, we have not been able to obtain the glass state. Tert-butanol crystallizes in different phases. We have been able to obtain two different stable (at least in a determined range of temperatures) crystals. The crystal-I, once obtained, does not transform in any other phase from 270 K until melts at $T_m = 293$, but transforms in crystal-II when it is cooled below 270 K (a few Kelvin below its temperature formation). On the other hand, crystal-II is stable in the whole range from 77 K to 285 K, and then it presents instability close to the pre-melting region. It exhibits an endothermic transition at 288 K when it is obtained after annealing

the SCL at 290 K. According to Oetting [Oetting 1963], this transition corresponds to the transition from crystal-I to crystal-III. Following another thermal process, when the SCL is cooled very slowly without a further annealing, the crystal-II presents an exothermic transition close to the melting transition. This exothermic peak has been also attributed by Oetting to a transition from crystal-II to crystal-I. In any case, these solid phases of tert-butanol are not fully stable at all, and transformations occur in determined ranges of temperature, depending of the thermal history of the SCL. We also want to remark that the specific heat of crystal-II is significantly higher than that of crystal-I, though being the stable crystalline state below 285 K.

4.4 Experimental results on isobutanol

Finally, the fourth isomer isobutanol is also a good glass former: when cooling from the liquid state very slowly we easily obtain the glass around 115 K, as can be seen in Fig 4.20. By heating this obtained glass at a constant power of heating, we observe the glass transition at T_g= 113 K. By further heating to higher temperatures we do not observe any significant variation or phase transition (see Fig 4.21).

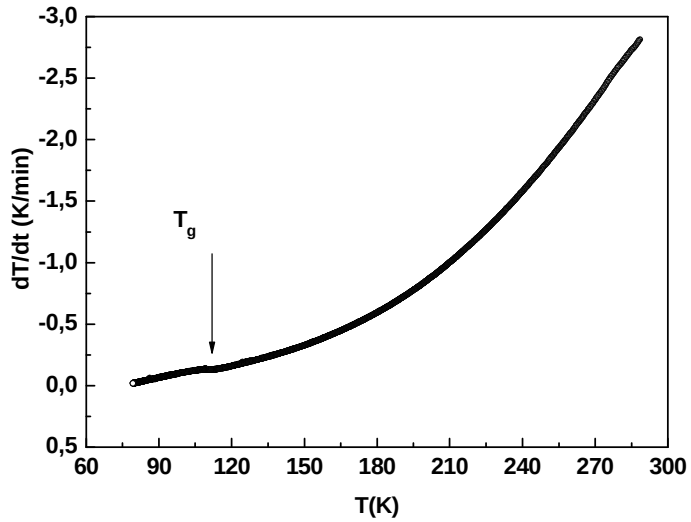

Fig 4.20 *dT/dt* for the "standard" cooling of liquid of iso-butanol.

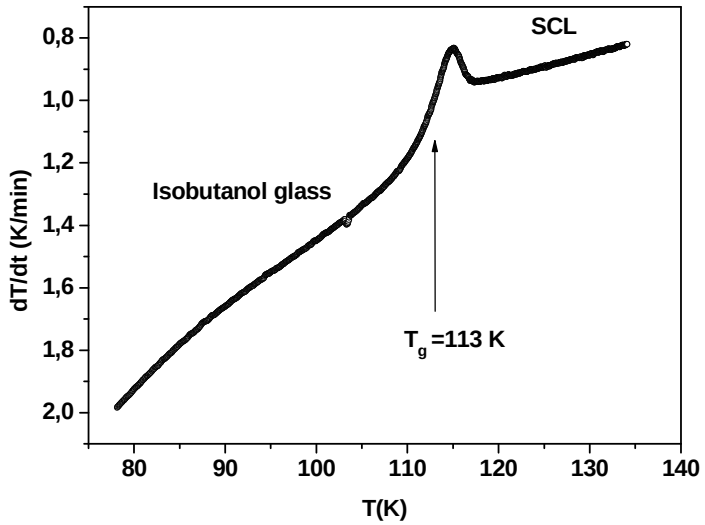

Fig 4.21 Heating run of isobutanol glass, T_g = 113K.

To prepare the crystal of isobutanol, we heat the glass state, then we stabilize the temperature around 143 K, and after a few hours in this temperature the SCL crystallizes. Then we cool this crystal to nitrogen temperature. In this cooling process we do not observe any variation in *dT/dt* around the glass transition, T_g = 113 K. By heating the crystal, we observe that it is stable until 155 K, then we observe an endothermic transition followed by two small peaks (see Fig 4.22 (a)), and finally the melting at T = 168 K. We were also able to obtain the crystal by cooling the liquid of isobutanol and stabilize the supercooled liquid around 143 K. When performing the heating process, all happens the same as before, confirming we had obtained the same crystal phase.

Additionally, to check if the crystal presents any difference before and after the endothermic transition, we performed several different thermal cycles to explore the features observed (see Fig 4.22 (b)).

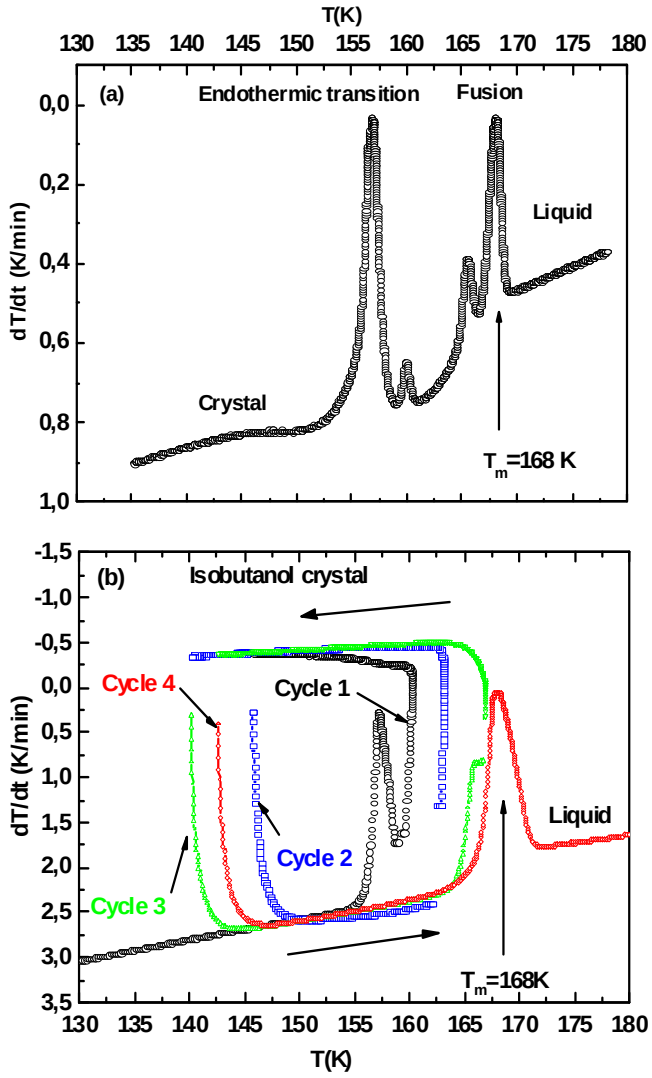

Fig 4.22 Thermogram of crystal isobutanol. In (a) we show the crystal presenting an endothermic transition at 155K, followed by two endothermic small peaks. In (b), we show subsequent and repeated cooling and heating cycles after each transition or peak, showing the irreversibility of the transitions, finally heating the stable crystal to the melting point (T_m = 168 K).

After having characterized the diagram phase of isobutanol, we finally present in Fig 4.23 the obtained specific-heat data for the different states of

isobutanol (measured at +2 K/min), glass, the stable crystal and the liquid state. The glass transition is observed at $T_g \approx 113$ K, and the melting point $T_m = 168$ K.

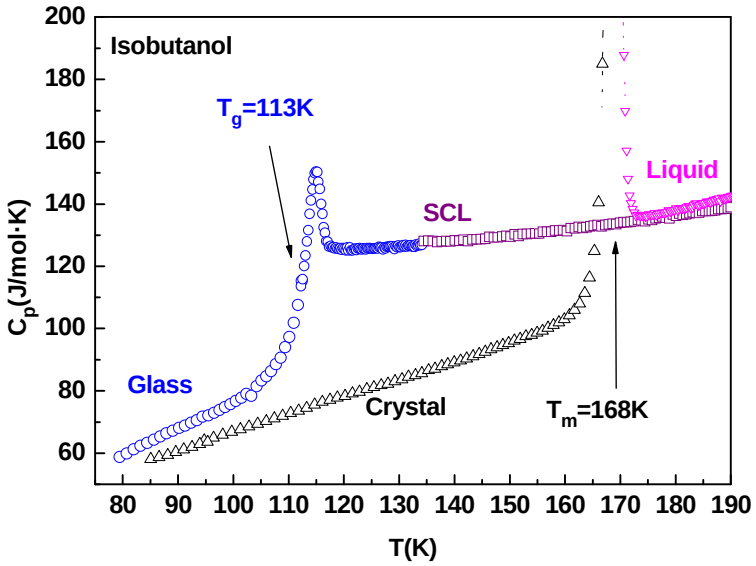

Fig 4.23 Molar specific heat of isobutanol for the glass (○), crystal (Δ), SCL( ) and liquid (∇) states. The glass transition temperature is found at T_g= 113 K, and the melting temperature at T_m=168 K.

In the same way we did with the two first isomers, n-butanol and sec-butanol, we have measured two differently prepared glasses of 2-butanol, either by slow cooling (SC) or by fast cooling (FC) of the corresponding liquid, at around –0.2 K/min and –20 K/min, respectively. All measurements were performed by applying the same heating power of 2.5 mW, which corresponds to heating rates of ≈ 1 K/min, measured around its glass transitions.

Again, the temperature T_g of the glass transition has been determined as the midpoint temperature of the jump between the specific-heat extrapolated curves of the glass and supercooled liquid states, as graphically indicated in Fig. 4.24. In the same way, we have also determined the discontinuity $\Delta C_p(T_g) = C_p^{\text{liquid}}(T_g) - C_p^{\text{glass}}(T_g)$ between the linearly extrapolated specific heat of the glassy state and that of the SCL evaluated at T_g. Following this method, we have obtained T_g = 113±1 K and $\Delta C_p(T_g)$ = 40±2 J/mol·K for isobutanol.

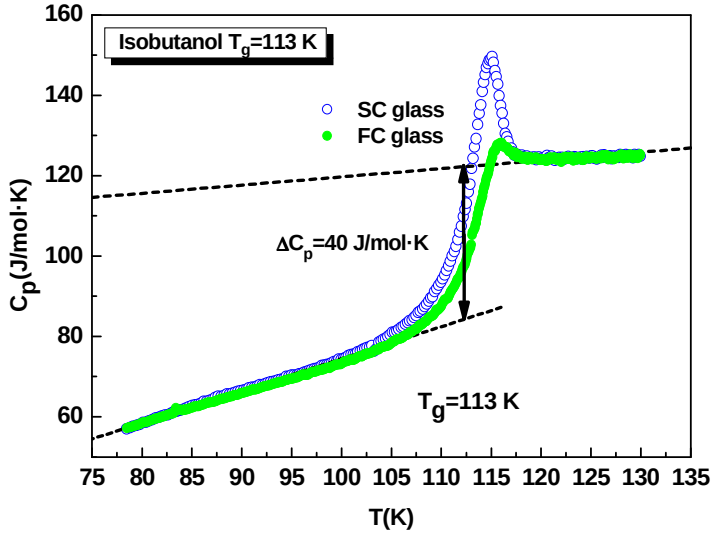

Fig 4.24 Specific heat of differently prepared glasses of isobutanol. Open symbols correspond to glass from slowly cooling of the liquid (–0.2 K/min) whereas the solid green symbols correspond to a much faster cooling (–20 K/min). Glass-transition temperatures T_g and specific-heat discontinuities $\Delta C_p(T_g)$ are shown by arrows.

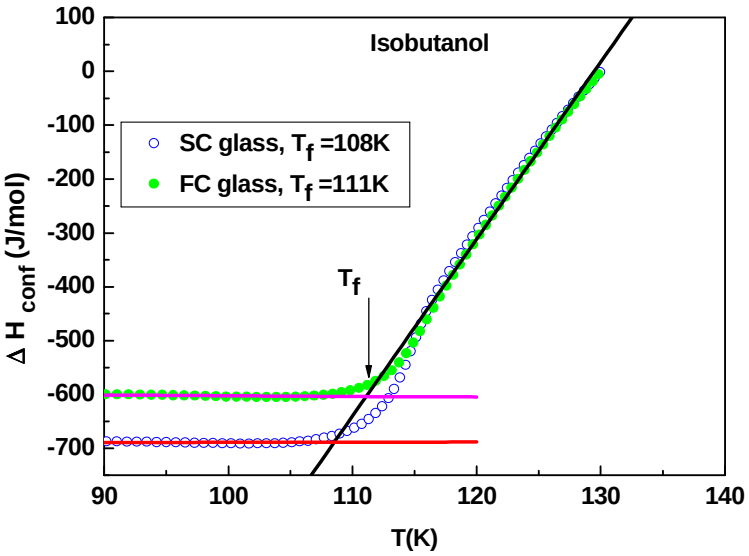

Fig 4.25 Configurational enthalpy of a fast cooled (FC) glass, and a slow cooled (SC) glass for isobutanol. The method followed to determine their fictive temperatures, T_f, is also graphically shown.

From the specific-heat curves Fig. 4.24 of the different studied glasses, we have also calculated, and plotted in Fig. 4.25, the corresponding curves for their configurational enthalpy by means of equation (4.1). We obtain T_f =111K for the FC glass and T_f =108 K for the SC one.

Therefore, as expected, the fictive temperature T_f decreases with slower cooling of the liquid to obtain the glass state. This is directly related to the "overshoot" in the C_p peak that implies larger enthalpy or entropy losses at the glass transition, when the glass was previously formed by cooling the liquid.

4.5 Other experiments

In the previous section we have investigated through calorimetric experiments the phase diagram of the four butanol isomers, and measured the specific heat of the different phases. In this section we will present other experiments to complement the results obtained calorimetrically, and explore the physical nature of the so-called "glacial state" of n-butanol.

4.5.1 X-ray diffraction

In this particular case of n-butanol, and especially to investigate the very nature of the "glacial phase", another experimental technique was conducted. The structural properties of liquid and solid states of n-butanol were investigated by means of X-ray diffraction experiments in collaboration with Dr. Ivan M. Shmyt'ko. The experiments were realized in the Institute of Solid State Physics of Russian Academy of Sciences, Chernogolovka, Russia.

4.5.1.1 Experimental setup and measuring procedures

An X-ray diffractometer D-500 (Siemens) with a secondary graphite monochromator and Cu-K_α radiation was used in transmission geometry. The liquid sample was inserted into a disk-like sample holder with beryllium disks of ~20 mm in diameter as windows. The thickness of the beryllium disks is ~0.1 mm and the distance between windows is ~1.0 mm. Besides the direct use of the

beryllium disks as X-ray windows, they also served for adjusting the sample under investigation on the vertical axis of the X-ray goniometer.

This experimental set-up allowed to vary temperature and rate of cooling in a wide interval of rates, and provided a temperature control better than 0.1 K at a given constant temperature. For more details, see Ref [Shmyt'ko 2010].

Two different measuring procedures were used. A first kind of procedure was used to conduct a detailed investigation of possible structural changes in *n*-butanol in a wide temperature interval. It consisted in a series of controlled temperature steps, where diffraction spectra were recorded, with the temperature decreasing from room temperature down to 96.8 K. The effective cooling rate of the sample in this case was very slow because the recording time of a single diffraction spectrum was approximately 2.5 hours, that often was increased up to 15 hours to improve statistics. A second procedure was used to specifically obtain some crystalline or glassy phases of *n*-butanol. To obtain the stable crystal phase, slow cooling of the sample was performed from room temperature to a crystallization temperature $T_{crystal}$ a few degrees below the melting point T_m. In order to obtain the glassy state, the sample was heated a few tens of degrees above T_m and then was quenched below the glass transition $T_g \approx 111$ K (in our case, into liquid nitrogen). After this, the quenched glass was slowly heated to several measuring temperatures, and also annealed at different temperatures for a few hours to observe and investigate crystallization processes.

4.5.1.2 Results

We will not present all the results obtained for the different phases of n-butanol that are described in Ref [Shmyt'ko 2010]. We will focus here only on the results obtained for the so-called "glacial state".

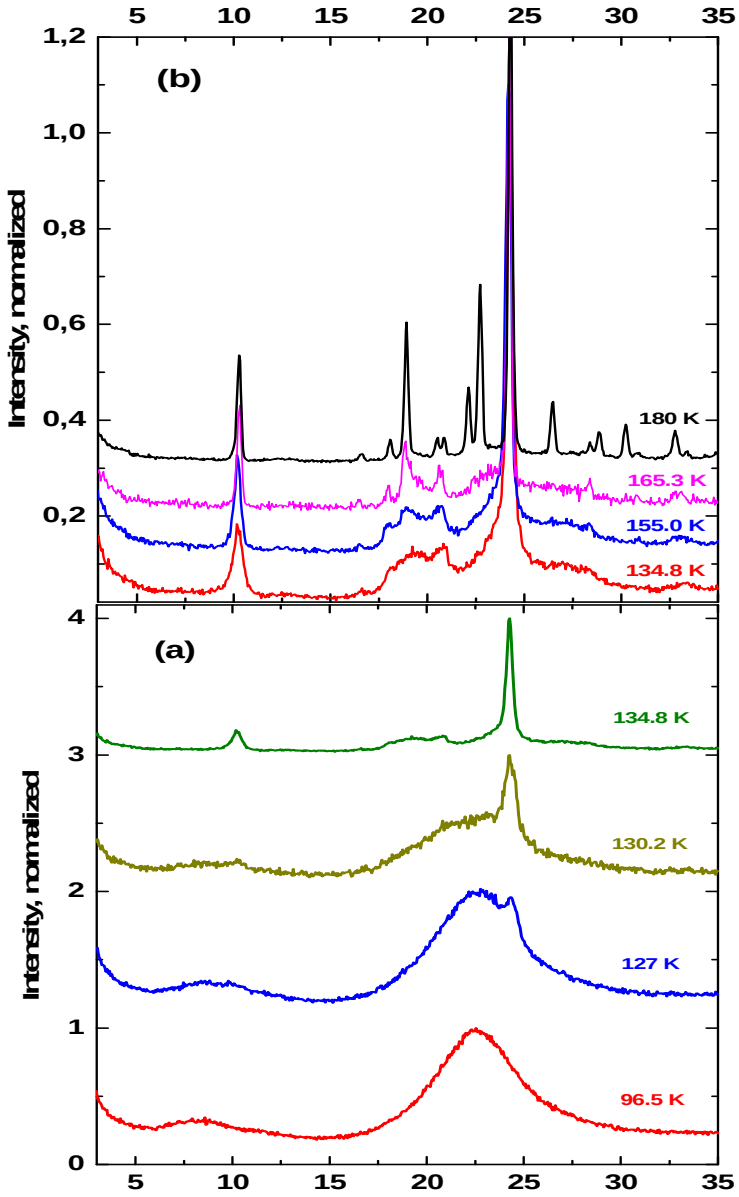

Fig 4.26 Evolution with temperature of X-ray diffraction spectra at slow heating, starting from the glassy state: (a) emergence of crystalline peaks superimposed on the amorphous pattern for the so-called "glacial phase" at 127 K; (b) full crystallization of *n*-butanol above 155 K. All spectra have been shifted vertically for clarity.

Fig. 4.26 shows the evolution with temperature of X-ray diffraction spectra at slow heating, starting from the frozen liquid (i.e. the glass state) at 96.5 K. The figure is split in two temperature regions: (a) the formation of the so-called "glacial state"; (b) the second crystallization step from the previous "glacial state" to the fully-ordered crystalline state.

In Fig. 4.26a, superimposed on the amorphous background (of the SCL) one can clearly see the emergence of crystalline peaks at 127 K, that becomes better defined at 130.2 K and is already completed at 134.8 K. It is to be noted that the growth of these crystalline reflections is however accompanied by keeping a big part of the amorphous background. As shown in Fig. 4.26b, subsequent heating of the sample up to 155 K does not produce any further structural changes. Above 155 K, the previously formed "glacial phase" begins to transform into the fully-ordered crystalline phase of *n*-butanol, that is undoubtedly observed at 180 K. Let us remark that the emergent crystalline peaks at 127 K in the "glacial phase" are exactly the main Bragg peaks of the stable crystal phase.

In summary, these X–ray diffraction experiments [Shmyt'ko 2010] clearly support our earlier observations by calorimetry (see Figs. 4.3, 4.4 and 4.6) and the corresponding conclusions, as we will discuss more in detail in section 4.6.1.

4.5.2 Brillouin scattering

To investigate the phase diagram of n-butanol, another experimental technique employed was Brillouin-scattering experiments [Hassaine 2009], which were conducted by Dr. Rafael J. Jiménez-Riobóo, in the Instituto de Ciencia de Materiales de Madrid, Consejo Superior de Investigaciones Científicas (ICMM-CSIC), Madrid.

4.5.2.1 Experimental setup and measuring procedures

High-resolution Brillouin scattering experiments in the temperature range 77 K– 300 K were conducted by using an Ar^+ ion laser (wavelength = 514.5 nm) and a Sandercock-type 3+3 tandem Fabry-Pérot interferometer.

A volume of 0.4 ml of *n*-butanol was extracted using a virgin syringe from the bottle and rapidly introduced in a rectangular cuvette with transparent windows (11×41 mm^2) and an optical path of 1 mm (21/g/1 Starna®); the n-butanol sample occupied the whole cuvette so that no air was left inside. The cuvette was closed using the Teflon stopper provided and placed inside an optical cryostat. In order to control the quality of the n-butanol sample, the refractive index of the liquid was determined by using a standard Abbe refractometre (Krüss) obtaining $n^{D}_{22.8°C} = 1.3980 \pm 0.0001$. This value confirms the quality and purity of the employed n-butanol. Low temperatures were achieved by using liquid nitrogen. An ITC-4 temperature controller (Oxford Instruments) was used in the experiments, obtaining a temperature stability of ±0.05 K.

4.5.2.2 Results

The whole temperature-dependent evolution of the HRBS phonon peaks obtained in backscattering geometry is presented in Fig. 4.27. The temperature behaviour of the longitudinal acoustic phonon has been obtained on heating and starting in the glass phase at 90 K (circles in Fig. 4.27). It is clear that there are at least four structural transitions in the temperature range investigated. Starting from the lowest temperatures, the first one is the observed transition from the glass phase to the viscous liquid at about 110 K; then, the structural transition from the viscous liquid to a crystalline-like state (presumably, the so-called "glacial phase") at about 132 K; an anomalous temperature dependence of the longitudinal phonon is seen to begin at 156 K, that softens at 174 K; and finally the transition to the liquid at 184 K.

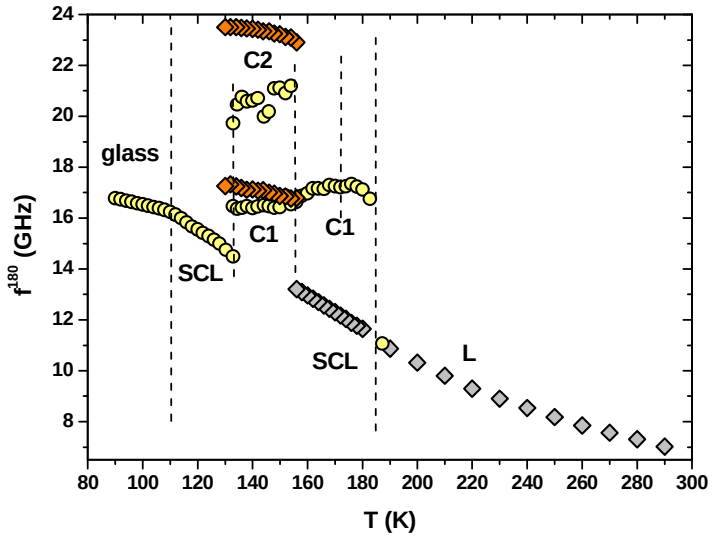

Fig 4.27 Brillouin backscattering frequency shift(s) as a function of temperature for the different phases of *n*-butanol. The circles represent the heating run beginning at 90 K from the glass state. The diamonds correspond to the cooling run of the liquid followed by crystallization below 156 K. The different phases correspond to: glass, supercooled liquid (SCL), liquid (L); C1 and C2 are the phonon peaks observed in the crystalline phases, see Fig. 5a,b in [Hassaine 2009]. The lines mark the temperatures where the different phase transitions or changes take place.

On the other hand, when the sample is cooled down slowly from room temperature (diamonds in Fig. 4.27), only one structural transition is observed in the temperature range 290 K > T > 130 K. An excellent agreement is found between the frequency values in the liquid phase obtained by either heating or cooling. Also the extrapolation of the SCL curve obtained on cooling fits extremely well with the SCL curve obtained on heating from the glass. In both cases there are two phonon peaks (C1 and C2) coexisting for the obtained crystalline phases in the intermediate temperature range.

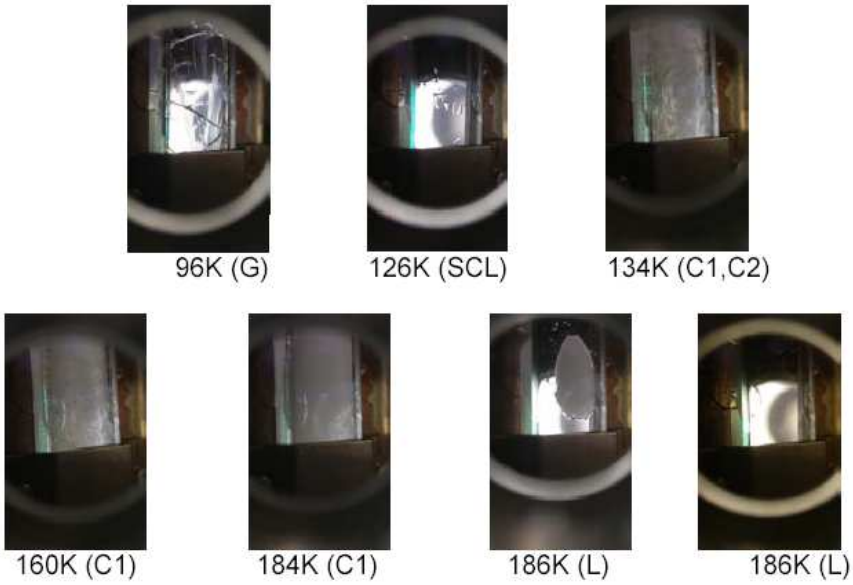

Fig 4.28 Optical photographs at different temperatures showing the different aspects of the sample throughout the different phases. The sample is found inside the cryostat. The round bright features in the photographs correspond to the frame of the inner window of the cryostat and are brighter when the sample is transparent and the light from the laboratory can come through.

Fig. 4.28 shows the evolution of the sample on heating after quenching from room temperature to 90 K. At 90 K the sample is completely transparent, as expected for a sample in the glassy state, except for some macroscopic cracks arising from stresses between the n-butanol sample and the cuvette surface due to different thermal expansion coefficients. At 126 K the sample is in the supercooled liquid state after passing through the glass transition (exhibiting a kink-like anomaly). In this case the sample is completely transparent and no cracks are visible, as expected for a liquid. When the sample goes below 130 K, entering the so called "glacial phase", something dramatically changes. The picture taken at 134 K is a very good witness of it. The sample is no more transparent, what is in clear contradiction with a typical liquid or glass, since both of them are isotropic. If there would be a liquid state, it should be only a part of the whole, because opacity is a clear sign either of micro cracks, what

could hardly be understood in a liquid, or of the existence of microcrystalline structures embedded in a liquid matrix, or of the existence of a unique non-cubic polycrystalline phase. At higher temperatures (see the photograph at 160 K) the picture does not change significantly, even though it is well established the existence at about 156 K of a phase transition from the so called "glacial" phase to the crystalline stable phase. At 184 K the sample seems to be more homogeneous just before the beginning of the melting process, what is clearly visible in the photographs taken at 186 K at two different times.

4.6 Discussion

4.6.1 The so-called "glacial state" of n-butanol

The possible existence of first-order transitions between two liquid states of a single-component substance or, more generally, between two distinct amorphous states of that substance, has been recently under active discussion. This unexpected phenomenon was termed *polyamorphism* [Angell 1995, Senker 2001], by analogy with the term "polymorphism" referred to solids presenting different crystalline structures.

The first "polyamorphic" transition for a *molecular* glass-forming liquid was reported to occur in triphenyl phosphite (TPP) by Kivelson and co-workers [Ha 1996]. They observed a new solid phase denoted by them as "glacial phase", obtained by a first-order, exothermic transformation from the supercooled-liquid state of TPP, either by slowly (~ 0.5 K/min) heating the glass above its glass-transition temperature ($T_g \approx 205$ K) or by an isothermal transformation of the supercooled liquid within the temperature range around 210–230 K. By further heating this "glacial phase", another first-order transition into the crystal state was observed at about 237 K. If the supercooled liquid was heated much faster instead, it directly crystallized around 240–245 K. All this phenomenology was confirmed by Rössler and co-workers [Wiedersich 1997] through further experiments of DSC calorimetry, Brillouin scattering, and dielectric and nuclear magnetic resonance.

There is no consensus in the literature whether the glacial state is a crystalline or an amorphous structure. Some groups have proposed to explain its origin as a defect-ordered phase within the theory of frustration-limited domains [Cohen 1996, Demirjian 2001, Alba-Simionesco 2000], others as a second amorphous state [Senker 2001], related to the existence of a liquid-liquid transition [Tanaka 2004, Kurita 2004, 2005], and also that it may be a liquid-crystal or a plastic-crystal state [Johari 1997]. On the other hand, Hédoux *et al*. have conducted experiments of Raman spectroscopy [Hédoux 1998], X-ray diffraction [Hédoux 1999], and differential scanning calorimetry (DSC) [Hédoux 2002], and have interpreted this transformation process as an aborted crystallization because of a high nucleation rate in a temperature range where the crystal growth is low. Therefore the "glacial state" would be rather a mixture of nanocrystallites and untransformed supercooled liquid.

More recently, the same case of a new solid phase (presumably amorphous) was reported by B.V. Bol'shakov and A. G. Dzhonson [Bol'shakov 2003, 2005] in n-butanol at ambient pressure, from the analysis of free radical oxidation kinetics: under isothermal conditions in the range 130–160 K, the supercooled liquid transformed gradually into a white or slightly opalescent solid phase. Kurita and Tanaka [Kurita 2005] observed the pattern evolution of the supercooled liquid of n-butanol to the new "glacial state" during first-order irreversible transformation at around 120 K, applying phase-contrast microscopy, as also they had done with TPP. The transformation of one supercooled liquid to a glassy state of another liquid —with an estimated T_g=133 K, around 15–20 K above the conventional glass transition of *n*-butanol– was interpreted as a new evidence of a liquid-liquid transition (hence, of polyamorphism). It has been proposed [Kurita 2004] that a liquid-liquid transition can exist in various molecular liquids which have a tendency to form long-lived locally-favored structures due to the anisotropic interaction.

Again, these interpretations of the "glacial state" as an exotic defect-ordered phase or as a result of a liquid-liquid transition, were contested by Hédoux and co-workers [Wypych 2007] on the basis of Raman-scattering experiments only. They claimed, as in the case of TPP, that the so-called "glacial phase" was nothing else that a mixed crystal-liquid state, not a new amorphous state.

With the aim of shedding light on these debated issues, we have investigated through non-commercial calorimetry (section 4.1), elasto-acoustic Brillouin (section 4.5.2) and X-ray (section 4.5.1) experiments the phase diagram of n-butanol, and we have measured the specific heat for its three different states in the wide range temperature (77-220 K), as presented before in Fig 4.7. Furthermore, we have also measured the specific heat and the thermal conductivity at low temperature for its three different states, glass, crystal and so-called "glacial" states, which will be presented in the next chapter 5.

The three kinds of experiments have allowed us to exhaustively investigate the previously reported "glacial phase", obtained from the undercooled liquid at temperatures ranging between 122 K and 140 K. At higher temperatures, typically starting above 155 K, this glacial phase transforms into the stable crystalline state of n-butanol.

All our calorimetric and thermodynamic studies pointed to the conclusion that it is neither a second amorphous state (we do not see any trace of a second glass transition), nor a distinct (metastable or disordered) crystalline phase, but rather a mixture of nanocrystalline grains and a disordered matrix, either liquid or solid. This mixture state could be likely due to an aborted crystallization process because of a high nucleation rate in a temperature range where the crystal growth is low [Hédoux 2002, Wypych 2007]. As a matter of fact, when we further force to interrupt the "*glaciation*" process by entering helium exchange gas in the internal vacuum chamber at the right moment, a fraction of the sample exhibits a glass-transition feature (at the very same glass-transition temperature of the canonical glass, as shown in the inset of Fig. 4.6) followed by a smaller exothermic process at 135–140 K (see curves e and f in Fig. 4.6), that is the continuation of the interrupted "*glaciation*" process. In any case, all these "mixture phases" exhibit first-order transitions into the stable crystalline state around 160 K.

Brillouin-scattering measurements have also shown the presence of a mixture of elasto-acoustic peaks in the so-called glacial state (see Fig. 4.27). One of those Brillouin peaks (C2) clearly corresponded to the same acoustic peak of the stable crystal state, obtained by isothermal crystallization at 167 K. Moreover, it is worth noting that this crystalline peak C2 is more intense and better defined, the

higher the temperature of the *glaciation* process is [Hassaine 2009]. This is in full agreement with the calorimetric interpretation, namely that the *glaciation* is only a first step of frustrated or aborted crystallization, due to a low crystalline growth rate. This rate increases gradually with temperature, producing less small nanocrystallites (and/or a smaller disordered volume of the sample) with temperature increase. Eventually, above 160 K the substance is able to crystallize completely.

Finally, our X-ray diffraction experiments (section 4.5.1) have even more clearly demonstrated and supported the same interpretation that the so-called "glacial phase" is not a second amorphous state, but rather the result of a frustrated crystallization process that produces many nanocrystallites embedded in a more or less disordered matrix. In all our experiments, we have not seen any trace of a second glass transition, nor of a second amorphous state, as claimed in the literature [Tanaka 2005, Bol'shakov 2005].

4.6.2 Thermodynamic properties

In this section, we present and discuss the calorimetric and thermodynamic results found in the different butanol isomers, at the glass and crystal melting transitions. In particular, we will calculate the so-called fragility or steepness index m, and check whether some proposed correlations found in the literature of the thermodynamic magnitudes with the fragility of the glass-forming liquid. These thermodynamic data will be completed by the determination of the residual entropy (i.e., the entropy of the glass S_g at $T = 0$ K) in the next chapter 5 (section 5.6.4).

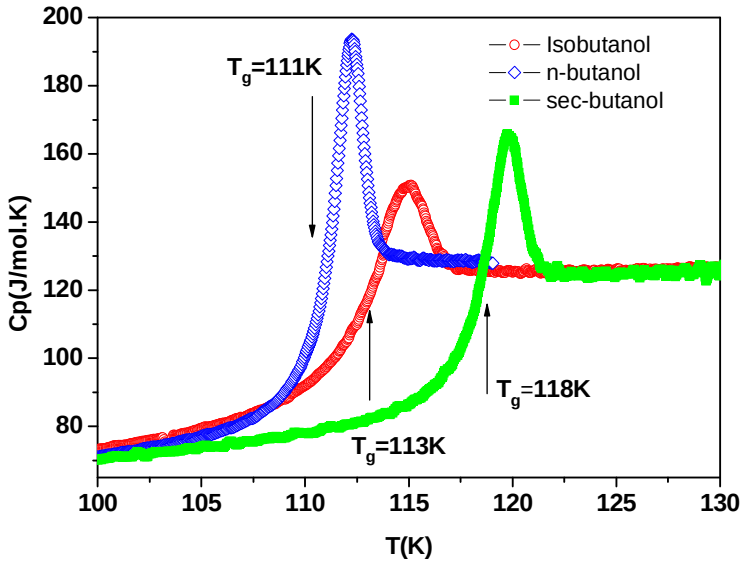

Fig 4.29 Specific heat of the three obtained butanol glasses by slow cooling (–0.2 K/min) and heated in all cases by the same power (1 K/min), showing the glass transition of each one: n-butanol glass (blue symbols), T_g=111K; isobutanol glass (red symbols), T_g=113K; and sec-butanol glass (green symbols), T_g=118K.

Fig 4.29 shows the glass transition of the three position isomers of butanol, obtained by using the same experimental conditions, and especially by subjecting the samples to the same thermal treatment (cooling rate about –0.2 K/min around T_g and heating rate about 1 K/min around T_g), knowing that the experimental glass-transition temperature T_g can be dependent on the cooling rate: T_g typically increases with increasing cooling rates.

As we can see in Fig 4.29, the specific heat values of the three substances n-, sec-, and isobutanol are almost identical, but the overshoot at the glass transition differs from one to another, and it is more expressed in n-butanol. The discontinuity ΔC_p at T_g is also slightly larger in n-butanol but similar in the two other isomers. After the transitions, the specific heat of the supercooled liquid (SCL) is also slightly higher in n-butanol compared to sec- and isobutanol, which have exactly the same specific heat.

As indicated in chapter 2, many theories and models were proposed to establish a link between kinetic or relaxation dynamics and thermodynamics. Many attempts have been made to correlate the kinetic properties of undercooled

liquids with their thermodynamic behavior around the glass transition. The experimental results for T_g have been correlated with molecular structure parameters, and other physical properties such as melting points, boiling points and fragility. Wang and Angell [Wang 2003, 2006] found a good correlation between kinetic and thermodynamic fragilities (the so-called *m* values of the liquids) for more than 50 glass-forming materials, with very few exceptions, where they characterize kinetics by their activation energies at T_g and, on the thermodynamic side, by the discontinuity ΔC_p at T_g, and the melting enthalpy ΔH_m.

Thus, we have calculated the fragility index *m* for the different glass-forming liquids of butanol isomers, n-butanol, sec-butanol and isobutanol, using the empirical equation [Wang 2006]:

$$m = 56\frac{T_g \Delta C_p(T_g)}{\Delta H_m} \tag{4.2}$$

In the previous sections we have obtained $\Delta C_p(T_g)$ for the different glasses (see Figs. 4.8, 4.12 and 4.24). Now we will present the method used and will graphically show the procedure followed to calculate the enthalpy and/or the entropy of melting.

In an ideally adiabatic system, the enthalpy corresponds to the amount of heat supplied ($Q = P_{total} \cdot \Delta t$), where P_{total} is given by:

$$C_p\left(\frac{dT}{dt}\right) = P_{total}\ ; \quad \text{and hence,} \qquad \Delta H = \int_{t_1}^{t_2} C_p(T)\left(\frac{dT}{dt}\right) dt \tag{4.3}$$

Considering that the specific heat C_p (T) does not vary considerably in the range of transition, the average value of C_p is taken at the temperature corresponding to the center of the transition region, t_1 and t_2 being the onset and the end of the wide range of the transition, as indicated in Fig 4.30.

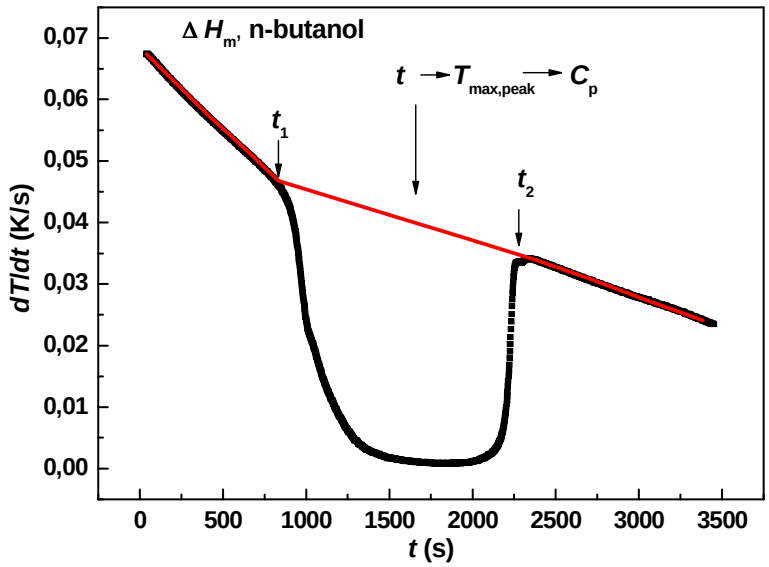

Fig 4.30 Melting transition observed by representing dT/dt vs the experimental time t. The mean value C_p is taken at the temperature corresponding to the midpoint of the transition, t_1 and t_2 are the onset and the end of the wide range of the transition, and the red curve represents the background of the transition.

After having systematically followed the same procedure to determine $\Delta C_p(T_g)$ and ΔH_m, we have calculated the fragility index m. The so calculated values m_{calc} are presented in Table 4.1, together with some values m_{meas} obtained from the literature for n-butanol [El Goresy 2008] and sec-butanol [Jakobsen 2008], in both cases measured in dielectric experiments. No good agreement is found between measured and calculated values, at least for these two cases. Moreover, it is difficult to understand the corresponding increase in the fragility index going from n-butanol to sec-butanol, when the latter is the best glass-former of all butanols.

Table 4.1: Relevant calorimetric and thermodynamic data of glass transition and crystal melting for the different butanol isomers. The fragility index m_{meas} is taken from measured values of dielectric experiments in the literature, and m_{calc} is calculated by eq. (4.2). The effective number of beads N_{beads} is calculated by eq. (4.4).

Butanol isomer	T_g (K)	T_m (K)	$\Delta C_p(T_g)$ (J/mol·K)	ΔS_m (J/mol·K)	$\Delta H(T_m)$ (kJ/mol)	m_{mea}	m_{calc}	$N_{beads} = \Delta S_m/1.68R$
n-butanol	111	183	48±2	51.14	9.28	59	32	3.6
sec-butanol	118	184.7	40±2	32.32	5.97	63	44	2.3
tert-butanol	-	293	-	39.5	6.65			-
Isobutanol	113	168	40±2	37.90	6.36		40	2.6

Another interesting concept, traditionally used to rationalize the thermodynamic magnitude for the glass transition and crystal melting processes, is the number of ‘‘beads’’, i.e. more or less spherical and compact units that constitute the molecule and account for their configurational degrees of freedom. Wolynes and co-workers [Lubchenko 2003, Stevenson 2005] proposed counting the beads from the entropy of melting and found an entropy of fusion per particle for Lennard–Jones spheres, $S_{LJ}=1.68k_B$. They proposed a general relation:

$$N_{beads} = S_m/1.68R \tag{4.4}$$

By making use of equation (4.4), we have obtained the corresponding estimations of the number of configurational beads per molecule, for glasses of n-butanol, sec-butanol and isobutanol, that are also shown in Table 4.1.

In a previous work [Ramos 2011], we observed an increase in N_{beads} with increasing chain length for the first primary monohydroxy alcohols (methanol, ethanol, n-propanol and n-butanol). However, this trend is broken for secondary alcohols, as sec-butanol or isobutanol, where the intermolecular connections change significantly.

In summary, by comparing kinetic and thermodynamic data for this model system of butanol isomers, and other monohydroxy alcohols, we found that the proposed phenomenological correlations proposed for the fragility of supercooled

liquids is not fulfilled for these – and probably other– hydrogen-bonded liquids, which behave kinetically as strong liquids but thermodynamically as fragile liquids. For them, the enthalpy/entropy of crystal melting and the specific-heat jump at the glass transition does not seem to directly correlate with the kinetic fragility index of the supercooled liquid.

References

[Alba-Simionesco 2000]: Ch. Alba-Simionesco and G. Tarjus, Europhys. Lett. 52, 297 (2000).

[Angell 1995]: C. A. Angell, Science 267, 1924 (1995).

[Andon 1971]: R. J. L. Andon, J. E. Connett, J. F. Counsell, E. B. Lees, and J. F. Martin, J. Chem. Soc. (A), 661 (1971).

[Bol'shakov 2003]: B.V. Bol'shakov and A.G. Dzhonson, Dokl. Phys. Chem. 393, 318 (2003).

[Bol'shakov 2005]: B.V. Bol'shakov and A.G. Dzhonson, J. Non-Cryst. Solids. 351, 444 (2005).

[Counsell 1965]: J. F. Counsell, J. L. Hales and J. F. Martin Trans. Faraday Soc 61, 1869 (1965).

[Cohen 1996]: I. Cohen, A. Ha, X. Zhao, M. Lee, T. Fischer, M. J. Strouse, and D. Kivelson, J. Phys. Chem. 100, 8518-8526 (1996).

[Demirjian 2001]: B. G. Demirjian, G. Dosseh, A. Chauty, M. Ferrer, D. Morineau, C. Lawrence, K. Takeda, D. Kivelson, and S. Brown, J. Phys. Chem. B 105, 2107 (2001).

[El Goresy 2008]: T. El Goresy and R. Böhmer, J. Chem. Phys. 128, 154520 (2008).

[Elliott 1990]: S. R. Elliott, *Physics of Amorphous Materials*, 2nd ed. (Longman, 1990).

[Gutzow 1995]: I. Gutzow and J. Schmelzer, *The Vitreous State*, (Springer, Berlin (1995).

[Ha 1996]: A. Ha, I. Cohen, X. Zhao, M. Lee, and D. Kivelson, J. Phys. Chem. 100, 8518 (1996).

[Hassaine 2009]: M. Hassaine, R. J. Jiménez-Riobóo, I. V. Sharapova, O. A. Korolyuk, A. I. Krivchikov and M. A. Ramos, J. Chem. Phys. 131, 174508 (2009).

[Hédoux 1998]: A. Hédoux, Y. Guinet, and M. Descamps, Phys. Rev. B 58, 31 (1998).

[Hédoux 1999]: A. Hédoux, O. Hernandez, J. Lefèbvre, Y. Guinet, and M. Descamps, Phys. Rev. B 60, 9390 (1999).

[Hédoux 2002]: A. Hédoux, Y. Guinet, M. Foulon, and M. Descamps, J. Chem. Phys. 116, 9374 (2002).

[Jakobsen 2008]: B. Jakobsen, C. Maggi, T. Christensen and J. Dyre, J. Chem. Phys. 129, 184502 (2008).

[Johari 1997]: G.P. Johari and C. Ferrari, J. Phys. Chem. B 101, 10191 (1997).

[Kurita 2004]: R. Kurita and H. Tanaka, Science 306, 845 (2004).

[Kurita 2005]: R. Kurita and H. Tanaka, J. Phys.: Condens. Matter. 17, 293 (2005).

[Lubchenko 2003]: V. and P.G. Wolynes, J. Chem. Phys. 119, 9088 (2003).

[McGregor 2006]: P. A. McGregor, D. R. Allan, S. Parsons, S. J. Clark Acta Crystallogr Sect B: Struct Sci B 62, 599 (2006).

[Nan 2007]: Z. Nan and Z.C. Tan, J. Therm. Anal. Cal 87, 539 (2007).

[Oetting 1963]: F. L. Oetting J. Phys. Chem, 67, 2757. (1963).

[Ramos 2006]: M.A. Ramos, I.M. Shmyt'ko, E.A. Arnautova, R.J. Jiménez-Riobóo, V. Rodríguez-Mora, S. Vieira, and M.J. Capitán, J. Non-Cryst. Solids 352, 4769 (2006).

[Ramos 2011]: M. A. Ramos, B. Kabtoul and M. Hassaine, Philosophical Magazine 91, 1847 (2011).

[Shmyt'ko 2010]: I. M. Shmyt'ko, R. J. Jiménez-Riobóo, M. Hassaine and M. A. Ramos, J. Phys. Condens.Matter 22, 195102 (2010).

[Senker 2001]: J. Senker and E. Rössler, Chem. Geol. 174, 143 (2001).

[Stevenson 2005]: J.D. Stevenson and P.G. Wolynes, J. Phys. Chem. B 109, 15093 (2005).

[Tanaka 2004]: H. Tanaka, R. Kurita, and H. Mataki, Phys. Rev. Lett. 92, 02570 (2004).

[Wang 2003]: L. M. Wang and C. A. Angell, J. Chem. Phys. 118, 10353 (2003).

[Wang 2006]: L. M. Wang, C. A. Angell, R. Richert, J. Chem. Phys. 125, 074505 (2006).

[Wiedersich 1997]: J. Wiedersich, A. Kudlik, J. Gottwald, G. Benini, I. Roggatz, and E. Rössler, J. Phys. Chem. B 101, 5800 (1997).

[Wypych 2007]: A. Wypych, Y. Guinet, and A. Hédoux, Phys. Rev. B 76, 144202 (2007).

5 Thermal properties at low temperature of butanol isomers

As described in chapter 2, glasses or amorphous solids exhibit *universal* thermal properties at low temperatures, which are very different from those of crystalline solids. Let us remember the behavior of specific heat at low temperature. Below 1 K, the specific heat C_p of glasses is much larger than the corresponding values found in their crystalline counterparts. C_p depends approximately linearly on temperature in clear contrast to the cubic dependence observed in crystals. Above 1 K, C_p deviates strongly from the expected $C_{Debye} \propto T^3$ dependence, exhibiting broad maximum in C_p / T^3 which is directly related to the so-called *boson peak* observed by neutron or Raman vibrational spectroscopies. Thermal conductivity also presents *universal* properties at low temperatures, which are very different from those of crystalline solids. Below 1 K, the thermal conductivity κ of glasses is orders of magnitude lower than the corresponding values found in their crystalline counterparts. In the same temperature range of the broad maximum in C_p/T^3, the thermal conductivity exhibits a *plateau*.

In this thesis we have conducted experiments at low temperatures with the four position isomers (also named as chemical or structural isomers) of butanol (see chapter 3, Fig 3.4), though only in three of them we were able to obtain the glass state. Also in three out of the four cases, we were able to obtain the fully crystalline state and measured their specific heat as a useful reference. This will allow us to carry out a comparative study for different glasses of the same substance, butanol, in order to assess the effects of changing the spatial arrangement of atoms and the position of hydrogen bonds in the lattice on the low-temperature thermal and elastoacoustic properties around the universal *boson peak* feature in glasses.

In this chapter we present specific-heat $C_p(T)$ measurements at low temperatures, in the temperature range 1.5–30 K, for all the available solid states from different isomers butanol: for glasses of n-butanol, sec-butanol and isobutanol, for the crystals of n-butanol, isobutanol and tert-butanol, as well as

for the "glacial state" of n-butanol. We will also present thermal conductivity $\kappa(T)$ measurements of the different isomers butanol glasses between 2 and 200 K, as well as Brillouin-scattering measurements of both longitudinal and transverse sound velocities measured down to 10 K, performed in other laboratories by some collaborators.

Finally, we will combine these low-temperature specific heat C_p data with those shown in the previous chapter at higher temperatures in order to assess the excess entropy of these glasses over their correspondent crystals, and hence determine its Kauzmann temperatures and their "residual entropy" at zero Kelvin.

5.1 Experimental results on n-butanol

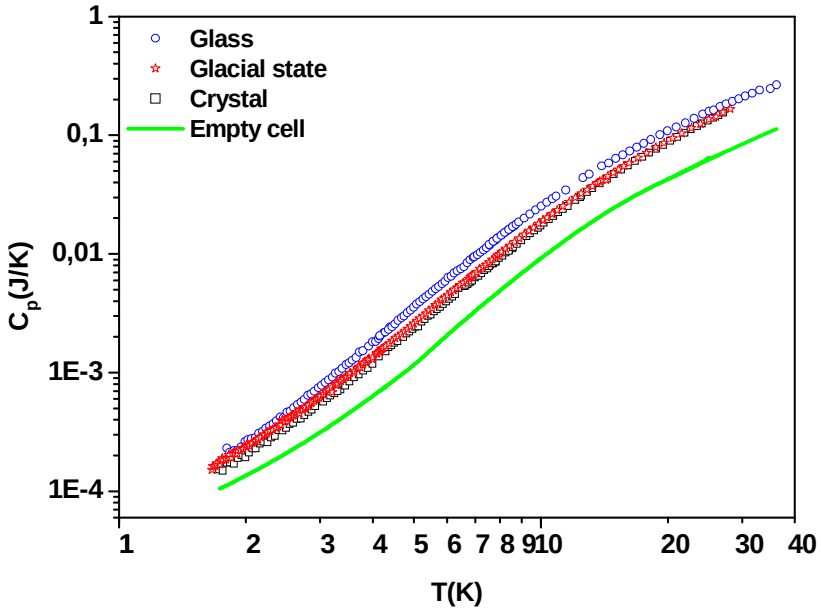

Fig 5.1 A log-log representation of the total heat capacity C_p for the three measured different states of n-butanol (glass, crystal and "glacial state") plotted together with the heat capacity of the empty cell.

In chapter 4 we have characterized the phase diagram of n-butanol and measured the specific heat of its different phases at nitrogen temperatures. We prepared again its solid phases in the same thermal conditions as before, and then we replaced the liquid nitrogen by liquid helium in our cryostat, to measure the specific heat of the desired solid state at low-temperatures, choosing between the two relaxation methods described in chapter 3.

As described in section 3.5.2, it is important to check that the heat capacity of the sample is significantly greater than that of the empty cell. As a real example, in Fig 5.1 we present the heat capacity of the empty cell (addenda) together with the total heat capacity of the three measured phases of n-butanol. The total heat capacity of the n-butanol crystal (the smallest one), is still clearly high compared to the heat capacity of the empty cell (addenda) down to 2 K, the lowest temperatures where the heat capacity is small and the contribution of the addenda is most important. After subtracting the heat capacity of the empty cell and dividing by the corresponding amount of butanol sample, the required molar specific heat can be determined.

In Fig 5.2 we present the specific-heat data for the three solid phases of n-butanol, i.e. glass, "glacial" and crystal ones, in a typical C_p/T^3 plot. This representation emphasizes how well the expected cubic behavior from the Debye model for C_p is fulfilled at $T \leq 4$ K for the fully-ordered crystal, in clear contrast with the broad maximum in C_p/T^3 at around 5 K (the universal "boson peak") exhibited by the glass in the same low-temperature range. The so-called "glacial phase" is seen to present an intermediate quantitative behavior, but qualitatively is neither that of a fully-ordered crystal nor that typical of a glass or amorphous solid.

As anticipated in Fig. 5.2, the specific heat of the crystal state of n-butanol follows at low temperature the expected behavior from the Debye model, $C_p = C_D T^3$ (a straight line passing through zero), with C_D=1.40±0.03 mJ/mol·K^4, as shown by the linear fit (dashed line) in the C_p/T vs T^2 plot shown in Fig. 5.3.

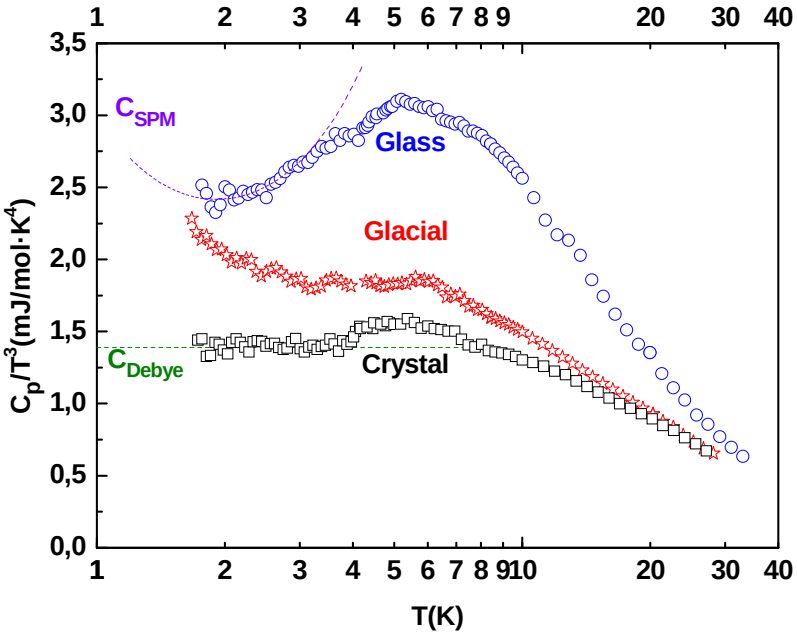

Fig. 5.2 Molar specific heat plotted as C_p/T^3 for the three obtained phases of n-butanol: glass (circles), "glacial" (stars) and crystal (squares). The results from the fits to the Debye model for the crystal and to the SPM for the glass (see Fig. 5.3) are indicated with dashed lines.

We have also determined the Debye temperature Θ_D, by using the "molecular" definition of the Debye temperature Θ_D. By *molecular* Debye temperatures, we mean considering in the Debye formula the number density of molecules (assumed to be the primitive cells) per unit volume n rather than the atomic number density, as is usually done . We are therefore making use of the Debye approximation for the (three) acoustic branches and Einstein approximation for the optical branches, as described in [Ashcroft 1976]:

$$C_D \approx 234\left(\frac{Nk_B}{\rho\Theta_D^3}\right) \tag{5.1}$$

Hence, by making use of this definition and the obtained C_D from the fit, we obtain $\Theta_D = 112 \pm 1$ K for crystal n-butanol.

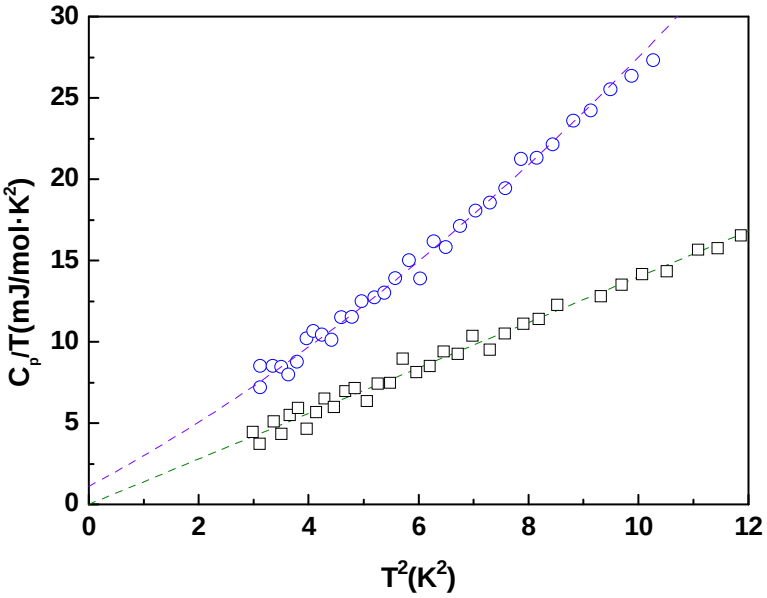

Fig. 5.3 Experimental data for the glass (circles) and crystal (squares) states of n-butanol at the lowest temperature, in a C_p/T vs T^2 representation, together with the corresponding fits to the Debye model (crystal) and Soft-Potential Model (glass), as described in the text.

On the other hand, in order to analyze the specific-heat data of glasses we are going to make use of the SPM (sec.2.2.2).A simple fit to the SPM for the specific heat of the glass state is also shown in Fig. 5.3. In the original version of the SPM [Karpov 1983, Ilin 1987], the *soft* vibrations responsible for the broad maximum in C_p/T^3 are predicted to rise as $C_p \propto T^5$ at the lower temperature side of the "boson peak". Therefore, it has been suggested [Ramos 2002, 2003] that the most simple and reasonable fit of low-temperature specific-heat data to the SPM is done by using a quadratic polynomial ($C_p = C_{TLS}\, T + C_D\, T^3 + C_{sm}\, T^5$, see eq 2.42). To be consistent, the fit should be performed [Ramos 2003] very approximately in the temperature range $0 < T < (3/2)T_{min}$, where T_{min} is the temperature of the minimum value of C_p/T^3, which marks the crossover from the temperature range dominated by tunneling states to that dominated by *soft* modes (quasiharmonic vibrations). From now on, we will denote with a star label those coefficients obtained out from these direct polynomial fits of the specific-heat measurements: $C_p = C^*_{TLS}\, T + C^*_D\, T^3 + C^*_{sm}\, T^5$.

By following the described procedure for n-butanol, and considering the minimum at T_m = 1.9 K, we obtain from the polynomial fit shown in Fig. 5.3: C_p [mJ/mol·K] = 1.11 (± 0.58) T + 1, 81 (± 0.21) T^3 + 0, 083 (± 0.017) T^5.

For the glass phase, we have also determined the Debye temperature Θ_D through eq. (5.1). By making use of C_D^*=1.81 mJ/mol·K^4, we obtain Θ_D = 103 ± 2 K for the glass of n-butanol.

We will summarize all these obtained data and others in Tables 5.1 and 5.2.

5.2 Experimental results on sec-butanol

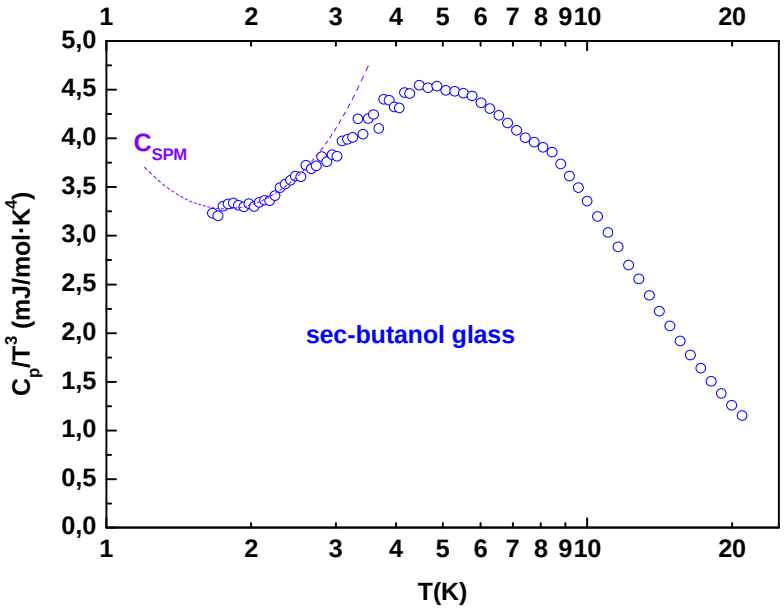

Fig. 5.4 Low-temperature specific heat in a semi logarithmic C_p/T^3 vs T plot for sec-butanol, with the corresponding fit to the Soft-Potential Model (glass), as described in the text.

As reported in chapter 4, sec-butanol showed no tendency to crystallize, and we were not able to obtain its crystalline state. Therefore, we have measured its glass state at low-temperature, as shown in Fig 5.4 in the typical C_p/T^3 vs T plot. The broad maximum (*boson peak*) of the sec-butanol glass is significantly higher and its peak position slightly lower ($C_{p,max}$ = 4.5 mJ/mol·K^4, T_{max} = 4.8 K) than in

n-butanol ($C_{p,max}$ = 3 mJ/mol·K^4, T_{max} = 5.4 K). We summarize all these data for glasses in Table 5.2.

As previously mentioned, to analyze the specific-heat data of the sec-butanol glass through the SPM, the fit should be performed very approximately in the temperature range $0 < T < (3/2)T_{min}$, where T_{min} is the temperature of the minimum value of C_p/T^3. From the experimental data shown in fig 5.4, with the minimum at T_m = 1.7 K, and by systematically using the same procedure as before, we obtain the polynomial fit, shown in Fig. 5.5, C_p [mJ/mol·K] = 2,20 (±1.00) T + 1,91 (±0.42) T^3 + 0,214 (±0.042) T^5 for the glassy state of sec-butanol.

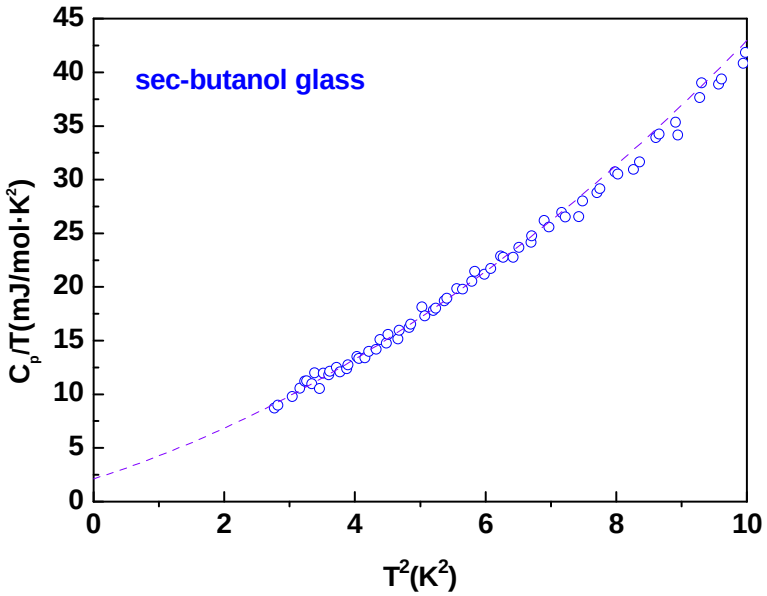

Fig. 5.5 Experimental data for the sec-butanol glass at the lowest temperatures, in a C_p/T vs T^2 representation.

Once C_D^* has been obtained (C_D^* = 1.91 mJ/mol·K^4), we have determined the Debye temperature Θ_D by using the "molecular" definition of the Debye temperature Θ_D described in section 5.1, obtaining Θ_D = 101 ± 2 K for sec-butanol glass.

5.3 Experimental results on tert-butanol

Contrary to the previously measured butanol isomers n- and sec-butanol, tert-butanol is not a good glass former. We were not able to obtain its glass state in spite of using the maximal rate of cooling allowed by our experimental system. Nevertheless, we have measured the specific heat of its stable crystal (crystal II) below 285 K.

Fig 5.6 shows the specific heat data of the crystal (crystal-II) of tert-butanol, plotted in the typical representation C_p/T^3 vs T, together with the corresponding fit to the Debye model. The specific heat of tert-butanol crystal follows the expected Debye behavior at low temperatures, showing the usual "shallow maximum" of crystals at $T = 10$ K.

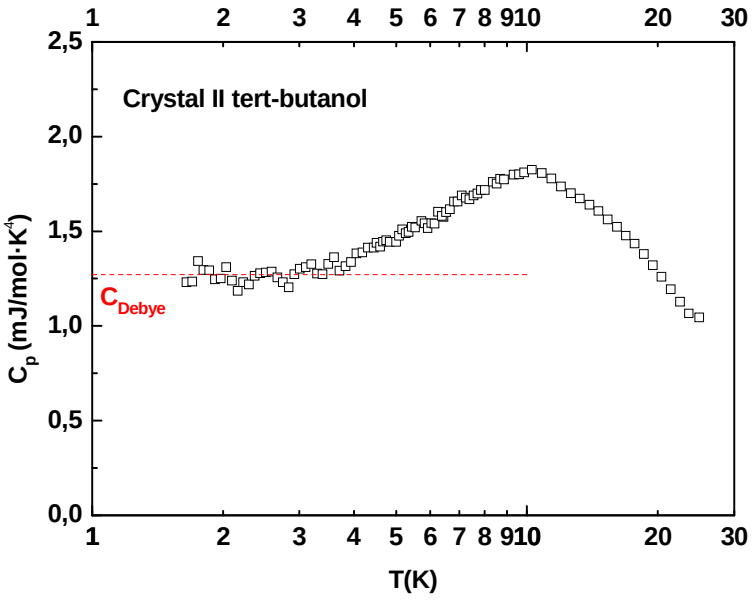

Fig 5.6 Low-temperature specific heat in a semi logarithmic C_p/T^3 vs T plot for the sec-butanol crystal, with the corresponding fit from the Debye model.

Fig. 5.7 shows the specific heat of the crystal (crystal-II) of tert-butanol that follows at low temperature the expected behavior from the Debye model, C_p =

$C_D T^3$, (a straight line passing through zero) with C_D=1.28±0.03 mJ/mol·K^4, as shown by the linear fit (dashed line) in the C_p/T vs T^2 plot.

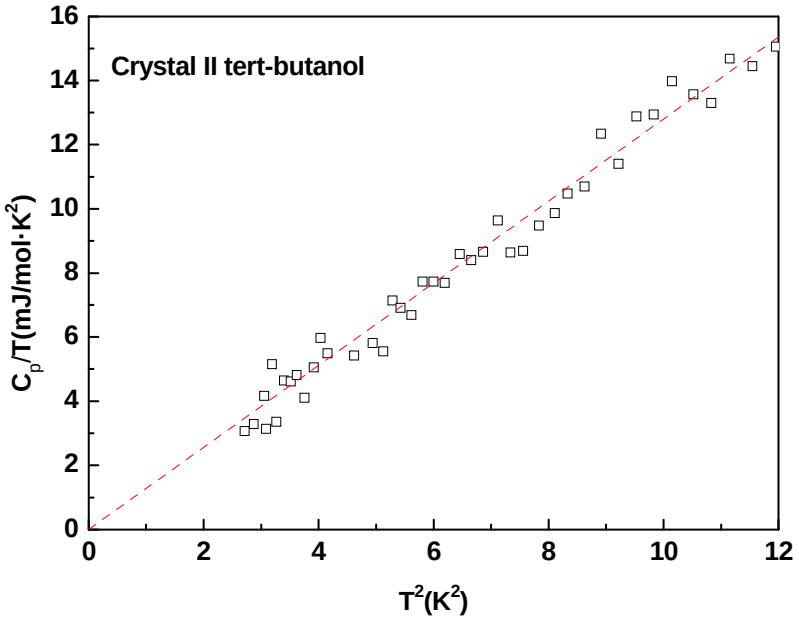

Fig 5.7 C_p/T vs T^2 representation of the experimental data for the tert-butanol crystal-II at the lowest temperatures.

We have also determined the Debye temperature Θ_D, by using the "molecular" definition of the Debye temperature Θ_D and the obtained C_D from the corresponding fit, finding Θ_D = 115 ± 2 K for this crystal.

5.4 Experimental results on isobutanol

Finally, isobutanol is a good glass former, and also crystallizes below its melting temperature as reported in chapter 4. We prepared its glass and crystalline states, following the same procedures employed at nitrogen temperatures. In the case of the crystalline state, we specify that the crystal measured at low temperatures was previously subjected to the thermal cycle below its melting temperature described in Fig. 4.22.

In Fig. 5.8 we present the specific-heat data for the glass and crystal of isobutanol, in the typical C_p/T^3 plot. The specific heat of the crystal state of isobutanol exhibits at $T \leq 5$ K the expected cubic behavior from the Debye model for fully-ordered crystals. Again, at temperatures below 10 K, the isobutanol glass presents the typical broad maximum in C_p/T^3 of glasses, often called the *boson peak*. One can see that this boson peak is significantly higher than in n-butanol and sec-butanol.

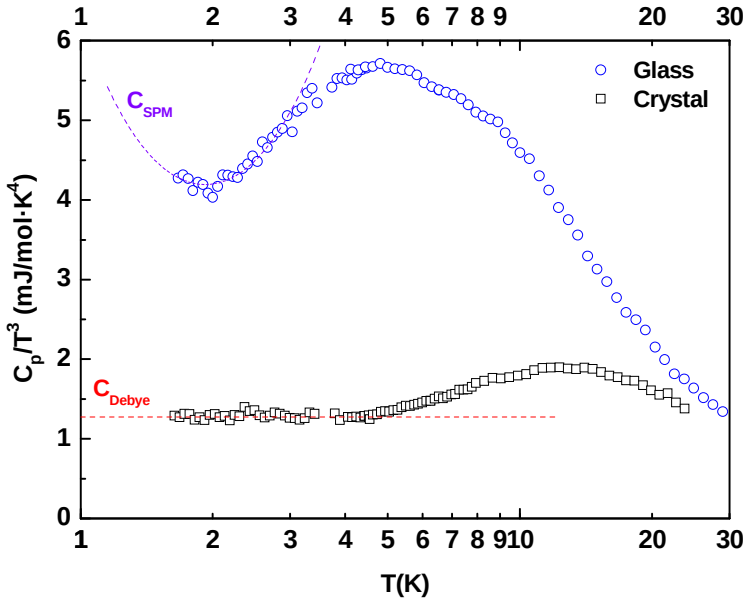

Fig. 5.8 Molar specific heat plotted as C_p/T^3 for the two obtained phases of isobutanol: glass (circles), and crystal (squares). The results from the fits to the Debye model for the crystal and to the SPM for the glass (see Fig. 5.9) are indicated with dashed lines.

As shown in Fig. 5.8, the specific heat of the crystal state of isobutanol follows at low temperature the expected behavior from the Debye model, $C_p = C_D T^3$, with C_D=1.28±0.03 mJ/mol·K^4, as shown by the linear fit in the C_p/T vs T^2 plot shown in Fig. 5.9 (a straight line passing through zero).

We have also determined the Debye temperature Θ_D, by using the obtained C_D from the corresponding fit, and we obtain $\Theta_D = 115 \pm 2$ K for the isobutanol crystal.

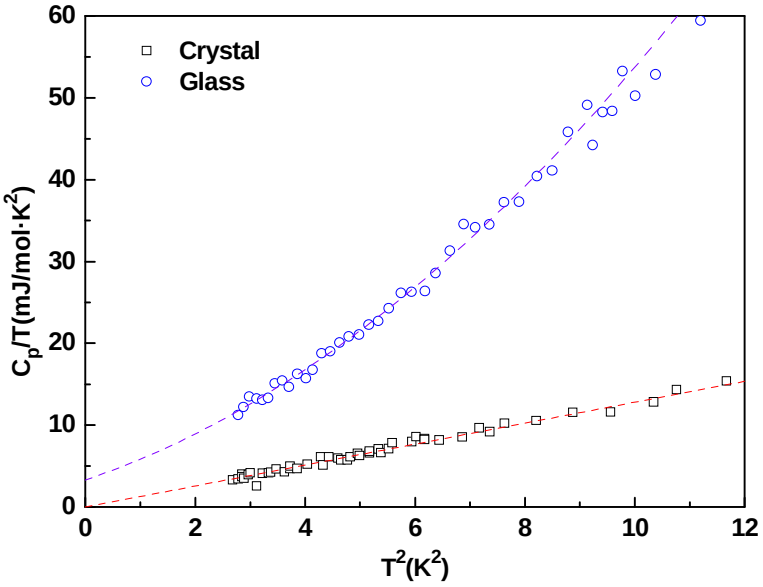

Fig. 5.9 Experimental data for the glass (circles) and crystal (squares) states of isobutanol at the lowest temperature, in a C_p/T vs T^2 representation, together with the corresponding fits to the Debye model (crystal) and Soft-Potential Model (glass).

The SPM quadratic fit of equation (2.42) has been applied for the isobutanol glass, by using the same criterion described above. By considering the minimum at $T_m = 2$ K, we obtain the polynomial fit shown in Fig. 5.9:

C_p [mJ/mol·K] = 4.04 (±1.56) T + 1.98 (±0.58) T^3 + 0,30 (±0.049) T^5.

As for the crystalline phase, we have also determined the Debye temperature Θ_D for the glass. By using the cubic coefficient C_D^*=1.98 mJ/mol·K^4 obtained from SPM, we get Θ_D = 99 ± 2 K for the glass of isobutanol. These and others physical data for the different solid states, as well as the corresponding specific heat coefficients obtained from the fits are compiled in tables 5.1 and 5.2, for crystals and glasses, respectively.

Table 5.1 Calorimetric data for the crystals of n-butanol, tert-butanol and isobutanol.

Substance (Butanol)	C_D (mJ mol^{-1} K^{-4})	Θ_D (K)	T_{max} (K)	$C_{p\,max}$ (mJ mol^{-1} K^{-4})
n-butanol	1.40 ± 0.03	112 ± 2	5.4	1.6
sec-butanol	-	-	-	-
tert-butanol	1.28 ± 0.03	115 ± 2	10.1	1.8
isobutanol	1.28 ± 0.03	115 ± 2	12.9	1.9

Table 5.2 Calorimetric data for the glasses of n-butanol, sec-butanol and isobutanol.

Substance (Butanol)	C^*_{TLS} (mJ mol^{-1} K^{-2})	C^*_D (mJ mol^{-1} K^{-4})	C^*_{sm} (mJ mol^{-1} K^{-6})	Θ_D (K)	T_{max} (K)	$C_{p\,max}$ (mJ mol^{-1} K^{-4})
n-butanol	1.11±0.58	1.81± 0.21	0.083±0.17	103 ± 2	5.4	3.1
sec-butanol	2.20±1.00	1.91± 0.42	0.21± 0.04	101± 2	4.8	4.5
tert-butanol	-	-	-	-	-	-
isobutanol	4.04±1.56	1.98± 0.58	0.30± 0.05	99± 2	4.8	5.7

5.5 Other experiments

In the previous section we have presented the measured specific heat of the solid phases of butanol isomers at low temperature. In this section we will present other experiments conducted to complement the results obtained by the specific heat measurements, and to explore other thermal and elastoacoustic properties. In particular, thermal conductivity $\kappa(T)$, as well as Brillouin-scattering

measurements of the longitudinal and transverse sound velocities, have been conducted at low temperature for glasses from the different isomers of butanol (n-butanol, sec-butanol and isobutanol), in collaboration with researchers of other laboratories.

5.5.1 Thermal conductivity

As described in chapter 2, glasses exhibit *universal* thermal properties at low temperatures, which are very different from those of crystalline solids. Among others, below 1 K the thermal conductivity κ of glasses is orders of magnitude lower than the corresponding values found in their crystalline counterparts. Furthermore, κ depends quadratically on temperature ($\kappa \propto T^2$), in clear contrast to the cubic dependences observed in crystals. Then, in the same temperature range of the *boson peak* observed in C_p/T^3, the thermal conductivity exhibits a *plateau*.

Thermal conductivity measurements were conducted at the Institute for Low Temperature Physics and Engineering of NAS Ukraine by Professor Alexander Krivchikov.

5.5.1.1 Experimental setup

The thermal conductivity of the different glasses of isomers butanol, as well as the different phases of solid n-butanol (glass, crystal and "glacial state") was measured under equilibrium vapor pressure in a experimental setup described elsewhere [Krivchikov 2011], using the steady-state potentiometric method. The sample container used was a stainless steel tube 40 mm long and 22 mm in diameter, with a wall thickness of 0.3 mm. The bottom of the container was fixed to the cold zone of the cryostat that is connected to a helium bath. The glasses were prepared by very fast cooling (above 50 K min^{-1}) of the liquid through the glass transition region.

5.5.1.2 Results

The temperature dependences of the thermal conductivity κ(T) for the three obtained glasses of butanol isomers are shown in Fig. 5.10, using a log-log plot. It can be seen that the temperature behavior of the thermal conductivity for all the butanol isomers is that typical of glasses. Firstly, the thermal conductivity of all glasses increases with increasing temperature (most intensively at the lowest temperatures) up to a maximum value. As expected, each curve has a smeared *plateau* around 5–10 K where the thermal conductivity practically does not vary with rising temperature. Then it continues to increase up to a saturation at $T \approx 50$ K, that essentially persists towards the glass transition temperature ($T_g \sim 110$–120 K in the three cases).

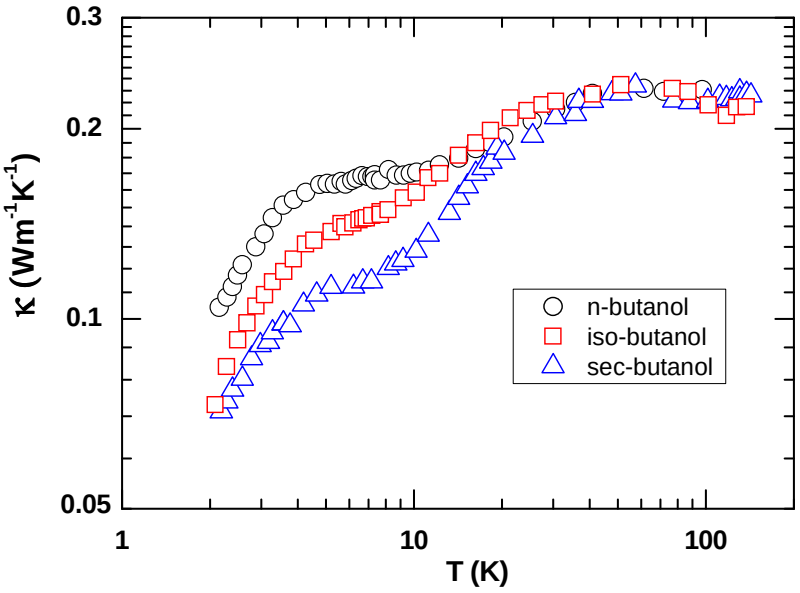

Fig 5.10 Temperature dependence of the thermal conductivity of n-butanol (circles), sec-butanol (squares), and iso-butanol (triangles), in their glass states.

5.5.2 Brillouin scattering at low temperatures

Brillouin-scattering measurements were conducted to measure longitudinal and transverse sound velocities of the different samples in their glass state in the temperature range 10–110 K. Brillouin-scattering experiments were conducted by Dr. Rafael J. Jiménez-Riobóo at the Instituto de Ciencia de Materiales de Madrid, Consejo Superior de Investigaciones Científicas (ICMM-CSIC), Madrid, Spain.

5.5.2.1 Experimental setup

High-resolution Brillouin-scattering measurements of both longitudinal and transverse sound velocities of the different samples in their glass state were conducted in the temperature range 10–110 K by using an Ar^+ ion laser (wavelength = 514.5 nm) and a Sandercock-type 3+3 tandem Fabry-Pérot interferometer. The experimental set-up was the same previously used and described in section 4.5.2.1 for the study above 100 K of the phase diagram of n-butanol [Hassaine 2009, Shmyt'ko 2010]. In order to obtain direct information of the sound propagation velocities, the 90A scattering geometry was used [Kruger 1989]. In this way the acoustic wave vector is independent of the refractive index of the sample, and hence the sound velocities can be obtained in absolute terms.

5.5.2.2 Results

The measurements of hypersonic longitudinal and transverse sound velocities as a function of temperature, $v_{L,T}(T)$, for the three butanol glasses below their glass-transition temperatures down to 10 K, are shown in Fig 5.11. Simple extrapolations to zero temperature $v_{L,T}(T=0)$, used to determine the elastic Debye coefficients and Debye temperatures through

$$C_{Debye} = \frac{2\pi^2}{5}\left(\frac{k_B^4}{\hbar^3 \rho v_D^3}\right) \tag{5.2}$$

where v_D is the Debye-averaged sound velocity $1/v_D^3 = 1/3\ (1/v_L^3 + 2/v_T^3)$, are also graphically indicated in Fig 5.11 and given in Table 5.3. N is taken as the number density of molecules for the reasons given above. The Debye sound velocity values v_D found for the three position isomers of butanol are very similar, ranging 1709–1763 m/s.

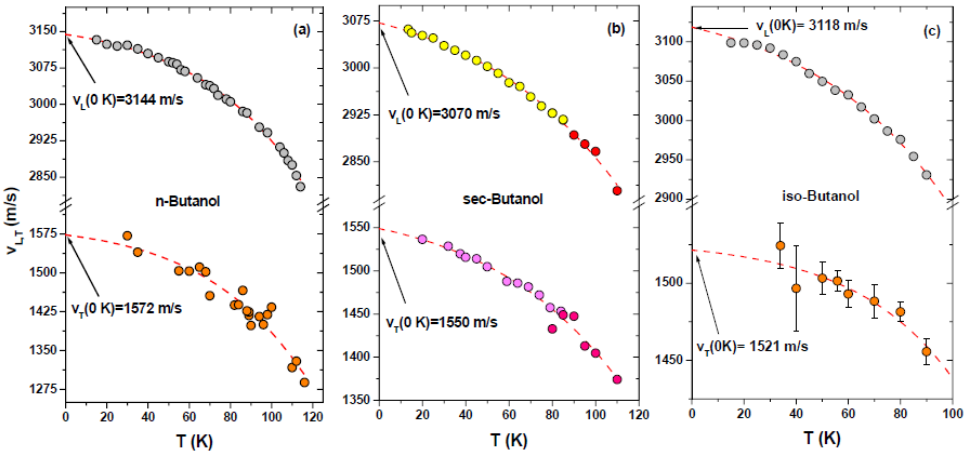

Fig 5.11 Temperature dependence (including extrapolation to zero temperature) for the longitudinal and transverse sound velocities of n-butanol, sec-butanol and iso-butanol isomers, in their glass states. Experimental error bars are only shown for the less favorable case of transverse sound in iso-butanol.

In order to assess the values of the mass density in the zero-temperature limit ρ_{0K}, we have obtained the ratios ρ_{RT}/ρ_{0K} between their values in the liquid state at room temperature (20 ºC) taken from the literature and those unknown at 0 K by assuming that the Lorentz-Lorenz specific refraction

$$r = \frac{n^2 - 1}{n^2 + 2}\frac{1}{\rho} \qquad (5.3)$$

remains constant [Bodmann 1969] as a function of temperature. From our Brillouin-scattering measurements we have obtained the refractive index both at room temperature and at low temperatures, and hence the corresponding extrapolated values ρ_{0K} for the three glassy isomers, which are given in Table 5.3.

The correspondingly determined values of the predicted Debye cubic coefficient C_D for the specific heat at low temperatures and the *molecular* Debye temperatures Θ_D are also displayed in Table 5.3. The elastic Debye coefficients agree very well, within experimental error, with the calorimetric ones obtained from a SPM analysis of the specific heat, as we can see in table 5.3 in the last column $C^*_D/C_D \approx 1$.

Table 5.3: Elastic data obtained for glasses: ρ_{RT} are mass-density values in the liquid state at 20ºC; ρ_{0K} are extrapolated values to low temperature using eq. (5.3); $v_L(0)$ and $v_T(0)$ are measured longitudinal and transverse sound velocities in the zero-temperature limit from Fig. 5.11, and v_D is their Debye-averaged sound velocity; C_{Debye} is the predicted Debye cubic coefficient for the specific heat and Θ_D is the corresponding *molecular* Debye temperature, after eq. (1).

Substance (Butanol)	ρ_{RT} kg/m^3	ρ_{0K} kg/m^3	$v_L(0)$ m/s	$v_T(0)$ m/s	v_D m/s	C_D mJmol^{-1}K^{-4}	Θ_D(K)	C^*_D/C_D
n-butanol	809.5	951.0	3144	1572	1763 ± 18	1.74 ± 0.09	104 ± 2	1.03
sec-butanol	806.3	947.6	3070	1550	1738 ± 17	1.82 ± 0.09	102 ± 2	1.05
tert-butanol	-	-	-	-	-	-	-	-
isobutanol	802	908.5	3119	1521	1709 ± 17	2.00 ± 0.10	99 ± 2	0.99

5.6 Discussion

5.6.1 The so-called "glacial state" of n-butanol

In chapter 4 we have investigated and discussed through specific heat, elasto-acoustic Brillouin and x-ray diffraction experiments, the "glacial state" of n-butanol between 77 and 300K. In the present section, we will focus on analyzing the low-temperature properties of the different solid phases of n-butanol presented before, namely their specific heat and thermal conductivity measurements. This will allow us to compare the behavior of the "glacial state" to the "universal" behavior of the glasses and crystals.

In Fig 4.2 we have seen that the so-called "glacial phase" presents an intermediate quantitative behaviour of its specific heat, but qualitatively is neither that of a fully-ordered crystal nor that typical of a glass or amorphous solid. The temperature dependences for the thermal conductivities $\kappa(T)$ of the different phases of n-butanol [Krivchikov 2011] are shown in Fig 5.12, using a double logarithmic plot. The $\kappa(T)$ curve for the fully-ordered crystal state of n-butanol presents the typical shape of fully-ordered molecular crystals. On the other hand, the behavior of $\kappa(T)$ for n-butanol glass is well representative of the universal thermal conductivity exhibited by glasses at low temperatures [Zeller 1971, Phillips 1972]. In particular, n-butanol glass exhibits the ubiquituous *plateau* at around 4–12 K. The so-called "glacial state" of n-butanol does not exhibit a glasslike $\kappa(T)$ at all, but rather is similar to that of a strongly defective crystal. It is also very different from that of the fully-ordered crystal.

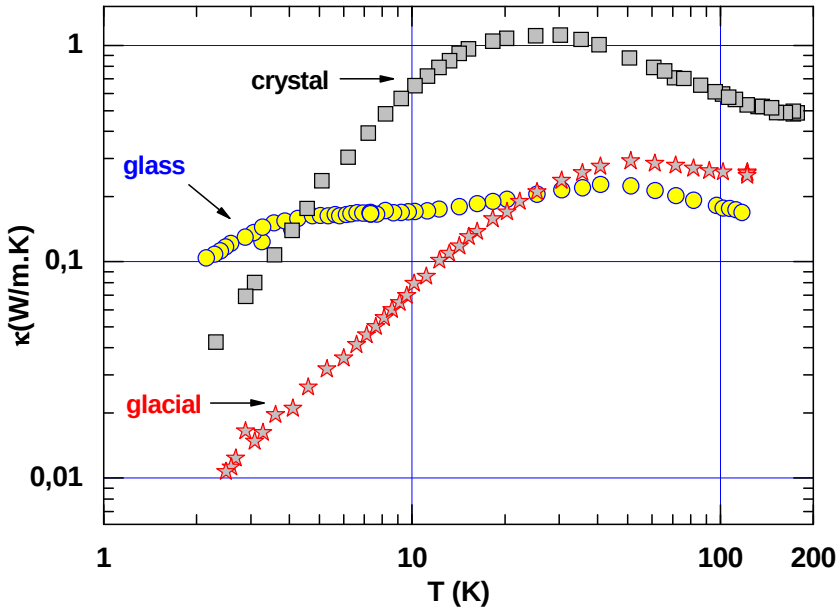

Fig 5.12 Temperature dependence of the thermal conductivity of n-butanol (solid symbols) for its three states: glass (circles), "glacial" (stars), and fully-ordered crystal (squares) [Krivchikov 2011].

Specifically, $\kappa(T)$ for the glacial state has a smeared phonon maximum near T=50 K. At $2 < T < 20$ K, $\kappa(T)$ grows with temperature roughly as $T^{1.35}$. In the interval T = 50–122 K, $\kappa(T)$ decreases, as in the glass state, at the rate $d\kappa/dT = -0.9\times10^{-3}$ $Wm^{-1}K^{-2}$. Note that $\kappa(T)$ of the glacial state is strikingly lower than that of the glass at $T < 25$ K. This fact shows that in the "glacial state" there exists strong phonon scattering which is different from the resonant phonon scattering typically found for glasses.

Figs 5.2 (specific heat) and 5.12 (thermal conductivity) show that both crystal and glass states of n-butanol exhibit the correspondingly expected behavior, but the low-temperature properties of the so-called "glacial state" undoubtedly are, either qualitatively or quantitatively, very different from the universal behavior presented by any glass or amorphous solid. This confirms our previous claims in section 4.6.1, and in [Wypich 2007, Hassaine 2009, Shmyt'ko 2010] against considering the "glacial phase" as a second amorphous phase and hence an evidence of *polyamorphism*. On the other hand, its low-temperature behavior is not that of a fully-ordered crystal either: The specific heat does not reach the expected cubic Debye limit at low temperatures and the thermal conductivity is one order of magnitude lower than that of the amorphous state.

5.6.2 Low-temperature specific heat of butanol crystals

As already shown at the beginning of this chapter, the Debye coefficients of the crystals (n-, sec- and tert-butanol), can be readily obtained from a least-squares straight-linear fit for C_p/T vs T^2 curves at low temperatures. All those data and fits have been collected in Fig 5.13. The Debye contributions in the crystals for tert-butanol and isobutanol are identical within experimental errors, and also very similar to that of n-butanol.

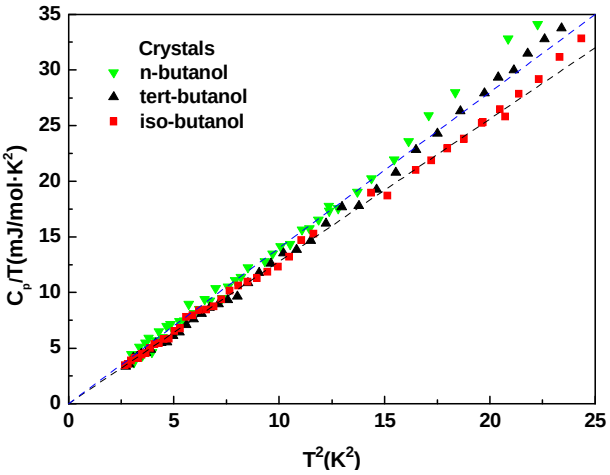

Fig 5.13 Low-temperature specific heat plotted as C_p/T versus T^2 for crystals of the different butanol isomers. Dashed lines are the corresponding fits to the Debye model (a straight line passing through zero).

In Fig. 5.14 we present together the C_p/T^3 curves for glass and crystalline phases. As can be seen, the glass of isobutanol has a C_p/T^3 peak height which doubles the one of n-butanol. Also, the glass of sec-butanol presents a C_p/T^3 peak that is 50% higher than the peak of n-butanol (see Table 5.2). In contrast, the Debye specific heat of the reference crystals remains essentially constant for the different isomers.

5.6.3 Low-temperature properties of butanol glasses

In previous sections 5.1, 5.2 and 5.4, and in Table 5.2, we have presented the results of a simple SPM analysis of our specific-heat data for glasses, by directly fitting the data to parabolic eq. (2.42).

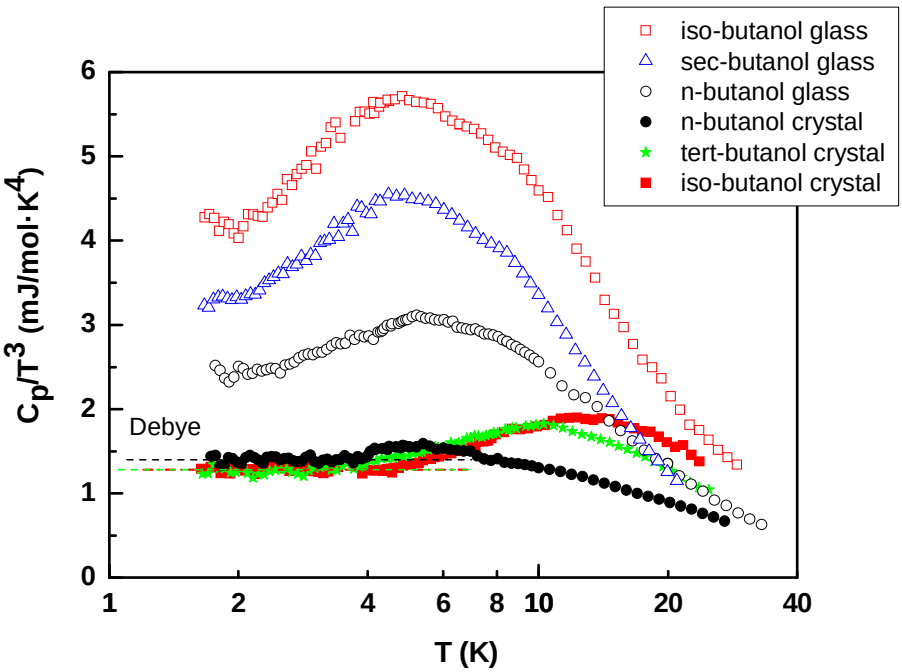

Fig 5.14. C_p/T^3 plots for glasses and crystalline phases of different position isomers of butanol, as indicated in the legend, showing similar Debye levels (dashed lines) for the crystals, but very different boson-peak heights for the glasses.

Nonetheless, for an accurate determination of those SPM parameters (especially the TLS coefficient), measurements at still lower temperatures would be needed in our case, since the TLS "soft modes" crossover for the specific heat occurs approximately between $k_B T_{min} \approx W/1.6$ [Buchenau 1991] and $k_B T_{min} \approx W/1.8$ [Buchenau 1997, Ramos 1998], that is around or below 2 K in this case, too close to the lowest temperatures in our experiments. A similar problem affects the thermal conductivity data. The crossover from the lowest-temperature region dominated by the resonant scattering of sound waves by tunneling states ($\kappa \propto T^2$) to that by soft modes (the plateau region) can be assessed from a plot of κ/T vs T, where a maximum is observed at $T_{max,\kappa}$ given by $k_B T_{max,\kappa} \approx W/1.6$. Therefore, rather than trying separate best fits for every measurement (probably inconsistent for the reasons given above), we will determine now a single W SPM-parameter for a given substance, taking a compromise between both

thermal properties. Then, the corresponding quantitative factors (C_{TLS}, C_{sm}, and $\overline{C}$) are fitted to scale the corresponding data (see Table 5.4).

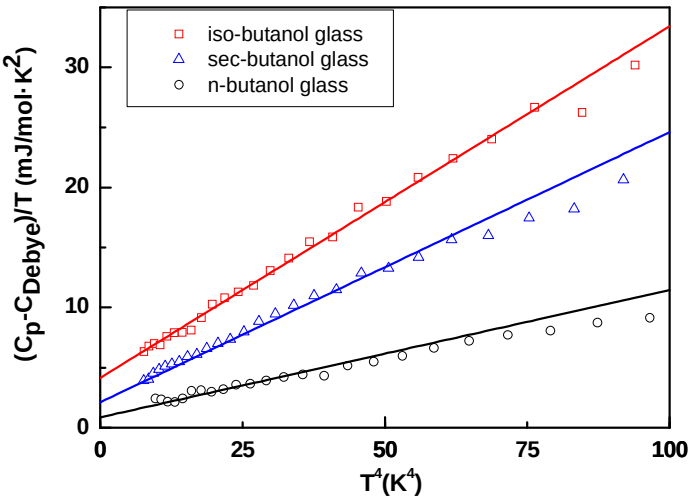

Fig 5.15 Excess low-temperature specific heat of butanol glasses after subtraction of the acoustically measured Debye level in a $(C_p - C_{Debye})/T$ vs T^4 plot, in order to obtain the T and T^5 coefficients of the Soft-Potential Model from the shown straight-linear fits (see text for more details)

Also for the lack of specific-heat data at very low temperatures and to avoid too many doubtful SPM parameters, a more reasonable and accurate procedure will be followed here than the previous direct fit to eq. (2.42). Since we have obtained the true Debye coefficient C_D from elastoacoustic measurements (Table 5.3), and the elastic Debye coefficients have been proved [Ramos 2004] to be equal to the calorimetrically obtained ones C^*_D, when properly fitted through eq. (2.42), we have fixed the measured C_D coefficient for each glass. The *excess* specific heat of the butanol glasses is clearly manifested after subtraction of the corresponding Debye coefficient, and plotted as $(C_p - C_{Debye})/T$ vs T^4, in order to obtain the missing T and T^5 coefficients of the SPM from simple straight-linear fits, as shown in Fig. 5.15 and Table 5.4. In those particular fits, the SPM parameters C_{TLS} and C_{sm} were further fixed to fulfill the abovementioned rule $W/k_B \approx 1.6–1.8\ T_{min} = 1.6–1.8\ (C_{TLS}/C_{sm})^{1/4}$, where W was determined from the

thermal conductivity data (see below). Let us stress that the observed linear behavior in the $(C_p - C_{Debye})/T$ vs T^4 plots for $0 < T^4 < (W/k_B)^4$ is indeed a non-trivial confirmation of the SPM qualitative predictions.

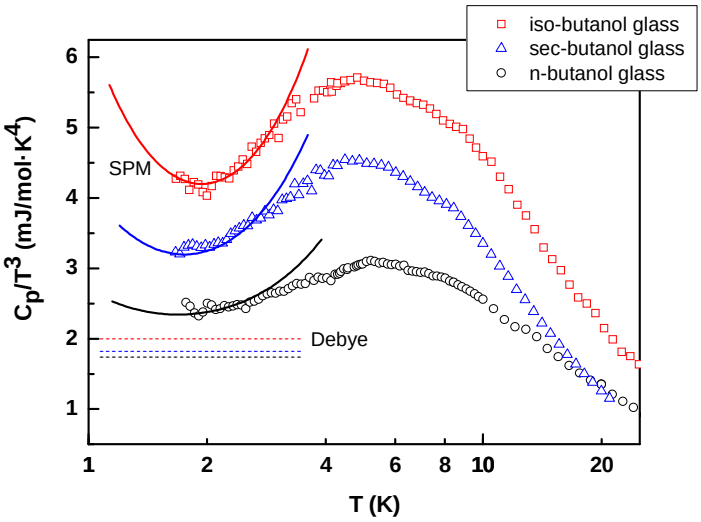

Fig 5.16 C_p/T^3 plots for the butanol glasses. Dashed lines indicate their (similar) Debye contributions obtained from Brillouin-scattering measurements (see Fig. 5.11): iso-, sec- and n-butanol, from above to below. The corresponding boson peaks follow the same order, but in contrast vary strongly. Solid lines indicate the total SPM fit (i.e. the one from Fig. 5.15 plus the Debye contribution, according to eq (2.42)).

As can be seen in Fig 5.16, the notable variation found in the boson peak amplitudes among different butanol isomers coexists with very similar Debye coefficients in all of them. This is in clear contrast to what was found in propanol isomers, where the different boson peaks found in them were correlated to the very different Debye levels between 1- and 2-propanol observed in both crystalline and glassy states [Ramos 2003, Talon 2001]. This clear finding opposes direct correlations between the boson peak in glasses and (mainly transverse) acoustic phonon dispersion curves, reported by some authors [Chumakov 2011, Ruta 2010, Caponi 2009, Monaco 2006]. As shown here, this cannot be a universal rule. The different amorphous networks built up from differently hydrogen-bonded butanol molecules produce significantly different

densities of quasilocalized vibrations at low frequencies and hence boson-peak heights whereas the acoustic properties and the Debye contribution remains practically the same. It is important to emphasize that these conclusions are independent on the conducted SPM quantitative analysis or fits, but are clearly deduced from the experiments. Therefore, our results do not support the idea that the boson peak can be explained by the elastic continuum transformation only.
Finally, for the sake of completeness, we will reproduce here the analysis of the thermal conductivity data conducted in [Hassaine 2012], using the SPM (already described in section 2.2.2).

For an elastic continuum such as a glass, the thermal conductivity $\kappa(T)$ is given by the standard expression obtained from the well-known phonon-gas kinetic equation, and using the Debye approximation for the density of states of the sound waves transporting heat. As said before, we will analyze our thermal conductivity results within the SPM [Buchenau 1992, Parshin 1994, Ramos 1997,1998] (see section 2.2.2), in which the inverse mean free phonon path $l_{SPM}^{-1}(\omega)$ can be subdivided into three components describing sound wave resonant scattering by tunneling states and quasilocalized low-frequency vibrations, as well as by classical relaxation processes:

$$l_{SPM}^{-1}(\omega)=\frac{\pi\omega C_{L,T}}{v_{L,T}}\left[1.1\tanh\left(\frac{\hbar\omega}{2k_BT}\right)+\left(\frac{T}{W}\right)^{3/4}\ln^{-1/4}\left(\frac{1}{\omega\tau_0}\right)+\frac{1}{8}\left(\frac{\hbar\omega}{W}\right)^3\right] \tag{5.3}$$

for longitudinal (L) and transverse (T) phonons, respectively.

In addition to the two SPM parameters W and P_s defined in chapter 2, section 2.2.2, for thermal conductivity and acoustic properties, the strength parameter $C_{L,T}$ (in turn linearly proportional to P_s/W) is introduced instead of P_s and appears explicitly in the equations. $C_{L,T}$ is essentially the same tunneling strength parameter defined in the TM characterizing the interaction between the acoustic sound waves and the two-level systems, but now generalized to all quasilocalized excitations within the SPM. To be more precise, $C_{L,T}^{(\mathrm{TM})} \sim 1.1\ C_{L,T}^{(\mathrm{SPM})}$ was found [Ramos and Buchenau, 1997, 1998]. Indeed, it is the astonishing universality of $C_{L,T}$ ($\sim 5\times10^{-4}$) what remains the key question concerning the low-temperature universal properties of glasses.

To compare with experiments, the thermal conductivity of the SPM can be calculated using the following expression [Ramos and Buchenau, 1997, 1998)]:

$$\kappa(T) \;= \frac{2k_B}{3\pi\overline{C}}\left(\frac{W}{h}\right)^2\left(\frac{1}{v_l}+\frac{2}{v_t}\right)F(z) \equiv \frac{2k_B}{\pi h^2}\frac{W^2}{\overline{C}\cdot\overline{v}}F(z) \qquad (5.4)$$

where $z = \frac{k_B T}{W}$, h is the Planck constant, $\frac{1}{v} \equiv \frac{1}{3}\left(\frac{1}{v_l}+\frac{2}{v_t}\right)$, $\overline{C}$ is the properly averaged value of C_L and C_T (which are nonetheless expected to be very similar), and

$$F(z) = \int_0^\infty dx \;\; \frac{x^3\, e^{-x}}{(1-e^{-x})^2} \;\; \frac{z^2}{1.1\tanh(x/2) + 0.7\, z^{3/4} + x^3\, z^3/8} \qquad (5.5)$$

The function $F(z)$ is hence universal and dimensionless, and only depends on the normalized temperature $z = k_B T/W$. In Ref. [Ramos 1997, 1998], it was found a good agreement between those SPM equations and the thermal conductivity data found in the literature for several glasses at low temperatures.

According to the SPM prediction, the magnitude $\kappa(T)\frac{\pi}{2k_B}\left(\frac{h}{W}\right)^2\overline{C}\cdot\overline{v}$ as a function of $k_B T/W$ (i.e. $F(z)$ as a function of z) should be independent of a particular substance structure or chemical composition, at least at low temperatures up to the plateau region. The SPM parameters W and $\overline{C}$ can thus be obtained through a comparison of experimental data and the universal dependence of $F(z)$ given by Eq. (5.5). The dependence of the renormalized thermal conductivity $\kappa(T)\frac{\pi}{2k_B}\left(\frac{h}{W}\right)^2\overline{C}\cdot\overline{v}$ on the reduced temperature ($z = \frac{k_B T}{W}$) obtained for our experimental data in the different isomers are shown in Fig. 5.17. Fitting parameters W and $\overline{C}$ are given in Table 5.4. As said above, a single W has been determined for a given substance as the best compromise to agree with both specific heat data and thermal conductivity data, specifically to agree with $F(z)$ for $z < 2$. Then $\overline{C}$ is just an overall constant factor for the thermal conductivity curve. It can be observed indeed in Fig. 5.17 that the universal behavior proposed by the SPM renormalization agrees well with experimental data in the low temperature region ($z<2$) for the three butanol isomers, as was

also observed in other structural and orientational glasses [Sharapova 2010, Krivchikov, 2011]. Obviously, this SPM scaling does not work above, say, z>4, where the basic SPM is longer valid and the similar obtained values of thermal conductivity at higher temperatures for all butanol glasses (see Fig. 5.10) would give different deviations from the universal SPM curve $F(z)$.

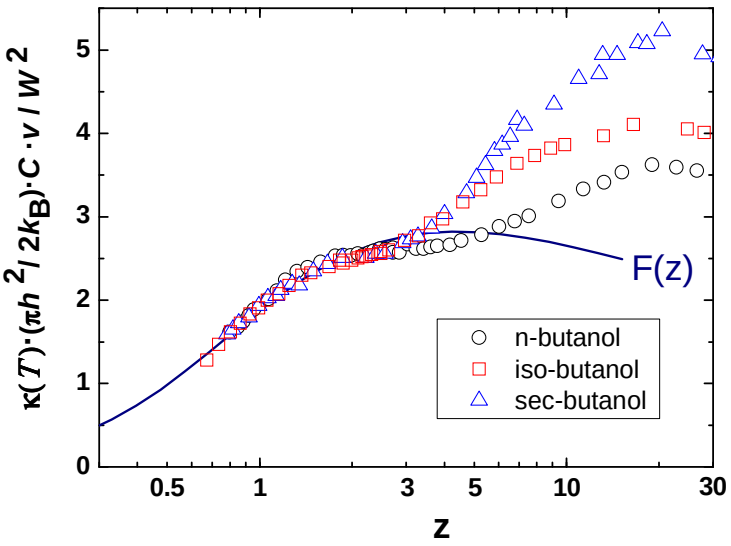

Fig. 5.17. Renormalized thermal conductivity data $\kappa(T)\frac{\pi}{2k_B}\left(\frac{h}{W}\right)^2\overline{C}\cdot\overline{v}$ plotted on the reduced temperature $z = k_BT/W$ from experimental data for butanol glasses (symbols as indicated in the legend). The solid line is the universal, dimensionless function $F(z)$, calculated by eq. (5.5).

Table 5.4. SPM-fitted specific-heat parameters for glasses: W has been determined to concurrently fit low-temperature thermal conductivity and specific heat data; the ratio C_{TLS}/C_{sm} is fixed from W; the density of soft modes P_s is directly derived from C_{sm}.

Substance	W/k_B (K)	C_{TLS} (mJ mol^{-1}K^{-2})	C_D (mJmol^{-1}K^{-4})	C_{sm} (mJ mol^{-1}K^{-6})	P_s (mol^{-1})	C ($\times 10^{-4}$)
n-butanol	2.7	0.86	1.74	0.106	1.20×10^{19}	2.25
sec-butanol	2.8	2.11	1.82	0.225	3.06×10^{19}	3.6
tert-butanol	–	–	–	–	–	–
iso-butanol	3.1	4.13	2.00	0.293	6.64×10^{19}	3.5

5.6.4 Residual entropy and Kauzmann temperature of butanol glasses

As mentioned in chapter 2, the entropy, $S_{liq}(T)$, of liquids decreases strongly and the structural relaxation time increases dramatically as the temperature T is lowered below the melting point, T_m, and decreases more rapidly on cooling towards the glass transition temperature, T_g. By extrapolating sharply the liquid entropy, it is found that the liquid entropy is less than the crystal entropy below the 'Kauzmann temperature' T_K. This would correspond to an apparent violation of the third law of thermodynamics. The situation is known as the entropy crisis or "Kauzmann paradox" [Elliott 1990], or even ''Kauzmann catastrophe" [Kivelson 1998].

Some models have been developed around the concept that something special takes place at T_K. It is interesting to note that T_K is quite close to a temperature T_{VF} or T_0, known as the VFT (or ideal glass) temperature (see section 2.1.4.2). Therefore, both a thermodynamic quantity (the entropy) and a dynamic quantity (the relaxation time or viscosity) would exhibit the same anomalous behavior, so indicating the possible existence of an underlying phase transition at a critical point. Richert and Angell [Richert 1998] have compared dielectric relaxation data of several glass-forming liquids with the predictions of the Adam–Gibbs

theory using experimental data for the configurational entropy $S_c(T)$. They found that the Kauzmann temperature T_K, at which S_c vanishes, coincides with the Vogel temperature T_0, at which the VFT fit to dielectric relaxation data τ (T) in the viscous regime diverges.

The heat capacities for both the crystalline and glassy states of most materials ($T < T_g$) are essentially (though not strictly) the same, and arise from vibrational contributions. The excess heat capacity measured for the glass above T_g is due to the configurational degrees of freedom which the material possesses in the supecooled liquid state [Elliott 1990]. The temperature dependence of the configurational entropy can be obtained by integration of the difference of the specific heat of the glass/liquid from its corresponding crystal.

As previously shown in chapter 4 and in this chapter, we have measured the specific heat in the whole temperature range from 1.5 K to the liquid state for all the obtained phases of butanol isomers. To complete the range between 0–1.5 K, we have used for the glass the fitted curve of the Soft Potential Model to specific-heat data, and the Debye model for the crystal. In this section we will calculate the residual entropy of glasses (n-butanol, sec-butanol and isobutanol) at 0 K, we will determine the Kauzmann temperatures T_K and, finally, we will compile all these data for the three isomers in Table 5.5, trying to find some hint or correlation.

5.6.4.1 n-butanol entropy

As shown in the previous sections, we have measured the specific heat of glasses and crystals of the butanol isomers. From these experimental data we are going to study the temperature dependence of the configurational entropy, and to determine the Kauzmann temperature T_K and the residual entropy at zero Kelvin.

In Fig 5.17 we show the specific heat curve of n-butanol glass, as well as of the fully ordered crystal, together with literature data of the n-butanol crystal [Counsell 1965], measured using another calorimetric method (adiabatic method), and presented here as a useful comparison.

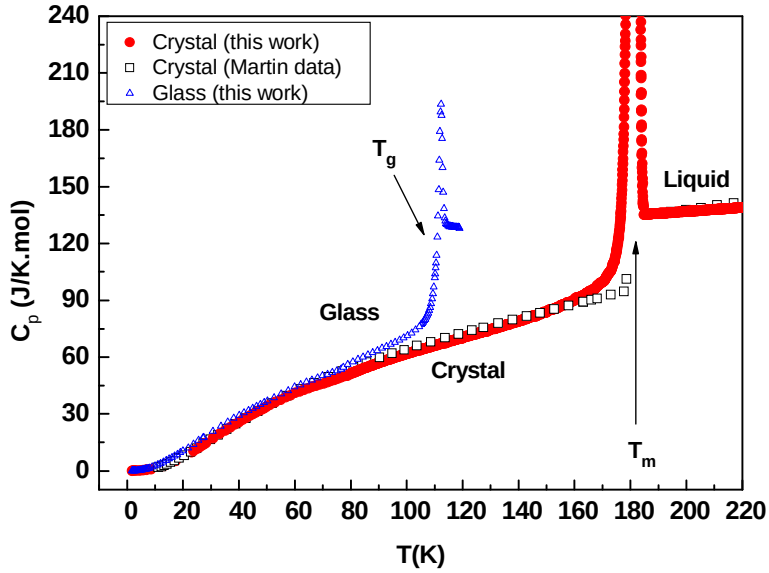

Fig 5.18 Molar specific heat of n-butanol glass (triangles) and its jump at T_g, of the fully ordered crystal (full circles) with the sharp peak at the melting point, followed by that of the liquid state. Literature specific-heat data [Counsell 1965] for the crystal (squares) are also shown.

In Fig 5.18 we plot the continuous functions of C_p/T versus T that we will use to calculate the entropy curves for n-butanol. Above the glass transition (~120 K), the specific heat of the SCL was extrapolated from this temperature to the liquid state. An interpolated curve was generated for the specific heat of the crystal from 0 K to the liquid state, except near the melting temperature, T_m=183 K, where a short extrapolation of the stable crystal measurement was done to smooth pre-melting effects. The entropy of melting calculated in chapter 4 (section 4.6.2) is also graphically shown in Fig 5.18.

This representation C_p/T against T, in addition to clearly show the differences in specific heat values between glass and crystal, will serve us as a direct tool to determine the entropy of the three different phases (crystal, glass and liquid states), by integrating C_p/T through the following equation:

$$S_{liq}(T_L) = \int_0^{T_m} \frac{C_{p,cry}}{T} dT + \frac{\Delta H_m}{T_m} + \int_{T_m}^{T_l} \frac{C_{p,liq}}{T} dT \qquad (5.6)$$

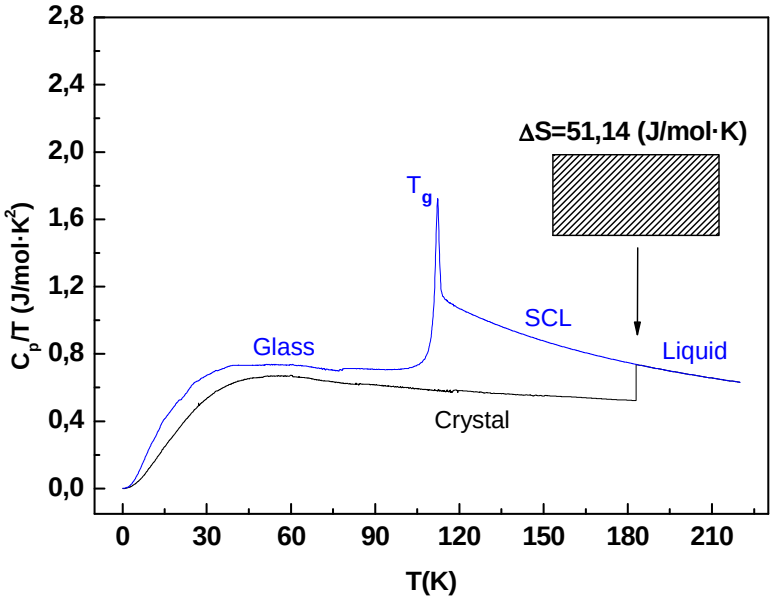

Fig 5.19 Continuous curves of C_p/T versus T obtained from interpolation of experimental data for the different states of n-butanol. The dashed area graphically indicates the entropy of melting.

Therefore, by integrating the specific heats in the representation C_p/T vs T (Fig 5.18), and making use of the measured entropy of melting $\Delta S_m=\Delta H_m/T_m$, we have obtained the entropy of each state from zero to a selected temperature T_L at the liquid state (in this case, T_L= 220 K).

Once the entropy of crystal and that of the liquid S_{liquid} at T_L by using eq (5.6) have been obtained, the residual entropy S_g (T = 0 K) of the glass at zero Kelvin can be determined as follows:

$$S_g(0) = S_{liq}(T_L) + \int_{T_L}^{0} \frac{C_{gl,SCL}}{T} dT \qquad (5.7)$$

Thus, for n-butanol we obtain $S_g(0)$ = 13.14 J/mol·K.

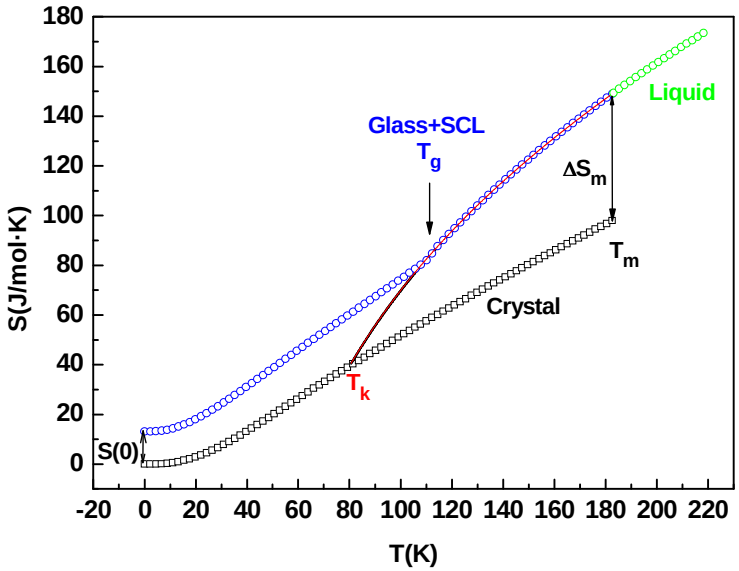

Fig 5.20 The entropy of n-butanol obtained by integrating the heat capacities shown in Fig 5.19, and using the measured entropy of melting (ΔS_m). We also show the temperature, T_K, at which the extrapolated entropy of the liquid crosses that of the crystal.

In Fig. 5.19 we show the corresponding entropy curves obtained for the crystal, glass and liquid states of n-butanol. It is graphically evident how starting from the zero entropy of the crystal at 0 K, one arrives after the whole thermal cycle at a non-zero residual entropy for the glass at 0 K.

On the other hand, assuming very similar vibrational contributions for crystals and glasses, the configurational entropy can be defined as: $S_c(T) = (S_{glass} - S_{crystal})$. According to the Adam-Gibbs (AG) theory:

$$S_c(T) = S_\infty(1 - T_K/T) \qquad (5.8)$$

Then, in order to determine the so-called Kauzmann temperature T_K, we perform a simple linear fit ($a+bx$) in the representation $S_c(T)$ against $1/T$ (not shown), where $S_\infty = a$, and $T_K = b/a$.

By doing so, we obtain S_∞ = 90.77 J/K·mol and the Kauzmann temperature T_K=80K (see Fig. 5.20).

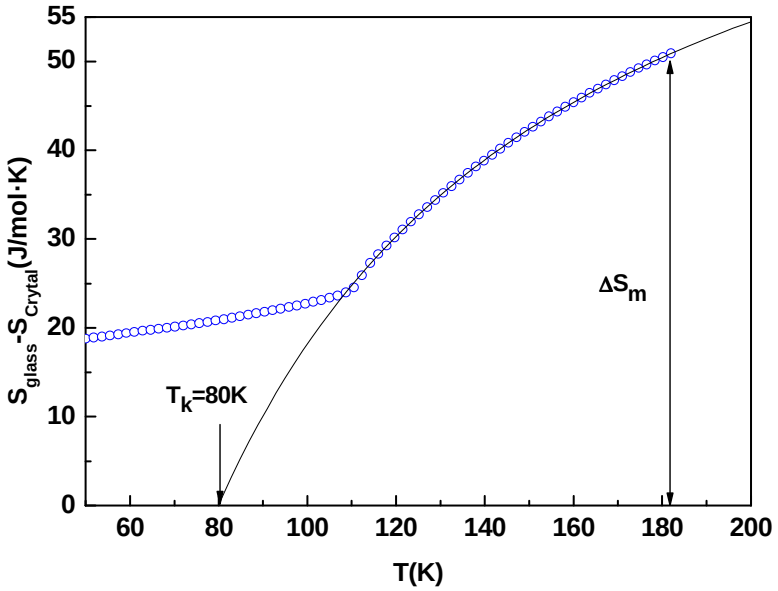

Fig 5.21 Variation of the obtained configurational entropy of n-butanol (S_{glass}-$S_{crystal}$) with temperature. The solid line is a fit using AG equation (5.8).

5.6.4.2 Sec-butanol entropy

As presented previously (chapter 4), sec-butanol is a very good glass former. In the literature it is found that it can crystalize but needs long time (days) below its melting temperature [Andon 1971]. We were not been able to obtain its crystalline state. Neverthless, we have used the literature specific heat data of its crystalline state [Andon 1971] and our measured specific heat data of its glass state to calculate the entropy. By comparing our data and those of [Andon 1971] for glass, we note that there is not a notable difference, so that we will employ both sets of data together.

In Fig 5.21 we show in a C_p/T versus T representation these combined molar specific-heat data of the crystal, glass and liquid states of sec-butanol, as well as its melting entropy ΔS.

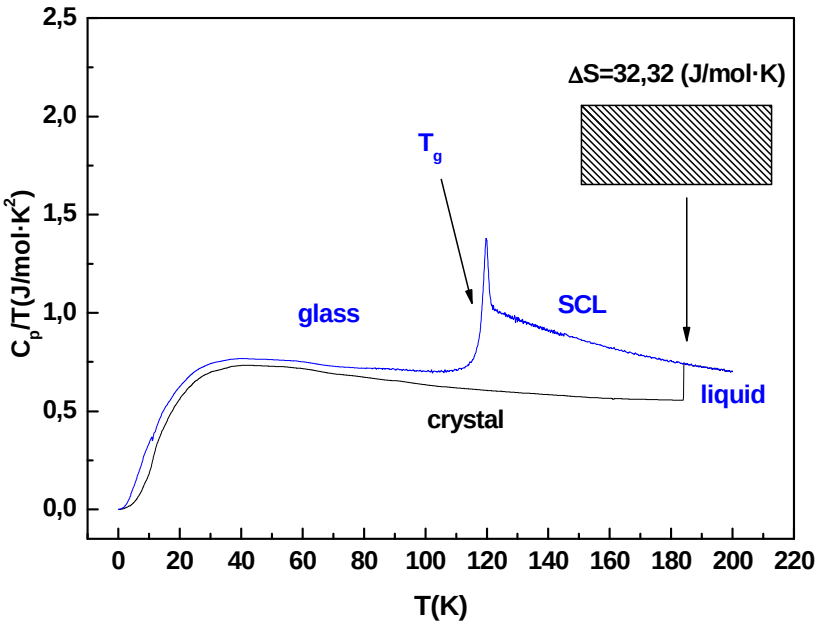

Fig 5.22 Continuous curves of C_p/T versus T obtained from interpolation of experimental data for the different states of sec-butanol. The dashed area graphically indicates the entropy of melting. The specific heat curve of the crystal and the melting entropy at T_m=185 K were taken from literature [Andon, 1971].

By following the same procedure as in n-butanol (previous section), we have calculated the entropy of the crystal, liquid and glass states of sec-butanol, as well as the resulting residual entropy at zero Kelvin $S_g(0)$ = 5.17 J/mol·K, what is shown in Fig 5.22.

Also, by performing a simple linear fit ($a+bx$) in the representation $S_c(T)$ against $1/T$, following eq. (5.8), we have obtained S_∞ = 67.9 J/mol·K and a Kauzmann temperature T_K = 96 K. As can be seen in Fig 5.23, the fit gives an excellent representation for experimental data in the range $T_g < T < T_m$. All these fit parameters are compiled in table 5.5, together with others parameters for the different isomers of butanol.

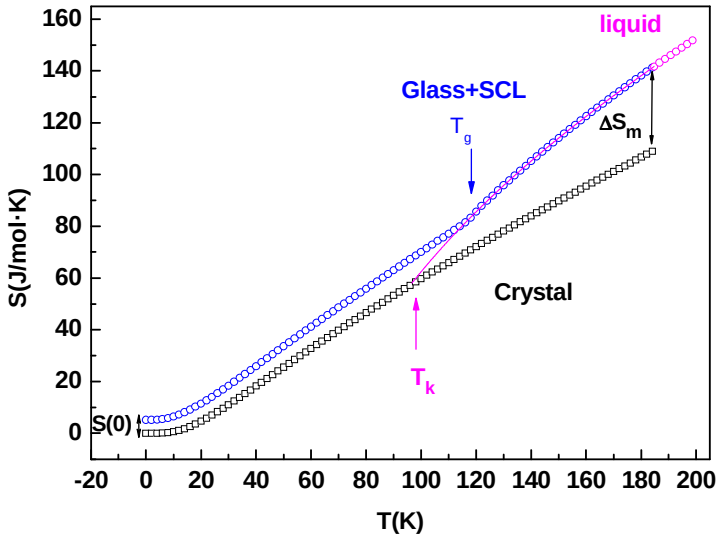

Fig 5.23 Entropy of sec-butanol obtained by integrating the specific heat shown in Fig 5.22, and using the measured entropy of melting (ΔS_m). We also show the temperature, T_K, at which the extrapolated entropy of liquid crosses that of the crystal.

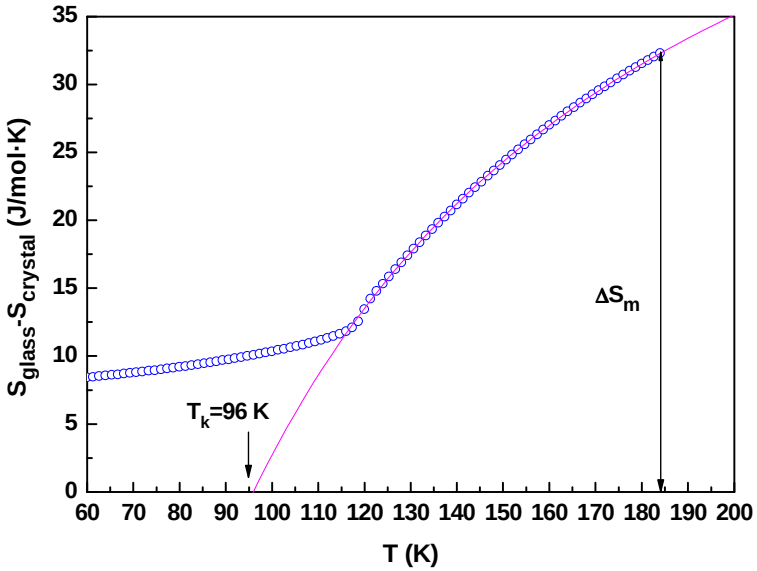

5.24 Variation of the obtained configurational entropy of sec-butanol (S_{glass}-$S_{crystal}$) with temperature. The solid line is a fit using AG equation (5.8).

5.6.4.3 Isobutanol entropy

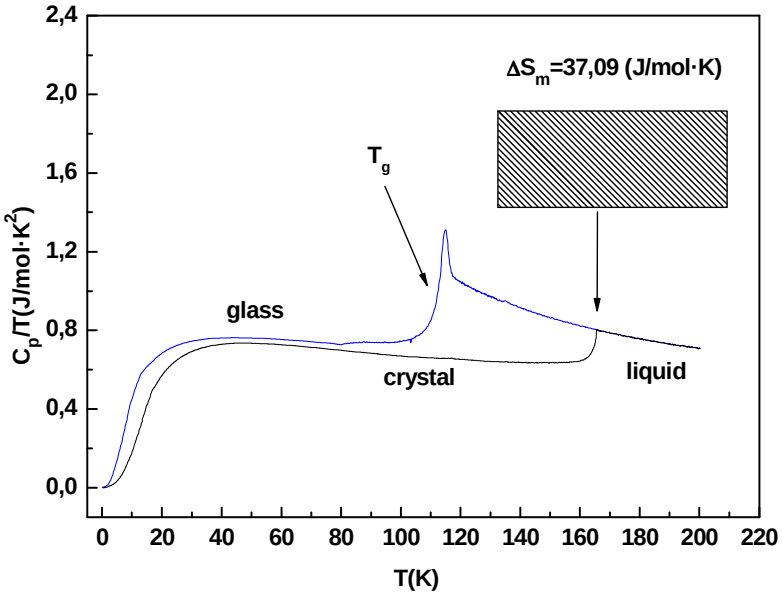

Fig 5.25 Continuous curves of C_p/T versus T obtained from interpolation of experimental data for the different states of isobutanol. The dashed area graphically indicates the entropy of melting obtained in chapter 4.

Finally, isobutanol is also a good glass former, but we have also been able to obtain its crystalline state. Fig 5.25 shows the molar specific heat (C_p/T) against T, of the glass, liquid and crystal, as well as the entropy of melting. We note that the temperature range between 20–77 K has been completed with data taken from literature [Counsell 1968].

By following the same procedure as in the two former studied isomers, we have calculated the entropy of the crystal, liquid and glass states of isobutanol, including its residual entropy $S_g(0)$, as shown in Fig 5.26.

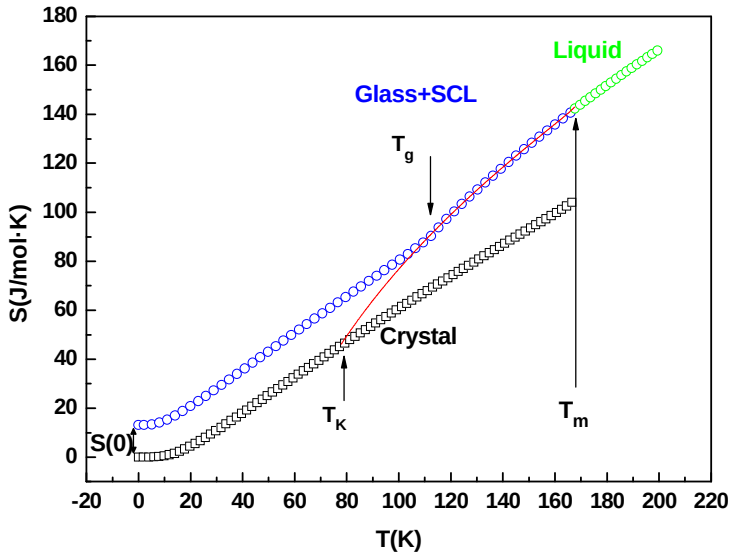

Fig 5.26 The entropy of isobutanol obtained by integrating the heat capacities shown in Fig 5.25, and using the measured entropy of melting (ΔS_m). We also show the temperature, T_K, at which the extrapolated entropy of liquid crosses that of the crystal.

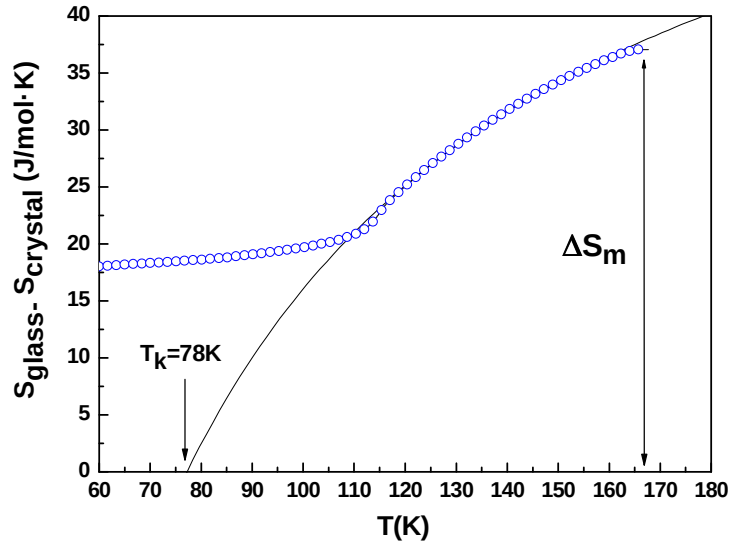

Fig 5.27 Variation of the obtained configurational entropy of isobutanol (S_{glass}-$S_{crystal}$) with temperature. The solid line is a fit using AG equation (5.8).

Finally, we have also determined T_K, as before, by a simple linear fit ($a+bx$) in the representation $S_c(T)$ against $1/T$. By doing so, we have obtained $S_\infty = 70.5$ J/K·mol and a Kauzmann temperature $T_K = 78$K.

5.6.4.4. General discussion

Fig 5.27 shows together all *excess* entropy curves (i.e. the difference between the entropy of the glass and that of the corresponding crystal in each substance, which we have also denoted as configurational entropy $S_c(T)$). To allow a better comparison, both excess entropy and temperature have been scaled to their melting values, ΔS_m and T_m, respectively.

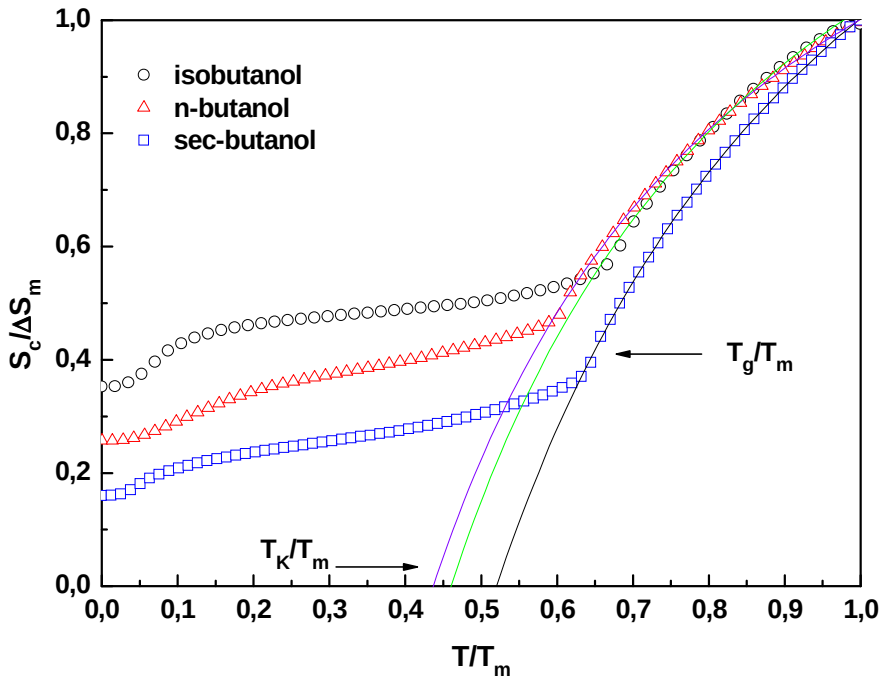

Fig 5.28 Temperature dependence of the *excess* entropy curves (i.e. the difference between the entropy of the glass and that of the corresponding crystal in each butanol isomer), normalized by their values at the melting point, T_m and ΔS_m. The lines cross the abscissa at the reduced Kauzmann temperature (T_K/T_m).

The solid lines also shown in Fig 5.27 are the previously described fits to the Adam-Gibbs equation, that can be regarded as the extrapolation of the ergodic SCL configurational entropy. These curves cross the abscissa at the reduced Kauzmann temperature T_K/T_m, which varies between 0.44 and 0.52 for these three isomers of butanol (see data in Table 5.5). A better scaling is found for T_g/T_m, which lies within 0.64±0.03, typical values for many glass-forming liquids. We do not find a significant scaling between T_K and T_g, since T_K/T_g ranges between 0.69 (isobutanol) and 0.81 (sec-butanol).

Table 5.5: Calorimetric and thermodynamic data for glasses of n-butanol, sec-butanol and isobutanol: T_m is the melting temperature, T_g the glass transition-temperature and T_K the Kauzmann temperature. ΔS_m is the entropy of melting, $S_g(0)$ the residual entropy of glass at zero Kelvin. $S_c(T_g) = S_{glass}(T_g) - S_{crystal}(T_g)$ is the difference between the entropy of the glass and its corresponding crystal at T_g (that is, the configurational entropy at the glass transition), $S_{vibr,exc}$ is the "excess" vibrational entropy $S_{vibr,exc} = S_c(T_g) - S_g(0)$. R is the gas constant: R=8.314 J/mol·K.

Butanol isomer	T_m (K)	T_g (K)	T_K (K)	ΔS_m J/mol·K	$S_g(0)$ J/mol·K	$S_c(T_g)$ J/mol·K	$S_{vibr,exc}$ J/mol·K	$S_g(0)/\Delta S_m$	$S_g(0)/R$
n-butanol	183	111	80	51.1	13.1	24.7	11.6	0.26	1.58
sec-butanol	185	118	96	32.3	5.17	12.3	7.15	0.16	0.62
isobutanol	168	113	78	37.3	13.1	21.3	8.24	0.35	1.57

From the data collected in Table 5.5, we can also observe that the residual entropies of n-butanol and isobutanol are the same, within experimental error, whereas the residual entropy of sec-butanol is less than one half of the others. Still, all these values are similar to those found in other molecular glasses [Johari 1980].

If we express the entropy in units of the gas constant R, we see that $S_g(0) \approx 1.6\ R$ for both n-butanol and isobutanol, whereas $S_g(0) \approx 0.62\ R$ in sec-butanol. Hence one may naively speculate that the residual entropy of n-butanol and isobutanol is $S_g(0) \approx k_B \cdot \ln 5$ and for sec-butanol is $S_g(0) \approx k_B \cdot \ln 2$, corresponding to 5 or 2 available configurations per molecule, respectively. Nevertheless, it is

important to stress that there are many sources of error until one obtains the residual entropy of one glass, and these numerical values should be considered with caution. However, it seems clear that the particular location of the hydroxyl group (OH), and hence the hydrogen bonding, in almost the centre of the butanol molecule for the case of sec-butanol, in contrast to the cases of n-butanol and isobutanol (see Fig. 3.3), makes sec-butanol a more *fragile* liquid than the others (see Table 4.1), with a stronger entropy reduction below T_m and a Kauzmann temperature closer to the glass transition T_g. Moreover, this could be associated to the lower residual entropy $S_g(0)$ of this isomer.

It is also worth mentioning that the obtained residual entropies $S_g(0)$ (i.e. the configurational entropies at 0 K) are always about one half of the "configurational entropies" at the glass transition, $S_c(T_g) = S_{glass}(T_g) - S_{crystal}(T_g)$. A similar amount of reduction of entropy down to 0 K is due to the differences between glass and crystal "vibrational entropies" between 0 K and T_g, quantified by the column $S_{vibr,exc} = S_c(T_g) - S_g(0)$ in Table 5.5. Therefore the assumptions sometimes invoked that the vibrational heat capacity (and hence entropy) of a glass can be approximated by that of the corresponding crystal are usually wrong.

References

[Andon 1971]: R. J. L. Andon, J. E. Connett, J. F. Counsell, E. B. Lees, and J. F. Martin, J. Chem. Soc. (A), 661 (1971).

[Ashcroft 1976]: N. W. Ashcroft and N. D. Mermin, *Solid State Physics*, Tokyo, Holt-Saunders, Chapter 23, (1976).

[Buchenau 1992]: U. Buchenau, Yu. M. Galperin, V. L. Gurevich, D. A. Parshin, M. A. Ramos, and H. R. Schober, Phys. Rev. B 46, 2798 (1992).

[Caponi 2009]: S. Caponi, S. Corezzi, D. Fioretto, A. Fontana, G. Monaco and F. Rossi, Phys. Rev. Lett. 102, 027402 (2009).

[Chumakov 2011]: A. I. Chumakov *et al.*, Phys. Rev. Lett. 106, 225501 (2011).

[Counsell 1965]: J. F. Counsell, J. L. Hales and J. F. Martin Trans. Faraday Soc 61**,** 1869, (1965).

[Counsell 1968]: J. F. Counsell, E. B. Lees, and J. F. Martin, J. Chem. Soc. (A), (1968).

[Elliott 1990]: S. R. Elliott, *Physics of Amorphous Materials*, 2nd ed. Longman, (1990).

[Hassaine 2009]: M. Hassaine, R. J. Jiménez-Riobóo, I. V. Sharapova, O. A. Korolyuk, A. I. Krivchikov, and M. A. Ramos, J. Chem. Phys 131, 174508 (2009).

[Hassaine 2012]: M. Hassaine, M.A. Ramos, A.I. Krivchikov, I.V. Sharapova, O.A. Korolyuk, and R.J. Jiménez-Riobóo, Phys. Rev. B 85, 104206 (2012).

[Ilin 1987]: M. A. Il'in, V. G. Karpov, and D. A. Parshin, Sov. Phys. JETP 65, 165 (1987).

[Johari 1980]: G. P. Johari, Philosophical Magazine 41, 41 (1980).

[Karpov 1983]: V. G. Karpov, M. I. Klinger, and F. N. Ignatiev, Sov. Phys. JETP 57, 439 (1983).

[Kivelson 1998]: D. Kivelson, G. Tarjus, J. Chem. Phys 109, 5481 (1998).

[Krivchikov (2011)]: A. I. Krivchikov, O. A. Korolyuk, I. V. Sharapova, O. O. Romantsova, F. J. Bermejo, C. Cabrillo, R. Fernandez-Perea, and I. Bustinduy, Journal of Non-Crystalline Solids 357, 483 (2011).

[Kruger 1989]: J. K. Krüger, in *Brillouin spectroscopy and its application to polymers in optical techniques to characterize polymer systems*, edited by A. Bässler Elsevier, Amsterdam, (1989).

[Monaco 2006]: A. Monaco, A. I. Chumakov, Y.-Z. Yue, G. Monaco, L. Comez, D. Fioretto, W. A. Crichton and R. Rüffer, Phys. Rev. Lett. 96, 205502 (2006).

[Parshin 1994]: D. A. Parshin, Phys. Rev. B 49, 9400 (1994).

[Phillips 1981]: W. A. Phillips (ed.), Amorphous Solids: *Low Temperature Properties*, Springer, Berlin, (1981).

[Ramos 1998]: M. A. Ramos and U. Buchenau, in: P. Esquinazi (ed.), *Tunneling Systems in Amorphous and Crystalline Solids*, Springer, Berlin, Chap. 9. (1998).

[Ramos 1997]: M. A. Ramos, and U. Buchenau, Phys. Rev. B 55, 5749 (1997).

[Ramos 2002]: M. A. Ramos, C. Talon, and S. Vieira, J. Non-Cryst. Solids 307-310, 80 (2002).

[Ramos 2003]: M. A. Ramos, C. Talon, R. J. Jiménez-Riobóo, and S. Vieira, J. Phys.: Condens. Matter 15, 1007 (2003).

[Richert 1998]: R. Richert and C. A. Angell, J. Chem. Phys. 108, 9016 (1998).

[Ruta 2010]: B. Ruta, G. Baldi, V. M. Giordano, L. Orsingher, S. Rols, F. Scarponi and G. Monaco, J. Chem. Phys. 133, 041101 (2010).

[Sharapova 2010]: I.V. Sharapova, A.I. Krivchikov, O.A. Korolyuk, A. Jezowski , M. Rovira-Esteva, J. Ll. Tamarit, L. C. Pardo, and M. D. Ruiz-Martin, F. J. Bermejo *Phys. Rev*. B 81, 094205 (2010).

[Shmyt'ko 2010]: I. M. Shmyt'ko, R. J. Jiménez-Riobóo, M. Hassaine, and M. A. Ramos, J. Phys.: Condens. Matter 22, 195102 (2010).

[Talon 2001]: C. Talón, M. A. Ramos, I. M. Shmyt'ko, N. Afonikova, A. Criado, G. Madariaga, and F. J. Bermejo, J. Non-Cryst. Solids 287, 226 (2001).

[Zeller 1971]: R. C. Zeller and R. O. Pohl, Phys. Rev B 4, 2029 (1971).

6 General conclusions

In this thesis, we have used the different butanol isomers (n-butanol, sec-butanol, isobutanol and *tert*-butanol) as a model system to shed light on our understanding of the low-temperature thermal and vibrational properties of glasses, specifically on the much controversial features known as the *boson peak* (in the reduced magnitudes $g(\omega)/\omega^2$ and C_p/T^3) and the thermal conductivity *plateau*. We have found that the main thermal properties of butanol glasses at low temperatures strongly vary among its different position isomers, when the hydrogen bond of the hydroxyl group (OH^-) locates in a different position of the butanol molecule. On the contrary, the Debye specific heat of their corresponding crystals remains essentially constant for the different isomers.

With the help of some complementary experiments (mainly Brillouin scattering), we have also shown that the *elastic* Debye coefficients agree well with the *calorimetric* ones obtained from a Soft-Potential Model (SPM) analysis of the specific heat. We have determined the *molecular* Debye temperatures Θ_D for the different solid states (glasses and crystals) of butanol isomers.

We have studied and determined the phase diagram of the different position isomers of butanol, obtaining their main calorimetric and thermodynamic data. We have discussed the proposed correlations in the literature with liquid *fragility* by comparing kinetic and thermodynamic data for this model system of butanol isomers, and with other monohydroxy alcohols. We have found that the proposed phenomenological correlations for the fragility of supercooled liquids is not fulfilled for these – and probably other– hydrogen-bonded liquids, which seems to behave kinetically as strong liquids but thermodynamically as fragile liquids.

From a comparative study of this model system of butanol isomers around the glass transformation range, it seems that competition between crystallization rate and glass-forming ability depends mainly on the aspect ratio of the

molecules, as well as on the hydrogen bonding location within the molecular structure, as can be seen through these butanol isomers, where the formation of crystal and glass strongly depends on the particular isomer and its intermolecular structure.

Another one of the aims traced in this thesis was to shed light on the controversial "glacial phase" of n-butanol. From the different experiments performed in this thesis, including x-ray diffraction and thermal conductivity conducted by some collaborators, we have found that this disputed solid phase, the so-called "glacial phase" is not a second amorphous state, but rather the result of a frustrated crystallization process at around 120 K that produces many nanocrystallites embedded in a more or less disordered matrix, presumably due to an aborted crystallization originated by a high nucleation rate in a temperature range where the crystal growth is low. In all our experiments, we have not seen any trace of a second glass transition, nor of a second amorphous state.

We have finally calculated the residual entropy in the zero-temperature limit and the so-called Kauzmann temperature T_K for all the studied glasses, as well as other thermodynamic data. Although an expected scaling was observed between the glass transition T_g and melting T_m temperatures, with T_g/T_m always lying within 0.64±0.03, we did not find any significant scaling between T_K and those temperatures.

On the other hand, it became clear that the particular location of the hydroxyl group (OH^-), and hence the hydrogen bonding, in almost the centre of the butanol molecule for the case of sec-butanol, in contrast to the cases of n-butanol and isobutanol where it is located at the end of the molecule, makes sec-butanol a more *fragile* liquid than the others, with a stronger entropy reduction below T_m and a Kauzmann temperature closer to the glass transition T_g, what could be associated with the lower residual entropy found for this isomer. It is however somewhat surprising that the most fragile liquid in this sense corresponds to the best glass former of the family of butanols.

It would be interesting in the future to perform complementary studies on this model system, by using other experimental techniques (e.g. neutron and Raman scattering in the glass states, or x-ray diffraction and dielectric relaxation time as a function of temperature in the liquid state, etc.) to explore different relevant issues about the influence of chemical isomerism and location of the hydrogen bonding on lattice dynamics, as well as others concerning molecular glass-forming liquids. Also, it would be very interesting to extend the low-temperature measurements on these butanol glasses to still lower temperatures to assess the real amount of tunneling states in each isomer and also to check the validity of the soft-potential model analysis in a more definite way.

Conclusiones generales

En esta tesis, hemos utilizado a los diferentes isómeros del butanol (n-butanol, sec-butanol, isobutanol y *tert*-butanol) como un sistema modelo para arrojar luz sobre nuestra comprensión de las propiedades térmicas y vibracionales de los vidrios, en concreto sobre las controvertidas propiedades características conocidas como *pico bosónico* (que aparece en las magnitudes reducidas $g(\omega)/\omega^2$ y C_p/T^3) y como *plateau* en la conductividad térmica a bajas temperaturas. Hemos encontrado que las principales propiedades térmicas de los vidrios de butanol varían fuertemente de unos isómeros posicionales a otros, al ocupar el puente de hidrógeno del grupo hidroxilo (OH^-) una posición diferente en la molécula de butanol. Por el contrario, el calor específico de Debye de los cristales correspondientes permanece esencialmente constante para los distintos isómeros.

Con la ayuda de algunos experimentos complementarios (principalmente de espectroscopía Brillouin), hemos demostrado también que los coeficientes de Debye *elásticos* están en buen acuerdo con los *calorimétricos* obtenidos de un análisis del calor específico empleando el Modelo de Potenciales Blandos (SPM). Asimismo hemos determinado las temperaturas de Debye moleculares Θ_D para los isómeros de butanol en sus diferentes estados sólidos (vidrios y cristales).

Hemos estudiado y determinado el diagrama de fases de los diferentes isómeros del butanol, obteniendo sus principales datos calorimétricos y termodinámicos. Hemos discutido las correlaciones propuestas en la literatura con la *fragilidad* del líquido, comparando los datos cinéticos y termodinámicos para este sistema modelo de isómeros de butanol, y con otros alcoholes monohidroxílicos. Hemos encontrado que las correlaciones fenomenológicas propuestas para la fragilidad de los líquidos sobreenfríados no se cumplen para estos –ni posiblemente para otros– líquidos de puente de hidrógeno, que parecen

comportarse cinéticamente como líquidos fuertes pero termodinámicamente como líquidos frágiles.

De un estudio comparativo de este sistema modelo de isómeros de butanol alrededor de su región de transformación vítrea, parece concluirse que la competición entre velocidad de cristalización y capacidad de formación del vidrio depende principalmente de la relación geométrica de las moléculas, así como de la ubicación del puente de hidrógeno dentro de la estructura intermolecular.

Otro de los objetivos que nos habíamos trazado en esta tesis era el de arrojar luz sobre la controvertida "fase glacial" del n-butanol. De los distintos experimentos realizados en esta tesis, incluidos los de difracción de rayos X y los de conductividad térmica llevados a cabo por algunos colaboradores, hemos concluido que esta debatida fase sólida, denominada "fase glacial", no corresponde a un segundo estado amorfo sino más bien a un proceso frustrado de cristalización alrededor de 120 K que produce muchos nanocristalitos dentro de una matriz desordenada, presumiblemente por el efecto de una cristalización abortada a causa de una velocidad de nucleación cristalina alta en un rango de temperatura donde la velocidad de crecimiento cristalino es baja. En todos nuestros experimentos no hemos encontrado ninguna evidencia de una segunda transición vítrea ni de un segundo estado amorfo.

Finalmente, hemos calculado la entropía residual en el límite del cero de temperaturas y la llamada temperatura de Kauzmann T_K para todos los vidrios estudiados, así como otros datos termodinámicos de interés. Aunque sí observamos la esperada proporcionalidad entre las temperaturas de transición vítrea T_g y de fusión T_m, con el cociente T_g/T_m siempre dentro del rango 0.64±0.03, no encontramos una correlación significativa entre T_K y dichas temperaturas.

Por otra parte, ha quedado claro que la particular ubicación del grupo hidroxilo (OH^-) y, por tanto, de los puentes de hidrógeno, cerca del centro de la

molécula para el caso del sec-butanol, en contraste con los casos del n-butanol y el isobutanol en los que se sitúa en un extremo de la molécula, hace del sec-butanol un líquido más *frágil* que los otros, con una reducción más acusada de la entropía por debajo de T_m y una temperatura de Kauzmann más cercana a la de transición vítrea T_g, lo que puede asociarse con la menor entropía residual encontrada para este isómero. Es, sin embargo, algo sorprendente que el líquido más frágil en este sentido se corresponda con el mejor formador de vidrio de la familia de los butanoles.

En el futuro, sería interesante llevar a cabo estudios complementarios en este sistema modelo, empleando otras técnicas experimentales (por ejemplo, dispersión de neutrones o Raman en los estados vítreos, o difracción de rayos X y tiempos de relajación dieléctrica en función de la temperatura en los estados líquidos, etc.) para explorar distintos aspectos interesantes relativos a la influencia del isomerismo químico y de la ubicación de los puentes de hidrógeno en la dinámica de la red, así como de otros relativos a los líquidos moleculares formadores de vidrios. También sería muy interesante extender las medidas a bajas temperaturas en estos vidrios de butanol a todavía más bajas temperaturas para determinar con precisión la cantidad real de estados de tuneleo en cada isómero y para comprobar la validez del análisis con el modelo de potenciales blandos de manera más definitiva.

Index of figures and tables

FIGURES

Figure 1.1: Schematic sketches of the atomic arrangements in.....12

Figure 1.2: The two general cooling paths by which an assembly of atoms in the liquid state can condense into the solid state.....13

Figure 2.1: Behavior of crystallization rate as a function of temperature.....17

Figure 2.2: Temperature dependence of a liquid's volume V or enthalpy H at constant pressure…….....…….20

Figure 2.3: Temperature dependence (using T_g as normalizing parameter) of viscosity logarithm for several glass-forming liquids…...……...22

Figure 2.4: Temperature dependence of the entropy difference between several supercooled liquids and their stable crystal……..…24

Figure 2.5: Visualization of the free-volume notion for a two-dimensional hard-sphere system……..……...26

Figure 2.6: Illustration of the relation between relaxation time, entropy, and excitation level on the potential energy hypersurface.....28

Figure 2.7: The dynamic correlation function in a Lennard-Jones system……...30

Figure 2.8: Specific heat (a) and thermal conductivity (b) of crystalline and amorphous phases of SiO_2……..……..…….33

Figure 2.9: Specific heat of vitreous SiO_2 and crystal quartz…....……34

Figure 2.10: Acoustic attenuation, expressed as internal friction Q^{-1}, of seven different amorphous solids….....…….……35

Figure 2.11: Schematic illustration of the double-well potential used in the TM, with its basic parameters……..…….……37

Figure 2.12: Single and double-well regions in the D_1-D_2 plane of the soft-potential model.....41

Figure 3.1 (a): Schematic illustration of the experimental system.....48

Figure 3.1 (b): photo of the calorimetric cell suspended from the circular support (ring) by nylon threads.....49

Figure 3.2: the calorimetric cell.....49

Figure 3.3: Schematic molecular structure of the four different position isomers of butanol.....51

Figure 3.4: Example of a real experimental point obtained for isobutanol using the standard relaxation method.....55

Figure 3.5: Example of a real experimental point obtained for isobutanol using the non-standard relaxation method.....55

Figure 3.6: Schematic illustration of the continuous method.....56

Figure 3.7: Experimental run of the empty cell using the continuous method.....57

Figure 3.8: Heat capacity of the empty cell by different experimental runs.....60

Figure 3.9: Polynomial fit to the experimental data 61

Figure 3.10: Heat capacity of the empty cell measured by using both the standard relaxation method and the fast relaxation.....62

Figure 3.11: Polynomials fits and its validity range.....63

Figure 3.12: Total heat capacity of the sample (in this case 2-butanol glass) together with the heat capacity of the empty cell.....63

Figure 4.1: A directly measured variation of temperature as a function of time, showing different rates of cooling.....66

Figure 4.2: Thermogram as a function of temperature from the glass to the liquid of n-butanol.....67

Figure 4.3: Typical thermogram, in absolute d*T*/dt units, showing the preparation of the metastable "glacial" state……..……68

Figure 4.4: Thermogram showing a first thermal cycle by heating the glacial state of *n*-butanol that exothermically transforms into the crystal state....69

Figure 4.5: glacial state obtained directly by cooling the liquid n-butanol...…...70

Figure 4.6 Heating thermograms of several *glacial phases* previously obtained following different crystallization histories.....71

Figure 4.7: Temperature dependence of the specific heat of *n*-butanol for the glass (Δ), *glacial* (∇) and crystal (O) states.....72

Figure 4.8: Specific heat of differently prepared glasses of n-butanol.....74

Figure 4.9: Configurational enthalpy of a fast cooled (FC) glass, and a slow cooled (SC) glass for 1-butanol……...……75

Figure 4.10: A directly measured variation of temperature as a function of time, showing the glass transition of 2-butanol…….....76

Figure 4.11: Molar specific heat of glass 2-butanol and its supercooled liquid (SCL) to above 200K……..……77

Figure 4.12: Specific heat of differently prepared glasses of 2-butanol.....78

Figure 4.13: Configurational enthalpy of a fast cooled (FC) glass, and a slow cooled (SC) glass for 2-butanol…….....79

Figure 4.14: Variation of temperature as a function of time, from 310 K to 77 K, showing the two consecutive crystallization processes of tert-butanol…...80

Figure 4.15: A directly measured variation of temperature as a function of time, showing the quench of liquid tert-butanol……...81

Figure 4.16: Heating of the crystal of tert-butanol obtained by the very fast cooling…..……81

Figure 4.17: *dT/dt* of the heating of the crystal-I from 275K and its liquid state, plotted together with crystal-II heated by the same heating power…….…82

Figure 4.18: Thermograms as a function of temperature of tert-butanol.....83

Figure 4.19: Specific heat of different crystals tert-butanol……...84

Figure 4.20: *dT/dt* of the "standard" cooling of liquid of iso-butanol……...85

Figure 4.21: Heating run of isobutanol glass, T_g = 113K……...……..…86

Figure 4.22: Thermogram of crystal isobutanol and its repeated cooling and heating cycles.....87

Figure 4.23: Molar specific heat of isobutanol for the glass (○), crystal (Δ), SCL (□) and liquid (∇) states.....88

Figure 4.24: Specific heat of differently prepared glasses of isobutanol.....89

Figure 4.25: Configurational enthalpy of a fast cooled (FC) glass, and a slow cooled (SC) glass for isobutanol…….……..89

Figure 4.26: Evolution with temperature of X-ray diffraction spectra at slow heating, starting from the glassy state…….……...……92

Figure 4.27: Brillouin backscattering frequency shift(s) as a function of temperature for the different phases of *n*-butanol…….……95

Figure 4.28: Optical photographs at different temperatures showing the different aspects of the sample throughout the different phases……..…96

Figure 4.29: Specific heat of the three obtained butanol glasses by slow cooling (–0.2 K/min) and heated in all cases by the same power……..…101

Figure 4.30: Melting transition observed by representing *dT*/*dt* vs the experimental time *t* (in the case of n-butanol).....103

Figure 5.1: A log-log representation of the total specific heat $C_{p\ total}$ for the three different states of n-butanol together with the heat capacity of the empty cell.....110

Figure 5.2: Molar specific heat plotted as C_p/T^3 for the three obtained phases of n-butanol…….....112

Figure 5.3: Experimental data for the glass and crystal states of n-butanol at the lowest temperature, together with the corresponding fits…….....113

Figure 5.4: Low-temperature specific heat in a semi logarithmic C_p/T^3 vs T plot for the sec-butanol glass, with the corresponding fit to the (SPM)…..…....114

Figure 5.5: Experimental data for the sec-butanol glass at the lowest temperature, in a C_p/T vs T^2 representation……115

Figure 5.6: Low-temperature specific heat in a semi logarithmic C_p/T^3 vs T plot for the sec-butanol crystal, with the corresponding fit (Debye model)……116

Figure 5.7: A C_p/T vs T^2 representation of the experimental data for the tert-butanol crystal-II at the lowest temperature……117

Figure 5.8: Molar specific heat plotted as C_p/T^3 for the two obtained phases of isobutanol: glass (circles), and crystal (squares)…….…….....118

Figure 5.9: Experimental data for the glass and crystal states of isobutanol at the lowest temperature, together with the corresponding fits.....119

Figure 5.10: Temperature dependence of the thermal conductivity of n-butanol, sec-butanol, and iso-butanol, in their glass states.....122

Figure 5.11: Temperature dependence (including extrapolation) for the longitudinal and transverse sound velocities of n-butanol, sec-butanol and iso-butanol isomers, in their glass states……..……..…124

Figure 5.12: Temperature dependence of the thermal conductivity of n-butanol for its three states: glass, "glacial", and fully-ordered crystal.....126

Figure 5.13: Low-temperature specific heat plotted in Cp/T versus T^2 for different crystals of isomers butanol…….....128

Figure 5.14: C_p/T^3 plots for glasses and crystalline phases of different position isomers of butanol…….....129

Figure 5.15: Excess low-temperature specific heat of butanol glasses after subtraction of the acoustically measured Debye level.....130

Figure 5.16: C_p/T^3 plots for the butanol glasses. Dashed lines indicate their Debye contributions obtained from Brillouin-scattering.....131

Figure 5.17: Renormalized thermal conductivity data κ (T) plotted on the reduced temperature z from experimental data for butanol glasses.....134

Figure 5.18: shows the molar specific heat of glass and crystal n-butanol and its jumps at T_g, T_m respectively, and the specific heat of the liquid.....137

Figure 5.19: C_p/T against temperature T plot for the glass, crystal and liquid of n-butanol…….....138

Figure 5.20: The entropy of n-butanol obtained by integrating the heat capacities, we also show T_K……139

Figure 5.21: Variation of the obtained configurational entropy of n-butanol with temperature, and the fit using AG equation…….……140

Figure 5.22: Continuous curves of C_p/T versus T obtained from interpolation of experimental data for the different states of sec-butanol.....141

Figure 5.23: Entropy of sec-butanol obtained by integrating the specific heat. We also show the temperature, T_K.....142

Figure 5.24: Variation of the obtained configurational entropy of sec-butanol with temperature, and the fit using AG equation.....142

Figure 5.25: Continuous curves of C_p/T versus T obtained from interpolation of experimental data for the different states of isobutanol……..…143

Figure 5.26: The entropy of isobutanol obtained by integrating the heat capacities. We also show the temperature, T_K.....144

Figure 5.27: Variation of the obtained configurational entropy of isobutanol with temperature, and the fit using AG.....144

Figure 5.28: Temperature dependence of the *excess* entropy curves normalized by their values at the melting point, T_m and ΔS_m.....145

TABLES

Table 4.1: Relevant calorimetric and thermodynamic data of glass transition and crystal melting for the different butanol isomers……...……..……104

Table 5.1: Calorimetric data for the crystals of n-butanol, tert-butanol and isobutanol.....120

Table 5.2: Calorimetric data for butanol glasses; n-butanol, sec-butanol and isobutanol…….…….120

Table 5.3: Elastic data obtained for butanol glasses……..125

Table 5.4: SPM-fitted specific-heat parameters for glasses.....135

Table 5.5: Calorimetric and thermodynamic data of glasses butanol isomers (n-butanol, sec-butanol and isobutanol)…….....146

List of publications

- *"Thermal-properties and Brillouin-scattering study of glass, crystal and "glacial" states in n-butanol"*,
M. Hassaine, R. J. Jiménez-Riobóo, I. V. Sharapova, O. A. Korolyuk, A. I. Krivchikov, and M. A. Ramos, J. Chem. Phys. 131, 174508 (2009).

- *"Structural and thermodynamic studies of n-butanol"*,
I. M. Shmyt'ko, R. J. Jiménez-Riobóo, M. Hassaine and M. A. Ramos, J. Phys. Condens. Matter 22, 195102 (2010).

- *"Low-temperature properties of glassy and crystalline states of n-butanol"*,
A. I. Krivchikov, M. Hassaine, I. V. Sharapova, O. A. Korolyuk, R. J. Jiménez-Riobóo, and M. A. Ramos, J. Non-Cryst. Solids 357, 524 (2011).

- *"Calorimetric studies at low temperatures of glass-forming 1-butanol and 2-butanol"*,
M. Hassaine and M. A. Ramos, Physica Status Solidi A 208, 2245 (2011).

- *"Calorimetric and thermodynamic study of glass-forming monohydroxy alcohols"*,
M. A. Ramos, B. Kabtoul, and M. Hassaine, Philosophical Magazine 91, 1847 (2011).

- *"Low-temperature thermal and elastoacoustic properties of butanol glasses: Study of position isomerism effects around the boson peak",*
M. Hassaine, M. A. Ramos, A. I. Krivchikov, I. V. Sharapova, O. A. Korolyuk, and R. J. Jiménez-Riobóo, Phys. Rev. B 85, 104206 (2012).

- *"Low-temperature properties of monoalcohol glasses and crystals",*
M. A. Ramos, M. Hassaine, B. Kabtoul, R.J. Jiménez-Riobóo, I. M. Shmyt'ko, A.I. Krivchikov, I.V. Sharapova, and O.A. Korolyuk, Low Temperature Physics/Fizika Nizkikh Temperatur 39, 600 (2013).